University of Alberta

Numerical Simulation of Granular Particle Movement in Fluid Flow

by

Siwa Tipthavonnukul

A thesis submitted to the Faculty of Graduate Studies and Research in partial fulfillment of the requirements for the degree of Master of Science

in

Geotechnical Engineering

Department of Civil and Environmental Engineering

Edmonton, Alberta

Fall 2002

National Library of Canada
Acquisitions and Bibliographic Services
395 Wellington Street
Ottawa ON K1A 0N4
Canada

Bibliothèque nationale du Canada
Acquisitions et services bibliographiques
395, rue Wellington
Ottawa ON K1A 0N4
Canada

Your file Votre référence

Our file Notre référence

The author has granted a non-exclusive licence allowing the National Library of Canada to reproduce, loan, distribute or sell copies of this thesis in microform, paper or electronic formats.

L'auteur a accordé une licence non exclusive permettant à la Bibliothèque nationale du Canada de reproduire, prêter, distribuer ou vendre des copies de cette thèse sous la forme de microfiche/film, de reproduction sur papier ou sur format électronique.

The author retains ownership of the copyright in this thesis. Neither the thesis nor substantial extracts from it may be printed or otherwise reproduced without the author's permission.

L'auteur conserve la propriété du droit d'auteur qui protège cette thèse. Ni la thèse ni des extraits substantiels de celle-ci ne doivent être imprimés ou autrement reproduits sans son autorisation.

0-612-81489-0

Canada

University of Alberta

Library Release Form

Name of Author: Siwa Tipthavonnukl

Title of Thesis: Numerical Simulation of Granular Particle Movement in Fluid Flow

Degree: Master of Science

Year this Degree Granted: 2002

Permission is hereby granted to the University of Alberta Library to reproduce single copies of this thesis and to lend or sell such copies for private, scholarly or scientific research purposes only.

The author reserves all other publication and other rights in association with the copyright in the thesis, and except as hereinbefore provided, neither the thesis nor any substantial portion thereof may be printed or otherwise reproduced in any material from whatever without the author's prior written permission.

Siwa Tipthavonnukul

563-565 Thachalab Rd., T.Talat,
Muang, Chanthaburi, 22000, THAILAND.

October 1, 2002

University of Alberta

Faculty of Graduate Studies and Research

The undersigned certify that they have read, and recommend to the Faculty of Graduate Studies and Research for acceptance, a thesis entitled Numerical Simulation of Granular Particle Movement in Fluid Flow submitted by Siwa Tipthavonnukul in partial fulfillment of the requirements for the degree of Master of Science in Geotechnical Engineering.

Dr. Dave Chan

Dr. Peter Steffler

Dr. Ben Jar

Date: October 1, 2002

ABSTRACT

A coupled method between discontinuum and continuum approaches has been developed to simulate granular particles moving in a flowing fluid. The movement of granules is modeled using the discrete element method, while the finite volume scheme is used to simulate fluid flow. The existence of granules in the flow region is assumed to cause a reduction in the amount of fluid flow. The flowing fluid is expected to induce drag forces, which are computed based on the relative velocities between the fluid and particles. Buoyant forces on a particle are equal to the weight of the fluid displaced by the particle. An existing computer program has been modified to include the solution of the Navier-Stokes equation. A few illustrative examples are given to demonstrate the possibility of the proposed method in simulating granular particles moving in a flowing fluid.

ACKNOWLEDGMENTS

I would like to express my sincere appreciation to Dr. Dave Chan, my supervisor, who always gives me the guidance, kind supports and helps me in every ways throughout my study.

To Dr. Peter Steffler and Dr. Ben Jar, members of my Examining Committee, for their helpful suggestions.

Special gratitude goes to Srboljub Masala for all his help and useful discussions, and to Haihua Lu for his valuable suggestions in computer programming. I appreciate very much for their kindness, their willingness to help and the helpful knowledge that I have learned from both of them.

I am also grateful to Andrew Corkum and Anna Ho for reviewing the most difficult chapters in my thesis and offering a number of helpful suggestions. Without their help the completion of this thesis would have taken longer. My thanks are extended to all of my colleagues and friends both in Canada and in Thailand for the priceless friendship they give to me.

Also I would like to thank the staff in the Department of Geotechnical and Geoenvironmental engineering for their collaboration and technical support.

Finally, I would like to express my gratitude to my mother, father and sisters for their encouragement and moral support in every steps of my life.

TABLE OF CONTENTS

CHAPTER	PAGE
1. INTRODUCTION	
1.1 General	1
1.2 Objective of Thesis	2
1.3 Scope and Organization	3
2. LITERATURE REVIEW	
2.1 Developments in the Discrete Element Method	4
2.2 Fundamentals on Fluid Mechanics	9
2.3 Coupling Mechanisms between Discontinuum and Continuum	15
3. THE SIMULATION OF GRANULAR MATERIAL	
3.1. Theory and Background Information	19
3.1.1 The discrete element method	19
3.1.2 Calculation cycle	21
3.1.2.1 Force-displacement law	22
3.1.2.2 Law of motion	26
3.1.3 Damping	27
3.1.4 Boundary conditions	29
3.1.5 Critical time-step determination in granular simulation	29
3.1.6 Contact detection	30
3.2. Explanation of Computer Codes	31
3.2.1 Contact detection scheme	31
3.2.2 Calculation of contact force	34
3.2.3 Calculation by the Law of Motion	34
3.2.4 Creation of graphical result	35
3.3. Limitation and Shortcomings of Granular Simulation	36
3.3.1 Size of the time-step	36
3.3.2 Search time in the contact detection algorithm	36
3.3.3 Material calibration	37
4. THE SIMULATION OF FLUID FLOW	
4.1. General Formulation	39
4.1.1 Differential equation of mass conservation	39
4.1.2 Differential equation of linear momentum	42
4.1.3 The Navier-Stokes equation	44

4.2. Modeling Methodology 46
4.2.1 General 46
4.2.2 Finite volume formulation 46
4.2.3 Boundary conditions 50
4.2.4 Solution algorithm 51
4.2.5 Critical time-step determination in fluid flow simulation 56

4.3. Explanation of Computer Codes 57
4.3.1 Discretization process 58
4.3.2 First approximation of flow variables 59
4.3.3 Pressure correction algorithm 60
4.3.4 Creation of graphical result 61

4.4. Limitations and Shortcomings of Fluid Flow Simulation 62
4.4.1 Computer time consumption 62
4.4.2 Range of solvable problems 62
4.4.3 Shortcomings of upwind differencing technique 63

4.5. Verification Problem 63
4.5.1 Problem statement 63
4.5.2 Closed-form solution 64
4.5.3 Numerical model 65
4.5.4 Results 66

5. FLUID-SOLID COUPLING
5.1. Modeling Solid-Fluid Couplings 68
5.1.1 Effects of fluid on the granular particles 69
5.1.1.1 Drag force 69
5.1.1.2 Buoyancy 71
5.1.1.3 Lift 72
5.1.2 Effect of granular particle on the fluid 73
5.1.3 Calculation cycle 74

5.2. Explanation of Computer Codes 75
5.2.1 Detection of fluid-particle contact 75
5.2.2 Simulation of particle interaction 76
5.2.3 Calculation of drag and buoyant forces 77

5.3. Limitations and Drawbacks 79
5.3.1 Range of solvable problems 79
5.3.2 Resolution of the flow field 79
5.3.3 Limitation of the two-dimensional model 80
5.3.4 Fluid/particle interaction 81
5.3.5 Calibration process 81

6. EXAMPLES OF COUPLED GRANULAR AND FLUID FLOW MODELING
6.1. Flow of Fluid and Granular Particles between Two Fixed

Parallel Plates 82
6.2. Granular Particles Dropped into Flowing Fluid 89

6.3. Discussions 103

7. CONCLUSION 109

REFERENCE LIST 111

LIST OF TABLES

	PAGE
Table 2.1. Range of Reynolds number	11
Table 4.1. Fluid properties in numerical simulation	66
Table 4.2. The comparison of flow velocities	67
Table 6.1. Summary of model parameters in the examples 6.1.1, 6.1.2 and 6.1.3	83
Table 6.2. Summary of model parameters in the examples 6.2.1, 6.2.2 and 6.2.3	90

LIST OF FIGURES

	PAGE
Figure 3.1. Calculation cycle in DEM	22
Figure 3.2. Two particles in contact	23
Figure 3.3. Sign convention for F_n and F_s	25
Figure 3.4. Spring and dashpot model	28
Figure 3.5. Flow chart of updating the contact list	32
Figure 3.6. Flow chart of detecting the new possible contact	33
Figure 3.7. Flow chart of calculating the contact force	33
Figure 3.8. Flow chart of applying the law of motion	35
Figure 4.1. Elemental Cartesian fixed control volume showing the inlet and outlet mass flows on the x faces	40
Figure 4.2. Notation for stresses	43
Figure 4.3. Elemental Cartesian fixed control volume showing the surface forces in the x direction only	43
Figure 4.4. Discretized flow field	47
Figure 4.5. Staggered-grid notation (shaded cell represents cell i, j)	47
Figure 4.6. Cell configurations for implementing boundary conditions	50
Figure 4.7 Entire process of fluid flow simulation	58
Figure 4.8. Discretization	59
Figure 4.9. Flow chart of pressure correction algorithm	61
Figure 4.10. Physical model	64
Figure 4.11. Simulated variations of fluid pressure	67
Figure 5.1. Drag coefficients for sphere and circular shaped objects	70
Figure 5.2. Calculation cycle of the whole simulation	74

Figure 5.3. Simulation of fluid interaction 78

Figure 5.4. All possible cases of particle dropping into fluid 78

Figure 5.5. Two different mesh sizes 80

Figure 6.1. Schematic of flow between two fixed plates 83

Figure 6.2. The simulation of granular and fluid flow between two fixed plates 84

Figure 6.3. The simulation of 6 granular particles and fluid flow between two fixed plates 85-86

Figure 6.4. The simulation of 45 granular particles and fluid flow between two fixed plates 87-88

Figure 6.5. Schematic of flow in the flow field with free surface on top 90

Figure 6.6. The simulation of granular and fluid flow in the free-surface flow space 91-93

Figure 6.7. The simulation of 6 granular particles and fluid flow in the free-surface flow space 94-97

Figure 6.8 The simulation of 45 granular particles and fluid flow in the free-surface flow space 98-102

Figure 6.9. Huge amount of overlap between particles 106

Figure 6.10. Too large contact forces 106

Figure 6.11. Instability calculation 108

CHAPTER 1 INTRODUCTION

1.1 *GENERAL*

Flow of a solid-fluid mixture occurs in a variety of natural and man-made phenomena. Fluid flow can be broadly classified as confined flow (pipe or closed-conduit flow) or unconfined flow (open channel flow). Solid and fluid coupled flow becomes an issue in science and engineering fields such as in fluid mechanics, geology, vehicle design and so on. Here are a few examples:

- In the field of hydro-transport, the transport of coal, ores, sand, cement, fly ash, or chopped wood through pipelines or in open channels;
- Dredging and filling in construction and navigation;
- Soil erosion and sedimentation in the field of conservation and water resources;
- Slurry pipelines, sewage sludge, collection of solid waste in sanitation;
- The movement of transportation vehicles in the air or in the design of sports equipment.

These examples show that the subject matter is diverse with lots of applications and, therefore, it is not surprising that solid-fluid flow is of interest to many professionals, which includes civil, mechanical, chemical and mining engineers, geologists, geographers, automobile designers, sport scientists and so on.

In this work, the simulation of granular material moving in the flowing fluid is considered. Solid and fluid are considered to have different physical properties. For example, a solid can resist static shear stresses but a fluid cannot. Any shear stress

applied to the fluid, no matter how small, will result in the motion of the fluid. From a computational point of view, different approaches have been used to model the movement of different materials. Granular material such as soil can be modelled as a collection of discrete interacting particles in an interstitial fluid using the discontinuum concept; whereas the simulation of fluid flow using the continuum concept has been well developed in the area of Computational Fluid Dynamics. Thus, the proper way to simulate movement of both materials is dissimilar. A coupled method between discontinuum and continuum approaches has been developed in this work to simulate the movement of granular material in fluid flow.

1.2 *OBJECTIVE OF THESIS*

The main objective of this thesis research is to develop the coupled continuum and discontinuum method in modeling the problem of wet granular flow. The term wet granular flow refers to large mobility of soil solids in a flowing fluid. The discontinuum approach to simulate movement of granular material and the continuum approach to simulate fluid flow are studied in this research. The governing equations in the simulation of each material, granular material and flowing fluid, are formulated separately. The coupling mechanisms, including the effect of fluid on the movement of the granular particles and the particle interaction with the flowing fluid, are explored. The limitations of each individual approach in the simulation techniques are discussed. Finally, in order to demonstrate the effectiveness of the proposed coupled method, a few illustrative examples are given.

1.3 *SCOPE AND ORGANIZATION*

Chapter 2 presents a review of existing literature on related topics. This includes the developments of the discrete element method (DEM), the basic fundamentals of fluid mechanics, and the past research on solid-fluid coupling to simulate the problem of granular material in a flowing fluid.

Chapter 3 contains the background information and descriptions of the theoretical basis for the simulation of granular material movement. This chapter also includes the explanation of the computer codes for DEM. Finally, the discussions on the limitations and shortcomings of the method are given.

In chapter 4, the background information and descriptions of the theoretical basis for the simulation of fluid flow are presented. The description of the computer codes for fluid flow simulation is given. The limitations and shortcomings of the simulation method are discussed. A verification problem is simulated and the numerical results are compared with the closed form solution.

Chapter 5 provides the details of coupling mechanisms that are incorporated into the simulation including drag, buoyancy and the method of introducing the particle effects. The explanation of the computer codes for solid-fluid coupling is given. The limitations of the coupling mechanisms are discussed at the end of this chapter.

Illustrative examples are given in chapter 6. Different numbers of particles are used in the simulations. The graphical results are created and are discussed in this chapter. Eventually the conclusion of the work is given in Chapter 7.

CHAPTER 2 LITERATURE REVIEW

In this chapter, a review of the literatures on related topics is given. Different approaches and the diversity of DEM applications are demonstrated. The basic fundamentals of fluid mechanics are reviewed. Finally, past research on coupling mechanisms between discontinuum and continuum approaches is summarized.

2.1 *DEVELOPMENTS IN THE DISCRETE ELEMENT METHOD*

The discrete element method, or DEM, was originally proposed by Cundall (1971); it was initially used to analyze the stability of jointed rock slopes by employing plane polygonal-shaped particles as elements. Enhanced later by Cundall (1988) and Hart et al. (1988), the method was able to deal with three-dimensional problems. DEM was later extended to applications in soils by Cundall and Strack (1979):

"The granular material is idealized as an assemblage of circular-shaped rigid disks or three-dimensional spherical elements".

Even though the simulation of circular-shaped particles has the advantage of being very simple in routine calculations, it could not represent the real behavior of materials such as sand due to the effect of the excessive rolling or rotation of the round-shaped particles (Ting et al., 1995). With the aim of emulating the natural media more closely, other complex shapes of particles have been proposed, such as the arbitrary polygonal-shaped element (Hopkins, 1992), or the elliptical-shaped element (Rothenburg and Barthurst,

1991). These more complex-shaped elements are able to account for particle shapes at the expense of more complicated computational algorithms. According to the work by Rothenburg and Bathurst (1991), the elliptical-shaped elements have the attractiveness of having two additional parameters to describe the individual granular particle. Ting (1992) developed an algorithm for ellipse-based granular assembly to overcome the problem of contact detections. In addition, another technique of simulating different particle shapes is "Clustering". A cluster, acting as one single larger particle, is formed by combining a number of simple circular-shaped particles and then applying bonds to the interparticle contacts between nearby particles within the cluster. The cluster is treated as a rigid body with the side-particles that can deform as the surface of the cluster. More details can be found in the work by Jensen et al (1999).

Besides the development of different particle shapes, the discrete element method has been advanced in other areas on implementation scheme, i.e., contact detection. Vinogradov (1992, 1993 and 1997), as well as Vinogradov and Sun (1997) and Gavrilov and Vinogradov (1997) suggested the algorithms to increase the computational efficiency and accuracy in the simulation of particle clusters, known as the multibody system. The proposed algorithms in these works were based on the path matrix, which is used to describe how particles are located in the assembly. These improvements of the algorithms for the implementation scheme have resulted in an increase in the computational efficiency and decrease in the search time of a calculation cycle. Furthermore, the extensions of the DEM to couple with the various mechanics have been developed. DEM coupling with fracture mechanics is dominantly used in solving rock mechanics problems. Taylor and Preece (1992) modified a DEM code to model rock motion

associated with conventional blasting. Trent and Margolin (1994) conducted numerical analysis based on DEM to model fracture in cemented granular materials. Potyondy et al. (1996) as well as Minchinton and Lynch (1996) made the simulation of crack generation in explosive rock by the discrete element method to study the importance of induced stresses and gas flow. Among the extensions of DEM related to various mechanics, DEM coupled with fluid mechanics was also revealed. Detournay and Cundall (1999) used a DEM commercial program, *FLAC3D*, to model free surface flow in porous media.

It is obvious that DEM has expanded into many applications. One useful advantage of the DEM is the ability to provide insight on how microscopic properties can have an impact on the macroscopic responses. Potyondy et al. (1996) described a computational methodology to simulate certain kinds of material testing using bonded assemblies of circular-shaped particles, similarly to the work by Potyondy and Cundall (1998). Cleary et al. (1998) used DEM to study the mixing processes. Ng (1999) applied DEM to revise the microscopic properties in granular materials. Antony (2000) also utilized DEM to analyze the normal contact force distribution and studied the effect of microstructure and contact fabric on stresses in granular media. The understanding of how the micro-properties affect the macro material responses can lead to more insight into the constitutive behavour of the material. Chang and Misra (1989) used the numerical simulation based on the DEM to compare the results with the micro-structural continuum model. Additionally, DEM has been applied in the field of powder technology and as well as in physical animation for computer graphics.

General description of the discrete element method

In discrete element modeling, the granular assembly is idealized by a collection of circular-shaped particles, or disks for two-dimensional problems. The particles displace independently and interact only at the contact points. Usually it is assumed that the particles are rigid and the behavior at the contacts is characterized by a soft-contact approach. The discussions on using hard- or soft-contacts can be found in the work by Cundall and Hart (1992). The contacts occur over a small area, at a point, relative to the particle sizes. At the contact points, rigid particles are allowed to overlap each other of a magnitude that is related to the contact force. This part of the chapter is based on the work by Cundall and Strack (1979) and the PFC2D manual (1999).

The contacts are described by three constitutive models; a stiffness model, a slip model and a bonding model. The stiffness model provides an elastic relationship between the contact force and the relative displacement. The contact forces are consisted of normal and shear components. The slip model enforces the relationship between shear and normal contact forces such that two contact particles may slip relative to each other. The Mohr-Coulomb criterion is generally used, $F^s_{\max} \le \mu \left| F^n_i \right|$, where $F^s_{\max}$ is the maximum shear force, μ is the frictional coefficient and F^n_i is the normal force. The bonding model is applied to the more complex behavior. The particles are bonded together at their contact points to form a clump of particles. The interparticle contacts may be modeled with an elastic spring and a dashpot.

The interaction between contact particles is treated as a dynamic process in which the movements of the particles are the results of the propagation through the particle

system of disturbances originating from the boundaries. The calculation alternates between the application of the force-displacement law and Newton's second law to keep track of the movement history of all individual particles in the assembly.

Initially, the positions of all granular particles are known. Any two particles in contact are detected and the contact list is being updated at the same time. By using the force-displacement law, the interaction forces between contact particles can be found from the magnitude of the particle overlap. Newton's second law of motion is then applied to find the particle movement resulted from the summation of all forces acting on a particle. It is assumed that the positions, velocities and accelerations of the particles are constant over a single time-step.

The solution scheme is identical to the one that is used in the explicit finite-difference method for continuum analysis. The use of an explicit, as opposed to an implicit, numerical scheme makes it possible for the scheme to simulate the non-linear interaction of a large number of particles without excessive memory requirements or the need for an iterative procedure. It is, however, conditionally stable. The time step needs to be small enough that during a single time step, disturbances cannot propagate from any particle further than its immediate neighbors.

In addition, the damping concept may be taken into account for increasing the systematic energy dissipation, rather than from frictional sliding only, and that induces the motion of the particle system to reach steady-state in a reasonable amount of time.

2.2 *FUNDAMENTALS OF FLUID MECHANICS*[1]

Fluids are aggregations of small molecules. The distance between molecules is very large compared with the molecular diameter, widely spaced for a gas, closely spaced for a liquid. The main focus, here, is on liquid. The molecules are not fixed but move about freely relative to each other and they cannot resist a shear stress. Such a fluid is called a *continuum*, which simply means that its variation in properties is so smooth that differential calculus can be used to analyze the substance.

The theory in fluid mechanics is often very limited, because it applies mainly to idealized situations which may be invalid in practical problems. Two main obstacles regarding the practicality of the theory are the geometry of the problem and the fluid viscosity. The basic equations of fluid motion are not likely to enable the analyst attacking with arbitrary geometric configurations. Therefore most problems in fluid mechanics are limited to simple geometry. Furthermore, the notion of fluid viscosity bounds the applications of fluid mechanics theories. It causes a destabilizing effect on all fluids, giving rise, at frustratingly small velocities, to a disorderly, random phenomenon called *turbulence*.

Basic Characteristic Terms for Fluid Properties

Viscosity

[1] This part could be referred to any text in fluid mechanics for more detailed discussions. The author refers mainly to two textbooks; Fluid Mechanics by White (1999) and Fundamentals of Fluid Mechanics by Gerhart et al. (1992).

When a fluid is sheared, it begins to move at a strain rate inversely proportional to a property called the *coefficient of viscosity* μ. The applied shear is also proportional to the velocity gradient for Newtonian fluids.

$$\tau = \mu \frac{d\theta}{dt} = \mu \frac{du}{dy} \tag{2.1}$$

where τ is the applied shear, μ is the fluid viscosity and $\frac{d\theta}{dt}$ as well as $\frac{du}{dy}$ are the velocity gradient.

Reynolds Number

The primary parameter correlating the viscous behavior of all Newtonian fluids is the dimensionless *Reynolds number*:

$$\mathrm{Re} = \frac{\rho VL}{\mu} = \frac{VL}{\upsilon} \tag{2.2}$$

where V and L are the characteristic velocity and length scales of flow, ρ is the fluid density and μ is the viscosity of fluid. The second form of Re, the right side of equation (2.2), condenses μ and ρ to give υ, the *kinematic viscosity*.

$$\upsilon = \frac{\mu}{\rho} \tag{2.3}$$

Reynolds number is used to determine the type of fluid flow. A very low value of Re (less than 1) indicates viscous *creeping* motion where inertia effects are negligible. Moderate Re implies a smoothly varying laminar flow: the flow ceases being smooth and steady (*laminar*) and becomes fluctuating and agitated (*turbulent*). The changeover is called *transition* to turbulence. The transition region depends upon many effects, e.g.,

wall roughness or fluctuations in the inlet stream, but the primary parameter is the value of Reynolds number. High Re probably spells *turbulent* flow, which is slowly varying in the time-mean but has superimposed strong random high-frequency fluctuations. Table 2.1 shows the approximate ranges of Reynolds number that determine the type of viscous fluid flow.

Table 2.1 Range of Reynolds number (White, 1999)

Ranges of Reynolds Number	Descriptions
$0 < Re < 1$	highly viscous laminar "creeping" motion
$1 < Re < 100$	laminar, strong Reynolds-number dependence
$100 < Re < 10^3$	laminar, boundary-layer theory useful
$10^3 < Re < 10^4$	transition to turbulence
$10^4 < Re < 10^6$	turbulent, moderate Reynolds-number dependence
$10^6 < Re < \infty$	turbulent, slight Reynolds-number dependence

These are representative ranges that vary somewhat with flow geometry, surface roughness, and the level of fluctuations in the inlet stream.

The Basic Governing Equations of Fluid Flow

Differential Equation of Mass Conservation or Continuity Equation

The continuity equation of fluid flow can be written as:

$$\frac{\partial \rho}{\partial t}+\frac{\partial}{\partial x}(\rho u)+\frac{\partial}{\partial y}(\rho v)+\frac{\partial}{\partial z}(\rho w)=0$$

or
$$\frac{\partial \rho}{\partial t}+\vec{\nabla}\cdot(\rho \vec{V})=0 \qquad (2.4)$$

where ρ is the mass density, $\vec{V}$ is the velocity vector, x, y, and z are the distances according to a Cartesian coordinate system, t is time and the gradient operator $\vec{\nabla}$ is $\vec{i}\frac{\partial}{\partial x}+\vec{j}\frac{\partial}{\partial y}+\vec{k}\frac{\partial}{\partial z}$.

The form of equation (2.4) can be modified following different assumptions of the problem.

Steady State Compressible Flow

If the flow is at steady state (independent on time), $\frac{\partial}{\partial t}=0$, and all properties are functions of position only, equation (2.4) becomes:

$$\frac{\partial(\rho u)}{\partial x}+\frac{\partial(\rho v)}{\partial y}+\frac{\partial(\rho w)}{\partial z}=0 \qquad (2.5)$$

Incompressible Flow

If the changes in density are negligible, density is constant regardless of whether the flow is steady or unsteady, and the density can be taken out of the divergence operator, equation (2.4) becomes:

$$\vec{\nabla}\cdot\vec{V}=0$$

or $$\frac{\partial u}{\partial x}+\frac{\partial v}{\partial y}+\frac{\partial w}{\partial z}=0 \qquad (2.6)$$

This equation is valid for both steady and unsteady incompressible flow. An exception occurs in the case of geophysical flows, when a change in density is imposed thermally or mechanically. An example is the layered flow of fresh water upon saltwater or warm air flow upon cold air in the atmosphere. Fluid stratification occurs in these situations. The vertical density changes must be taken into account even if the velocities are small.

Differential Equation of Linear Momentum

The original form of the basic differential linear-momentum equation is shown as:

$$\rho\vec{g}-\vec{\nabla}p+\vec{\nabla}\cdot\vec{\tau}_{ij}=\rho\frac{d\vec{V}}{dt} \qquad (2.7)$$

where $\frac{d\vec{V}}{dt}=\frac{\partial\vec{V}}{\partial t}+u\frac{\partial\vec{V}}{\partial x}+v\frac{\partial\vec{V}}{\partial y}+w\frac{\partial\vec{V}}{\partial z}$, $\vec{g}$ is the gravitational acceleration and p is the fluid pressure.

Again, the form of equation (2.7) can be modified depending the assumptions of the problem.

Inviscid or Frictionless Flow: Euler's Equation

The simplest assumption is the case of frictionless flow, where $\tau_{ij}=0$; equation (2.7) becomes:

$$\rho\vec{g} - \vec{\nabla}p = \rho\frac{d\vec{V}}{dt} \tag{2.8}$$

Newtonian or Viscous Fluid: Navier-Stokes Equations

For a Newtonian fluid, the viscous stresses are proportional to the element strain rates and the coefficient of viscosity; or $\tau = \mu\frac{d\theta}{dt} = \mu\frac{du}{dy}$. Apply this concept into a Newtonian fluid with constant density and viscosity, the three-dimensional differential momentum equation becomes

$$\begin{aligned}
\rho g_x - \frac{\partial p}{\partial x} + \mu\left(\frac{\partial^2 u}{\partial x^2} + \frac{\partial^2 u}{\partial y^2} + \frac{\partial^2 u}{\partial z^2}\right) &= \rho\frac{du}{dt} \\
\rho g_y - \frac{\partial p}{\partial y} + \mu\left(\frac{\partial^2 v}{\partial x^2} + \frac{\partial^2 v}{\partial y^2} + \frac{\partial^2 v}{\partial z^2}\right) &= \rho\frac{dv}{dt} \\
\rho g_z - \frac{\partial p}{\partial z} + \mu\left(\frac{\partial^2 w}{\partial x^2} + \frac{\partial^2 w}{\partial y^2} + \frac{\partial^2 w}{\partial z^2}\right) &= \rho\frac{dw}{dt}
\end{aligned} \tag{2.9}$$

Both basic governing equations, continuity and differential linear momentum, are valid for laminar and turbulent flows. For laminar flow problems, where there are no random fluctuations, equations (2.4) and (2.7) can be solved directly. Meanwhile, every fluid velocity and pressure term in the basic governing equations can vary randomly with time and space for turbulent flow. Special techniques are required to handle such instantaneous fluctuation in the variables that would occur in turbulent flow.

2.3 *COUPLING MECHANISMS BETWEEN DISCONTINUUM AND CONTINUUM*

The discrete element method was also developed to couple with other aspects of mechanics (i.e., solid, fluid, thermal and structural mechanics). Previous researches in the coupling approaches to simulate wet granular flow are reviewed here.

Thallak et al (1990) simulated the problem of hydraulic fracture in a granular assembly. In that work, granular particles were represented by contacting circular discs. The pores between the particles were connected together to form a channel network. To simulate the inter-pore flow, a geometrically-coupled channel network was created by assigning nodes to the pores, and the flow channels to the pore throats. The steady-state flow rate in channels was assumed to be linearly related to the pressure gradient according to the Hagen-Poiseuille equation. The aperture of a channel was proportional to the normal displacement at the associated contacts between particles. The pressure within pores could be built up and cause the contact between particles to break apart. This simulated the occurrence of hydraulic fracture in the granular assembly.

Babic′ and Shen (1990) applied a two-dimensional discrete element model to the problem of gravity-driven channel flow of uniform disks. The movement of the particles was modeled by the discrete element method. The fluid-solid interaction was included by considering the drag force between particles and the fluid. Therefore, particles were dragged along by the fluid flow. Sun and Vinogradov (1998) used the coupled approaches of DEM and potential flow theory to study the flow jam of solid particles transported by fluid in planar channels. Again, drag forces were incorporated in the simulation.

Chan (1993) described the method of incorporating fluid flow computation in discrete element modeling of wet granular deformation. Drag and buoyancy were included in the simulation as the fluid/particle interactions, while the technique of using different permeability was applied to represent the particle effect on the fluid flow calculation.

It could be noted that the coupling mechanisms were the major differences in the previous researches. Cundall (1999) classified the coupling mechanisms into five types of fluid/particle interactions. The categories, presented below, are based on solid density and the interacting effects between solid and fluid.

- *Uniform or hydrostatic pressure*

For the case in which particles are simply submerged in a fluid at rest under gravity, the buoyant (submerged) weight of each particle is used. This accounts for the effect of the hydrostatic gradient.

- *Low concentration of particles in fluid*

If particles move independently of each other (i.e., the particles are widely spaced) and they occupy a small fraction of the fluid volume, viscous ("Stokes") forces may be applied to each particle to represent the effects of the fluid. Such force vectors are functions of the relative velocity between the particle and the fluid.

- *Low concentration of fluid in the particle assembly*

When the total fluid volume is a small fraction of the total particle volume, the fluid probably exists at menisci, held by surface tension at contacts between particles. A special contact law can be used to capture the effects of the fluid. The law will have viscous and cohesive components, the latter being strongly dependent on the relative separation at the contact and the volume of fluid trapped.

- *Saturated particle assembly*

This category can be separated as two sub-cases regarding the size of pressure gradients within the assembly. One is the case of weak pressure gradients. This is when pressure fluctuations are small over distances equal to the mean particle radius. Thus a continuum flow calculation based on porosities and permeabilities averaged over the distances of several particle diameters can be used. Drag forces are applied to the particles, derived from calculated pressure gradients. In essence, the particle code feeds averaged permeabilities to the continuum code, which then feeds back mean flow-rate vectors, and hence particle body forces. This weakly coupled approach can capture mechanisms such as surface erosion, piping and channeling. Things are more complicated when dealing with the second sub-case of strong pressure gradients. The representative porosities and permeabilities over the concerned area could not be computed by the average technique. As well, these cause additional complexity in the calculation of the equivalent body forces. The scheme consists of a pipe/reservoir network, which is capable of reproducing quite complicated mechanisms, such as hydrofracturing and local erosion.

- *Strong pressure gradients and large deformations in the solid phase*

If the "solid" material breaks up and no longer retains a coherent structure, or if the void geometry changes dramatically, all of the schemes described before break down. An extreme example is that of "slurry flow" in which particles have similar velocity to the fluid: single particles or clumps of particles are, in essence, carried along by the fluid. Another, less extreme, example is that of an evolving, fluid-driven geological system, such as magma intrusion into brittle or ductile rock. In such cases it should be possible to reproduce the mechanisms by representing both fluid and solid as the particles.

CHAPTER 3 THE SIMULATION OF GRANULAR MATERIAL

This chapter contains the general idea and theoretical concepts for the simulation of granular material movement. There are three sections in this chapter. Section 1 gives the descriptions of the theoretical basis of the discrete element method. Both concepts and theoretical formulations are explained, including the theory and background information of the discrete element method, the calculation cycle, general descriptions of the boundary conditions, and the implementation scheme: contact detection algorithm. Section 2 describes computer codes that are used in the granular material simulation. Codes can be separated according to their functions into contact detection algorithm, contact force calculation, application of Newton's second law and graphic presentations. Section 3 discussed the limitations and shortcomings of the granular material simulation.

3.1 *THEORY AND BACKGROUND INFORMATION*

3.1.1 The Discrete Element Method

Soils are often considered as continuous media by many methods such as the finite difference method, the finite element method, etc. However, it is difficult to deal with the problem of large deformation, such as fracture and flow, using the continuum approach. Simulations involving large granular material moving in the fluid flow have utilized the discontinuum approach (Chan, 1993).

Discrete element method or DEM, which is based on discontinuum modeling, is a numerical procedure for simulating the mechanical behavior of a system of discrete,

interacting particles. DEM treats the granular material as an assembly of circular-shaped particles. Each particle will displace independently from one another and the particles in the interaction pair will interact with each other only at the contact point. This assumption can help to define the location of the resultant contact forces. The particles that comprise the granular assembly are assumed, here, to be rigid and behavior of the contacts is characterized using a soft contact approach. A finite normal stiffness is taken to represent the measurable normal stiffness that exists at a contact. At the contact point, each particle in the interaction pair is allowed to overlap with one another at a magnitude proportional to the contact force. The force-displacement law governs the relationship between the magnitude of the particle overlap and contact force. Then, all acting forces are summed for each individual granular particle, and each particle movement can be found. Newton's laws of motion provide the fundamental relationship between particle motion and forces causing that motion. Finally, mechanical behavior of the granular material is described in terms of the movement of each particle and inter-particle forces acting at each contact point (Cundall and Strack, 1979).

Four assumptions have been made so far:

1. Particles that comprise the granular assembly are assumed to be rigid.
2. Behavior of the contacts is characterized using a soft contact approach.
3. Contacts occur over a vanishingly small area (i.e., only at a point).
4. Magnitude of the particle overlap is related to the contact force, as described by the force-displacement relationship.

In addition, since the explicit numerical scheme will be used in the calculation cycle of the DEM, the chosen time-step needs to be small enough such that a single time-step disturbances cannot propagate from any particle further than its immediate neighbors. Otherwise the scheme is numerically unstable. The critical time-step of the discrete systems varies depending on the physical properties of the assembly, because the speed at which a disturbance can propagate is a function of the systematic physical properties of the material. More details are given later in the section for determining the critical time-step.

3.1.2 Calculation Cycle

Calculation cycle performed in the discrete element method alternates between the application of Newton's second law to particles, and a force-displacement law at the contacts (PFC2D manual, 1999). Newton's second law of motion gives the movement of a particle resulting from the action forces and moments, while the force-displacement law is used to find the contact forces that are induced by the relative motion between the contact particles.

At the starting point of each time-step, positions of all particles are known. The program will detect and update the set of contacts from the particle positions. The force-displacement law is then applied to each contact for the calculation of contact forces based on the magnitude of the particle overlap. Next, the law of motion is employed to update the particle velocities and position. The calculation cycle based on these two physical governing laws is shown in Figure 3.1. This allows the DEM to track the movement history of each individual particle in the granular assembly.

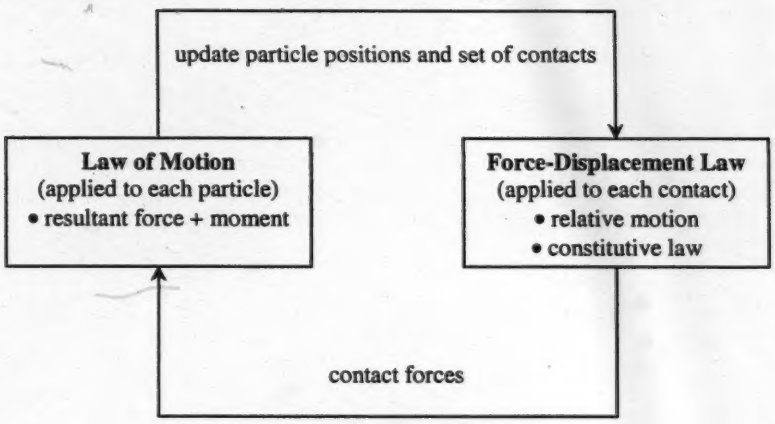

Figure 3.1 Calculation cycle in DEM

3.1.2.1 Force-Displacement Law[1]

The force-displacement law relates the relative displacement between contact particles to the contact force. Contact force is divided into two components: a normal component acting normal to the contact surface and a shear component acting in the tangential direction. Figure 3.2 illustrates the case of two particles (A and B) being in contact. The coordinates of the centers of particles A and B according to a Cartesian coordinate system are (x_{A1}, x_{A2}) and (x_{B1}, x_{B2}), respectively. The velocities of the particles are ($\dot{x}_{Z1}$, $\dot{x}_{Z2}$), which the subscript letter is used to designate the particle and the subscript number refers to the axis. The angular velocities are also presented in Figure 3.2 as $\dot{\theta}_A$ for particle A and $\dot{\theta}_B$ for particle B. Particles A and B have radii R_A and R_B and masses m_A and m_B respectively. Points P_A and P_B in Figure 3.2 are defined as the points of the intersection of the line connecting between two particle centers with the boundaries of particles A and B, respectively.

[1] All of the proofs in this section are referred to the work by Cundall and Strack (1979).

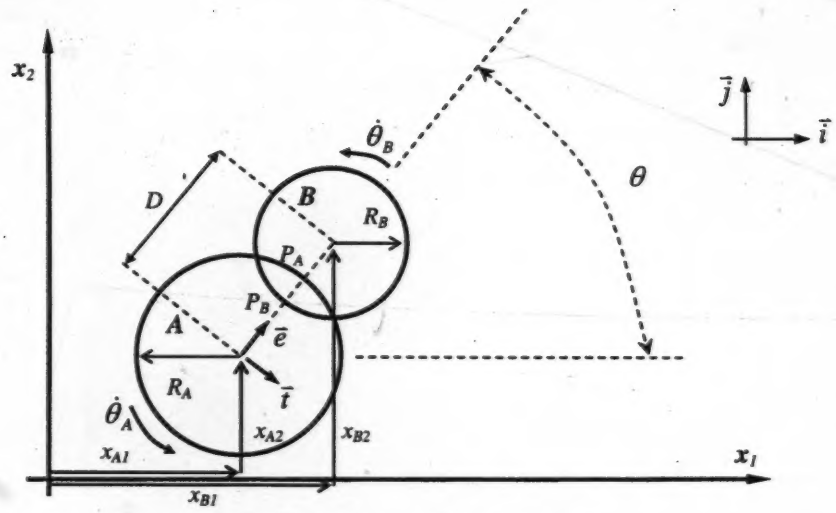

Figure 3.2 Two particles in contact

Two particles will be in contact, if the distance D between their centers is less than the summation of their radii; i.e. if

$$D < R_A + R_B \tag{3.1}$$

The unit vector $\vec{e} = (\cos\theta, \sin\theta)$ in Figure 3.2 points from the center of particle A to the center of particle B, i.e.

$$\vec{e} = \cos\theta\ \vec{i} + \sin\theta\ \vec{j} \tag{3.2}$$

$$= e_1\vec{i} + e_2\vec{j}$$

where $e_1 = \cos\theta$, and $e_2 = \sin\theta$.

And the unit vector $\vec{t}$ is obtained by a clockwise rotation of $\vec{e}$ through 90°, i.e.

$$\vec{t} = \sin\theta\ \vec{i} - \cos\theta\ \vec{j} \tag{3.3}$$

$$= e_2\vec{i} - e_1\vec{j}$$

If the coordinate of point P_A is given by

$$x_{PAi} = x_{Ai} + R_A e_i \tag{3.4}$$

The velocity of point P_A will be:

$$\dot{x}_{PAi} = \dot{x}_{Ai} + R_A \dot{e}_i \tag{3.5}$$

$$= \dot{x}_{Ai} - R_A \dot{\theta}_A t_i$$

Similarly, velocity of point P_B will be given by the same expression except that the angle θ in the equation (3.5) is replaced by $180+\theta$.

$$\dot{x}_{PBi} = \dot{x}_{Bi} + R_B \dot{\theta}_B t_i \tag{3.6}$$

The relative velocity of point P_A with respect to point P_B may be expressed as:

$$\dot{X}_i = \dot{x}_{PAi} - \dot{x}_{PBi}$$

$$= (\dot{x}_{Ai} - \dot{x}_{Bi}) - (R_A \dot{\theta}_A + R_B \dot{\theta}_B) t_i \tag{3.7}$$

Normal ($\dot{n}$) and tangential ($\dot{s}$) components of the relative velocities are the projections of $\dot{X}_i$ onto $\vec{e}$ and $\vec{t}$ respectively:

$$\dot{n}_i = (\dot{x}_{Ai} - \dot{x}_{Bi}) e_i \tag{3.8}$$

and

$$\dot{s}_i = (\dot{x}_{Ai} - \dot{x}_{Bi}) t_i - (R_A \dot{\theta}_A + R_B \dot{\theta}_B) \tag{3.9}$$

To give the components Δn and Δs of the relative displacement increment, the relative velocity components are integrated with respect to time:

$$\Delta n = (\dot{n}_i) \Delta t = \{(\dot{x}_{Ai} - \dot{x}_{Bi}) e_i\} \Delta t \tag{3.10}$$

and

$$\Delta s = (\dot{s}_i) \Delta t = \{(\dot{x}_{Ai} - \dot{x}_{Bi}) t_i - (R_A \dot{\theta}_A + R_B \dot{\theta}_B)\} \Delta t \tag{3.11}$$

These increments of the relative displacements are used with the force-displacement law to calculate the increments of the normal and shear forces, ΔF_n and ΔF_s.

$$\Delta F_n = k_n \Delta n = k_n \{(\dot{x}_{Ai} - \dot{x}_{Bi}) e_i\} \Delta t \tag{3.12}$$

and

$$\Delta F_s = k_s \Delta s = k_s \{(\dot{x}_{Ai} - \dot{x}_{Bi}) t_i - (R_A \dot{\theta}_A + R_B \dot{\theta}_B)\} \Delta t \tag{3.13}$$

where k_n and k_s represent the normal and shear stiffnesses, respectively.

Finally, at each time-step the force increments ΔF_n and ΔF_s are added into the summation of all force increments, F_n and F_s, determined for previous time-steps:

$$(F_n)_N = (F_n)_{N-1} + \Delta F_n \; ; \; (F_s)_N = (F_s)_{N-1} + \Delta F_s \tag{3.14}$$

where the indices N and N-1 refer to times t_N and t_{N-1} such that $t_N - t_{N-1} = \Delta t$. Sign convention for the normal and shear forces acting on a particle is indicated in Figure 3.3. F_n and F_s are taken as positive in the directions opposite to $\vec{e}$ and $\vec{t}$.

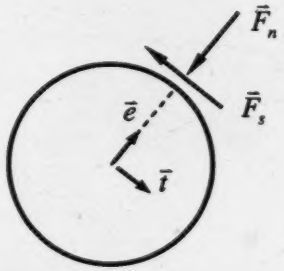

Figure 3.3 Sign convention for F_n and F_s

A Coulomb friction law is incorporated as follows. The magnitude of the shear force F_s found from the equation (3.14) is checked against the maximum possible value $(F_s)_{max}$ defined as:

$$(F_s)_{max} = F_n \tan\phi + c \tag{3.15}$$

where ϕ is the inter-particle friction angles and c is the cohesion. If the absolute value of $(F_s)_N$ of equation (3.14) is larger than $(F_s)_{max}$, the magnitude of $(F_s)_N$ is set equal to $(F_s)_{max}$, preserving the sign obtained from equation (3.14).

Once the normal and shear forces have been determined for each contact of a particle, they are resolved into 2 components according to the directions in the Cartesian coordinate system. Summation of all force components acting at the particle gives the resultant forces ΣF_{Zi}. Resultant moment on a particle, ΣM_Z, is positive if acting in the counter-clockwise direction, and is determined from $\Sigma M_Z = \Sigma F_s R_Z$ where the summation is taken over all forces acting on particle Z in the tangential direction.

The resultant forces and moments acting on the granular particle are used with Newton's second law of motion to determine the movement of the particle.

3.1.2.2 Law of Motion[2]

The motion of a single rigid particle, determined by the resultant forces and moments acting upon, can be described in terms of the translational motion of a point in the particle and the rotational motion of the particle. Translational motion of the particle mass center includes the particle position x_i, velocity $\dot{x}_i$, and acceleration $\ddot{x}_i$, while the rotational motion of the particle includes the angular velocity $\dot{\theta}_Z$ and angular acceleration $\ddot{\theta}_Z$. Newton's second law is applied to the particle as:

$$m_Z \ddot{x}_{zi} = \Sigma F_{Z\,i} \qquad (3.16)$$

[2] All of the proofs in this section are referred to the work by Cundall and Strack (1979).

and $$I_Z \ddot{\theta}_Z = \Sigma M_Z \tag{3.17}$$

where m_Z and I_Z represent the mass and moment of inertia of particle Z.

Assume that the time interval Δt is so small that the translational and angular acceleration, $\ddot{x}_i$ and $\ddot{\theta}_Z$, are constant over the interval. Equations (3.16) and (3.17) lead to the following expressions for the translational and angular velocities at the next time-step:

$$(\dot{x}_{zi})_{N+1} = (\dot{x}_{zi})_N + (\Sigma F_{zi}/m_Z)_N \Delta t \tag{3.18}$$

and $$(\dot{\theta}_Z)_{N+1} = (\dot{\theta}_Z)_N + (\Sigma M_Z / I_Z)_N \Delta t \tag{3.19}$$

where ΣF_{zi} is the term for the summation of all forces acting on the particle Z, including contact forces, as well as other forces such as body forces, drag forces and buoyant forces.

Finally, the new values for velocities are used to update the positions and rotations of the particles by a further numerical integration.

$$(x_{zi})_{N+1} = (x_{zi})_N + (\dot{x}_{zi})_N \Delta t \tag{3.20}$$

and $$(\theta_Z)_{N+1} = (\theta_Z)_N + (\dot{\theta}_Z)_N \Delta t \tag{3.21}$$

3.1.3 Damping

The contact model between particles both in normal and tangential direction may be conceived as a spring and a dashpot (see in Figure 3.4). The spring in the model is taken into account as the stiffness in the force-displacement law, while the dashpot is set

to provide some sort of damping for dissipating the system energy. The use of damping other than by friction alone is necessary in order that the assemblies reach a state of equilibrium for all conditions.

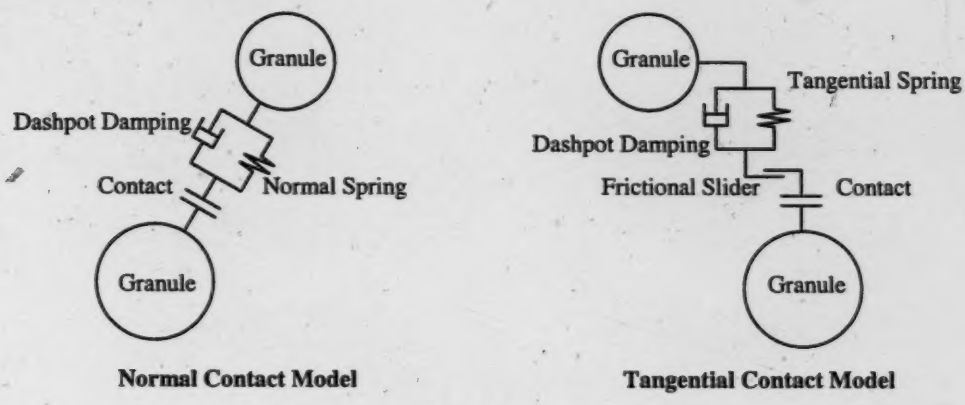

Figure 3.4 Spring and dashpot model

Damping forces are calculated based on the relative velocities at the contact. Formulations to calculate the damping forces are separated into two components:

Normal damping:

$$D_n = c_n \dot{n} \tag{3.22}$$
$$= c_n (\dot{x}_{Ai} - \dot{x}_{Bi}) e_i$$

Shear damping:

$$D_s = c_s \dot{s} \tag{3.23}$$
$$= c_s \{ (\dot{x}_{Ai} - \dot{x}_{Bi}) t_i - (R_A \dot{\theta}_A + R_B \dot{\theta}_B) \}$$

where c_n is the damping coefficient in the normal direction and c_s is the damping coefficient in the tangential direction. Note that if the shear force is greater than the maximum possible shear force, there will be no shear damping applied.

Damping forces D_n and D_s, found from the equations (3.22) and (3.23), are included in the total forces acting on a particle. It is assumed that the damping coefficients in the normal and tangential directions are taken to be proportional to the normal and shear stiffnesses k_n and k_s, respectively, with proportionality constant β (in this simulation, 0.01). Damping coefficients are (Cundall and Strack, 1979):

$$c_n = \beta k_n ; \; c_s = \beta k_s \tag{3.24}$$

3.1.4 Boundary Conditions

In general, a particle can move freely according to the resultant forces and governed by Newton's second law of motion, with the exception of the case when the particle moves and faces the boundary condition. Boundary conditions in this simulation refer to the boundaries of the flow field such as the sidewalls, or the bottom line of the flow field. Interaction of boundaries to a particle is similar to the interaction of particles in contact with each other. Therefore, granular particles will not be able to move across those boundaries. However, the particle can move along the boundaries, resulting in energy loss in the granular system due to the friction between the particle and the boundary. A particle will slip along the boundary, if the tangential force acting on the particle is greater than the maximum possible value of the shear force.

3.1.5 Critical Time-Step Determination in Granular Simulation

As a consequence of the explicit numerical scheme employed in the discrete element method, a time-step must be selected which is small enough that the numerical

simulation is stable or, during a single time-step, disturbances cannot propagate from any particle further than its immediate neighbors. This is the major disadvantage of the explicit numerical scheme. The scheme is conditionally stable. In the work by Thallak et al. (1990), the value of a critical time-step Δt_c is estimated by the natural period of a one-dimensional mass-spring system; i.e., from a single degree-of-freedom mass spring model with the lowest mass and the highest stiffness in the simulation, according to:

$$\Delta t_c = 2\sqrt{\frac{m_{\min}}{K_n}} \tag{3.25}$$

where $m_{\min}$ represents the mass of the smallest particle in the assembly and K_n the highest normal contact stiffness.

3.1.6 Contact Detection

From the positions of all particles in the assembly, the program must identify all pairs of particles that are in contact before calculating the contact forces. The position of one particle is checked against the position of every other particles to determine if contact will occur. Since the circular-shaped particle is used in the simulation, it avoids the ambiguities that usually occur in contact detection for other particle shapes. For instance, if the polygonal-shaped particles are used, it is necessary to determine whether the contact is an edge-edge type contact, edge-corner type contact or corner-corner type contact. But for the circular-shaped particle, the program needs only to compare the distance between the particles with the sum of the radii (see equation 3.1).

This approach is acceptable when the number of particles is not too high. The computation time of this approach will be proportional to the square of the particle

number in the assembly or n^2, where n is the total number of particles within the granular assembly.

3.2 *EXPLANATION OF COMPUTER CODES*

Discrete element method programs generally do three major tasks. The first task is to determine particle contacts. The other two tasks are to perform the calculation cycle based on the application of two basic governing equations: the force-displacement law to each contact and Newton's second law to particles. After these calculations, the information (including location, displacement, velocities, etc.) for each particle is revised and the computer can display graphical results.

3.2.1 Contact Detection Scheme

From the positions of all particles, the program must have the contact detection scheme to detect and update all contacts that can possibly occur in the granular assembly. The algorithm for contact detection incorporated into this simulation is very simple. Contact or no contact between any pair of particles is dependent on the distance between the particles, and the summation of their radii. The first thing for the program to do is to update contacts that are already in the contact list from the previous time-step. If the contact does not occur at the current time-step, the program will simply delete the contact information from the contact list. Then, the program will detect the new contact that can initially occur at the current time-step. The position of one particle is checked against the position of every other particle in the assembly. If the program finds that there is a

contact and it is not in the contact list yet, the program will create the new record for this new contact. The contact information is stored to be used later. Flow charts for these are shown in the Figures 3.5 and 3.6.

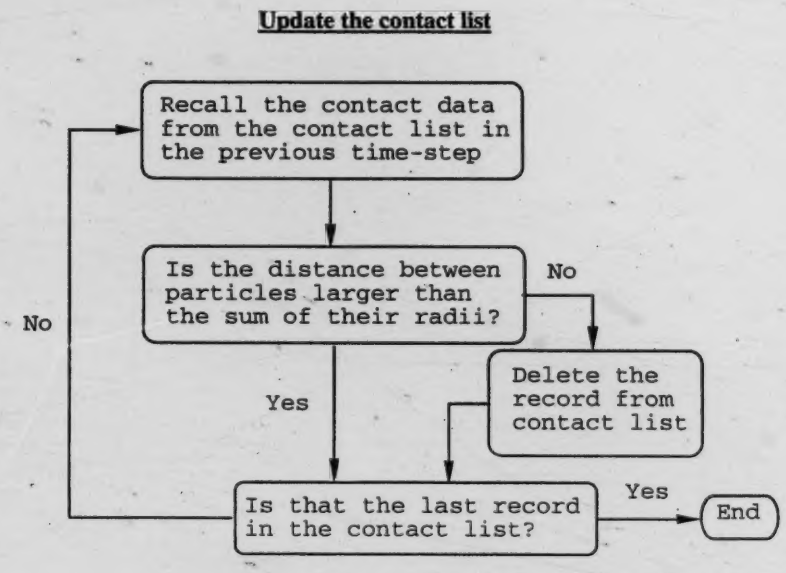
Update the contact list
Recall the contact data from the contact list in the previous time-step
Is the distance between particles larger than the sum of their radii?
No
No
Yes
Delete the record from contact list
Is that the last record in the contact list?
Yes
End

Figure 3.5 Flow chart of updating the contact list

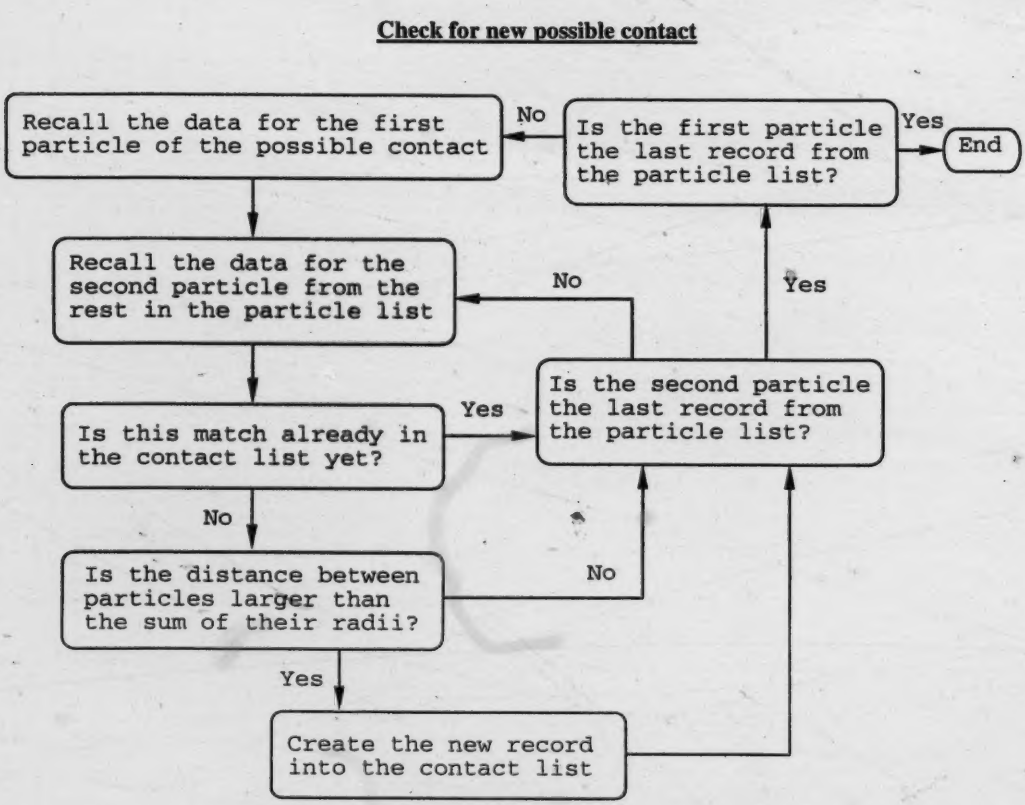
Check for new possible contact
Recall the data for the first particle of the possible contact
No
Is the first particle the last record from the particle list?
Yes
End
Recall the data for the second particle from the rest in the particle list
No
Yes
Is this match already in the contact list yet?
Yes
Is the second particle the last record from the particle list?
No
Is the distance between particles larger than the sum of their radii?
No
Yes
Create the new record into the contact list

Figure 3.6 Flow chart of detecting the new possible contact

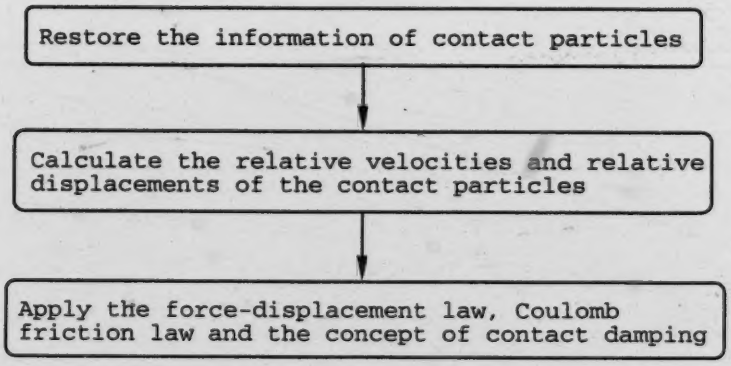
Restore the information of contact particles
Calculate the relative velocities and relative displacements of the contact particles
Apply the force-displacement law, Coulomb friction law and the concept of contact damping

Figure 3.7 Flow chart of calculating the contact force

3.2.2 Calculation for Contact Force

A flow chart to calculate the contact forces is shown in Figure 3.7. After the program has updated the contact list, it can calculate the contact force. The force-displacement law is applied to each contact including contact damping and the Coulomb frictional law.

3.2.4 Calculation by the Law of Motion

All resultant forces and moments acting on the particle are summed, and then the movement of the particle can be found by the application of Newton's second law of motion. Figure 3.8 shows the flow chart of applying the law of motion. Acceleration, velocity, and position of all particles are initially computed by the law of motion, as well as angular acceleration, and angular velocity. However, if the particle is in contact with the boundary, the friction force will be considered. This friction will be acting against the motion of the particle, changing its velocity. Again, Coulomb frictional law is used to calculate the friction force on the boundary. If the tangential force acting on the particle is greater than the maximum possible value of shear force, then the particle will slip along the boundary under a slip condition.

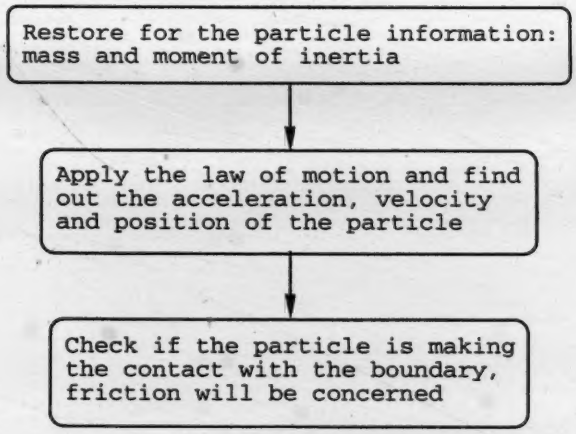
Restore for the particle information: mass and moment of inertia
Apply the law of motion and find out the acceleration, velocity and position of the particle
Check if the particle is making the contact with the boundary, friction will be concerned

Figure 3.8 Flow chart of applying the law of motion

3.2.5 Creation of Graphical Result

At the end of every calculation cycle, the discrete element method will give the solution in terms of the movement of the granular particles and the inter-particle forces acting at the contacts. The main focus of this simulation is the movement of the granular particles in fluid flow. Each particle in the assembly is located by the position of its center. Based on this information, the program can plot each particle as the circular-shaped object in the fluid flow and show it on the monitor. The special function from the OpenGL library is encoded into the simulation program helping the program to create the part of graphical display. OpenGL is a software interface for graphics hardware. This interface consists of hundreds of distinct commands, which can help the software developer to specify the objects and operations needed to produce interactive three-dimensional applications as well as graphical display. Complete information about OpenGL can be found at the website "www.opengl.org".

3.3 *LIMITATIONS AND SHORTCOMINGS OF GRANULAR SIMULATION*

3.3.1 Size of the Time-Step

As a result of the explicit numerical scheme employed in the discrete element method, the simulation will be stable if the time-step Δt is taken as a fraction or less than one of the critical time-step. The critical time-step is estimated on the basis of a single degree-of-freedom system of a mass m connected to the ground by a spring with stiffness k. The critical time-step for this case is equal to $2\sqrt{(m/k)}$. Therefore, the critical time-step is a function of the physical properties of the discrete system as described earlier. By the nature of the explicit numerical scheme, the concept is very simple but it suffers from the limitations that the time-step must be small. Therefore, a simulation will require a higher number of computation steps than the implicit scheme.

3.3.2 Search Time in the Contact Detection Algorithm

Although the approach of the contact detection used in this simulation is very simple and does not need a highly sophisticated organization of the data structure, it requires a large amount of searching time especially when the number of particles reaches several hundreds. Therefore, to maintain the computational time in a reasonable range, the number of particles in the simulation is limited.

In recent research, there are a number of developments in the contact detection algorithm. By using good organization of data structure and very keen approach, the overall search time can be improved. An example for reducing search time is to do one

exhaustive search at the start of the simulation, and then maintain a list of neighbors for each body. Subsequent searches will be restricted to the local area around each body instead of searching over the entire domain, so that search time will be proportional to the number of particles in the assembly (or n). Complete details can be found in the work by Munjiza and Andrews (1998), as well as, by Perkins and Williams (2001).

3.3.3 Material Calibration

Discrete element method describes the overall macro-mechanical material behavior in terms of the micromechanisms. The input properties of the DEM model are in the microscopic level, and are not usually known. In order to reproduce a material that behaves in the same way as the intended macro responses, the micro properties must be selected appropriately. Since there is no direct formulation that relates the micro parameters with the macro-responses, a calibration process to match the micro-scale properties with the relevant macro-responses may be required. In addition, it should be realized that the term "particle" used in the discrete element method differs from its more general definition. By the common sense in the field of mechanics, the term "particle" means to a body whose dimensions are negligible and thus occupies only a single point in space. In the DEM, the term "particle" denotes a body that occupies a finite volume of space. Thus, particle size does not correspond directly with the actual grain size of the granular material. Size of the particles must be chosen such that it is smaller than the smallest interesting features in the simulation. Therefore particles can be viewed as a collection of grains, especially when the grains of the material are very small, such as silt

and fine sands. Consequently, other causes related to the particle size such as particle shape, fabric and packing arrangement can also affect the behavior of the DEM model.

CHAPTER 4 THE SIMULATION OF FLUID FLOW

This chapter presents the ideas and theoretical concepts regarding the simulation of fluid flow. There are five sections in this chapter. Section 1 describes the theoretical formulations for modeling fluid flow. The derivations of the basic governing equations of fluid flow, both continuity equation and Navier-Stokes equations, are given here. In Section 2, the modeling methodology for fluid flow simulation is explained. The general concepts of the finite volume scheme, boundary conditions, solution algorithm and the determination of critical time-step size are also described in this section. Section 3 provides an explanation of the computer codes that are used in the simulation of fluid flow. The codes are structured depending on their functions related to the discretization of the flow field, calculation of fluid flow following the Navier-Stokes equation, adjustment of the first calculated variables based on the continuity equation and creation of the graphical results. The limitations and shortcomings of the simulation method are discussed in Section 4. Finally, in Section 5 a verification problem is provided. The numerical results of the simulation are compared with closed-form solutions.

4.1 *GENERAL FORMULATION*[1]

4.1.1 Differential Equation of Mass Conservation

[1] The derivation of these basic governing equations can be found in the general textbook of fluid mechanics. The author refers to two textbooks: Fluid Mechanics by White (1999) and Fundamentals of Fluid Mechanics by Gerhart et al. (1992).

Consider a system, which is defined as a fixed quantity of mass, denoted by m. An infinitesimal fixed control volume (dx, dy, dz), shown in Figure 4.1, is selected to represent this system.

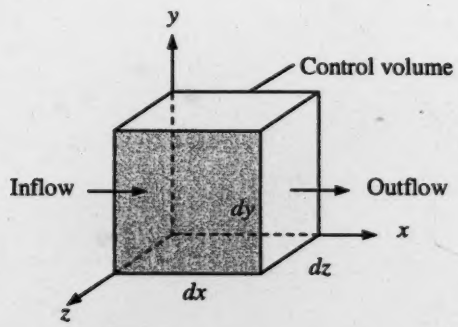

Figure 4.1 Elemental Cartesian fixed control volume showing the inlet and outlet mass flows on the x faces

Assuming the mass of the system is conserved and does not change, it can be expressed mathematically as:

$$m_{syst} = \text{const}$$

or

$$\frac{dm}{dt} = 0 \tag{4.1}$$

In mechanics, it is called *the conservation of mass*:

Thus,

$$\int_{CV} \frac{\partial \rho}{\partial t} d(Volume) + \sum_i (\rho_i A_i V_i)_{out} - \sum_i (\rho_i A_i V_i)_{in} = 0 \tag{4.2}$$

where ρ_i, A_i and V_i denote the density, area and velocity of the elemental control volume and i denotes the direction according to the Cartesian coordinate system. Note that the term velocity refers to the fluid velocity and not the solid velocity in this chapter.

The element is so small that the volume integral simply reduces to a differential term:

$$\int_{cv} \frac{\partial \rho}{\partial t} d(Volume) \approx \frac{\partial \rho}{\partial t} dxdydz$$

and the mass-flow terms occur on all six faces, three inflows and three outflows. The inflow and outflow terms on the x-face can be written as:

Inflow: $$\sum_i (\rho_i A_i V_i)_{in} = \rho u dydz \qquad (i = 1)$$

Outflow: $$\sum_i (\rho_i A_i V_i)_{out} = \left[\rho u + \frac{\partial}{\partial x}(\rho u)dx \right] dydz \qquad (i = 1)$$

Similarly, the inflow and outflow terms are expanded on the y- and z-faces. Substitute all of the expanded terms into equation (4.2):

$$\frac{\partial \rho}{\partial t} dxdydz + \frac{\partial}{\partial x}(\rho u)dxdydz + \frac{\partial}{\partial y}(\rho v)dxdydz + \frac{\partial}{\partial z}(\rho w)dxdydz = 0$$

Eliminating the element volume from all terms, leaving a partial differential equation involving the derivatives of the density and velocity:

$$\frac{\partial \rho}{\partial t} + \frac{\partial}{\partial x}(\rho u) + \frac{\partial}{\partial y}(\rho v) + \frac{\partial}{\partial z}(\rho w) = 0 \qquad (4.3)$$

Equation (4.3) is called the continuity equation for an infinitesimal volume in a continuum. If incompressible flow is assumed, therefore, density changes are assumed to be negligible, equation (4.3) becomes:

$$\frac{\partial u}{\partial x} + \frac{\partial v}{\partial y} + \frac{\partial w}{\partial z} = 0 \qquad (4.4)$$

where u, v and w are the velocities in x-, y- and z-directions respectively.

4.1.2 Differential Equation of Linear Momentum

Considering the same elemental control volume in Figure 4.1, Newton's second law of motion is applied to the elemental control volume:

$$\sum \vec{F} = m_{syst}\vec{a} \tag{4.5}$$

The mass of the elemental control volume is equal to:

$$m_{syst} = \rho d(Volume) = \rho(dxdydz)$$

and the acceleration of a fluid is equal to:

$$\vec{a} = \frac{d\vec{V}}{dt} = \frac{\partial \vec{V}}{\partial t} + \left(u\frac{\partial \vec{V}}{\partial x} + v\frac{\partial \vec{V}}{\partial y} + w\frac{\partial \vec{V}}{\partial z} \right)$$

Therefore, equation (4.5) becomes:

$$\sum \vec{F} = \rho \frac{d\vec{V}}{dt}(dxdydz) = \rho\left[\frac{\partial \vec{V}}{\partial t} + u\frac{\partial \vec{V}}{\partial x} + v\frac{\partial \vec{V}}{\partial y} + w\frac{\partial \vec{V}}{\partial z} \right](dxdydz) \tag{4.6}$$

The forces acting on the elemental volume are of two types, *body* forces and *surface* forces. Body forces are due to external fields (gravity, magnetism, electric potential) that act upon the entire mass within the element. In this case the only body force is gravity. Gravity force on the differential mass $\rho dxdydz$ within the control volume is:

$$d\vec{F}_{grav} = \rho\vec{g}dxdydz \tag{4.7}$$

where $\vec{g}$ is the gravitational attraction and may have an arbitrary orientation with respect to the coordinate system.

The surface forces are due to the stresses on the sides of the control surface. These stresses are the sum of hydrostatic pressure plus viscous stresses σ_{ij} which arise from motion with velocity gradients. The subscript notation for stresses is given in Figure 4.2.

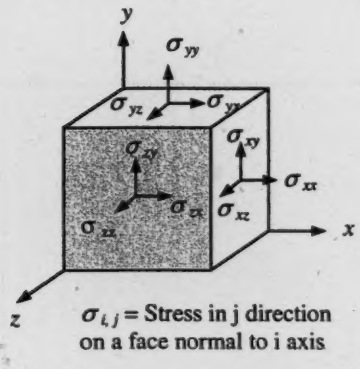

Figure 4.2 Notation for stresses

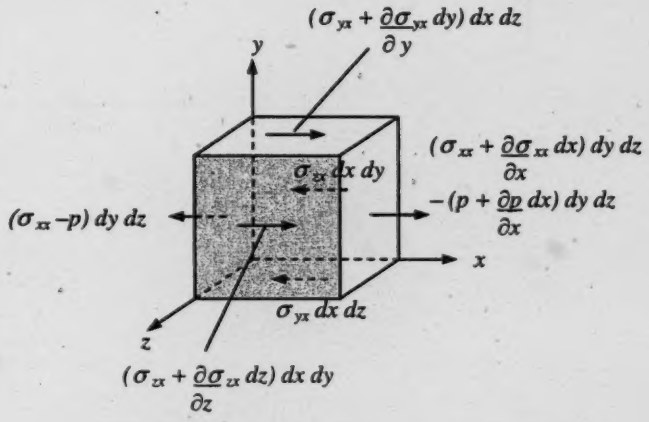
$(\sigma_{yx} + \frac{\partial \sigma_{yx}}{\partial y} dy)\, dx\, dz$
$(\sigma_{xx} + \frac{\partial \sigma_{xx}}{\partial x} dx)\, dy\, dz$
$-(p + \frac{\partial p}{\partial x} dx)\, dy\, dz$
$(\sigma_{xx} - p)\, dy\, dz$
$\sigma_{yx}\, dx\, dz$
$(\sigma_{zx} + \frac{\partial \sigma_{zx}}{\partial z} dz)\, dx\, dy$
x
y
z

Figure 4.3 Elemental Cartesian fixed control volume showing the surface forces in the x direction only

In Figure 4.3, the stress gradients or stress differences (shown only in x-direction) cause a net force on the surface. For example, the force acting in the left direction $\sigma_{xx}\, dy\, dz$ on the left face is balanced by the force acting in the right direction $\sigma_{xx}\, dy\, dz$ on the right face, leaving only the net rightward force $(\partial \sigma_{xx}/\partial x)\, dy\, dz$ on the right face. The same applies on the other four faces so that the net surface force in the x direction, including the pressure difference, is given by:

$$dF_{x,surf} = \left[-\frac{\partial p}{\partial x} + \frac{\partial}{\partial x}(\sigma_{xx}) + \frac{\partial}{\partial y}(\sigma_{yx}) + \frac{\partial}{\partial z}(\sigma_{zx}) \right] dxdydz;$$

Similarly for the net surface force in the y- and z-directions:

$$dF_{y,surf} = \left[-\frac{\partial p}{\partial y} + \frac{\partial}{\partial x}(\sigma_{yy}) + \frac{\partial}{\partial y}(\sigma_{xy}) + \frac{\partial}{\partial z}(\sigma_{zy}) \right] dxdydz;$$

$$dF_{z,surf} = \left[-\frac{\partial p}{\partial z} + \frac{\partial}{\partial x}(\sigma_{zz}) + \frac{\partial}{\partial y}(\sigma_{xz}) + \frac{\partial}{\partial z}(\sigma_{yz}) \right] dxdydz.$$

The total surface force is thus equal to the summation of the pressure-gradient vector and the divergence of the viscous-stress tensor.

$$d\vec{F}_{surf} = -\vec{\nabla} \cdot p + \vec{\nabla} \cdot \vec{\sigma}_{ij} \tag{4.8}$$

Substituting equations (4.7) and (4.8) into equation (4.6) and eliminating the element volume terms, *dx dy dz*, leads to:

$$\rho\vec{g} - \vec{\nabla}p + \vec{\nabla} \cdot \sigma_{ij} = \rho \frac{d\vec{V}}{dt} \tag{4.9}$$

where $\frac{d\vec{V}}{dt} = \frac{\partial \vec{V}}{\partial t} + \left(u\frac{\partial \vec{V}}{\partial x} + v\frac{\partial \vec{V}}{\partial y} + w\frac{\partial \vec{V}}{\partial z} \right)$.

Equation (4.9) can be written in terms of *x*-, *y*- and *z*- coordinates as follows:

$$\rho g_x - \frac{\partial p}{\partial x} + \frac{\partial \sigma_{xx}}{\partial x} + \frac{\partial \sigma_{yx}}{\partial y} + \frac{\partial \sigma_{zx}}{\partial z} = \rho\left(\frac{\partial u}{\partial t} + u\frac{\partial u}{\partial x} + v\frac{\partial u}{\partial y} + w\frac{\partial u}{\partial z} \right);$$

$$\rho g_y - \frac{\partial p}{\partial y} + \frac{\partial \sigma_{xy}}{\partial x} + \frac{\partial \sigma_{yy}}{\partial y} + \frac{\partial \sigma_{zy}}{\partial z} = \rho\left(\frac{\partial v}{\partial t} + u\frac{\partial v}{\partial x} + v\frac{\partial v}{\partial y} + w\frac{\partial v}{\partial z} \right); \tag{4.10}$$

$$\rho g_z - \frac{\partial p}{\partial z} + \frac{\partial \sigma_{xz}}{\partial x} + \frac{\partial \sigma_{yz}}{\partial y} + \frac{\partial \sigma_{zz}}{\partial z} = \rho\left(\frac{\partial w}{\partial t} + u\frac{\partial w}{\partial x} + v\frac{\partial w}{\partial y} + w\frac{\partial w}{\partial z} \right).$$

This is the linear momentum equation in differential form, which is valid for any fluid in any general motion, particularly fluids being characterized by the viscous-stress terms.

4.1.3 The Navier-Stokes Equations

Stress in fluid is related to the strain rate. The simplest possible model of this relationship is in a linear form. A fluid that follows this simple relationship is referred to

as a Newtonian fluid. The fluid property that is used to relate stress and strain rate is the viscosity of the fluid. For incompressible flow, the relationship of the stress and strain rate is given in equation (4.11).

$$\sigma_{xx} = 2\mu\frac{\partial u}{\partial x},\ \sigma_{yy} = 2\mu\frac{\partial v}{\partial y},\ \sigma_{zz} = 2\mu\frac{\partial w}{\partial z} \tag{4.11}$$

$$\sigma_{xy} = \sigma_{yx} = \mu\left(\frac{\partial u}{\partial y} + \frac{\partial v}{\partial x}\right),\ \sigma_{xz} = \sigma_{zx} = \mu\left(\frac{\partial w}{\partial x} + \frac{\partial u}{\partial z}\right),\ \sigma_{yz} = \sigma_{zy} = \mu\left(\frac{\partial v}{\partial z} + \frac{\partial w}{\partial y}\right)$$

where μ is the viscosity coefficient.

Substitute equation (4.11) into equation (4.10), assuming constant viscosity, gives the differential linear momentum equation for a Newtonian fluid with constant density and viscosity:

$$\begin{aligned}
\rho g_x - \frac{\partial p}{\partial x} + \mu\left(\frac{\partial^2 u}{\partial x^2} + \frac{\partial^2 u}{\partial y^2} + \frac{\partial^2 u}{\partial z^2}\right) &= \rho\frac{du}{dt};\\
\rho g_y - \frac{\partial p}{\partial y} + \mu\left(\frac{\partial^2 v}{\partial x^2} + \frac{\partial^2 v}{\partial y^2} + \frac{\partial^2 v}{\partial z^2}\right) &= \rho\frac{dv}{dt};\\
\rho g_z - \frac{\partial p}{\partial z} + \mu\left(\frac{\partial^2 w}{\partial x^2} + \frac{\partial^2 w}{\partial y^2} + \frac{\partial^2 w}{\partial z^2}\right) &= \rho\frac{dw}{dt}.
\end{aligned} \tag{4.12}$$

Equation (4.12) is known as the *Navier-Stokes* equation. There are four unknowns in the equation: p, u, v and w, or fluid pressure and flow velocities, respectively. To solve the problem of a viscous, incompressible fluid in motion, equation (4.4) or the continuity equation must be taken into account. A more detailed explanation is provided in the following section.

4.2 *MODELLING METHODOLOGY*[2]

4.2.1 General

Up to this point, the Navier-Stokes equations and the continuity equation were used to describe the motion of the viscous, incompressible fluid. In the long history of fluid mechanics, a variety of computational fluid dynamics (CFD) methods have been developed. The first step in most CFD methods is to divide the flow field into a finite number of subregions. The continuity and momentum principles are then applied to all subregions within the flow domain. A solution is found when the primary variables (flow velocities and fluid pressure) are all computed. Despite the fact that the solution procedure is for unsteady problems, a steady solution can be obtained by tracing the solution development over a time period long enough for all the primary variables to become constant with time. Similarly to the flow field being divided into a number of subregions, the time domain can be divided into a number of small time steps.

4.2.2 Finite Volume Formulation

In the fluid flow simulation, the following assumptions are made:

1. The flow is laminar.
2. Two dimensional flow.
3. The density and viscosity of the fluid are constant.

[2] This section is referred to "Fundamentals of Fluid Mechanics" by Gerhart et al. (1992).

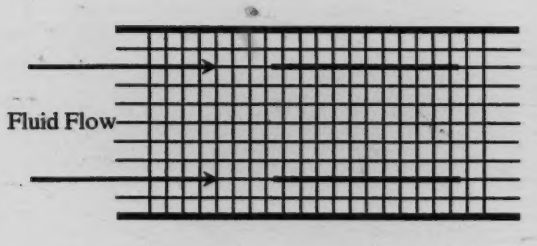

Figure 4.4 Discretized flow field

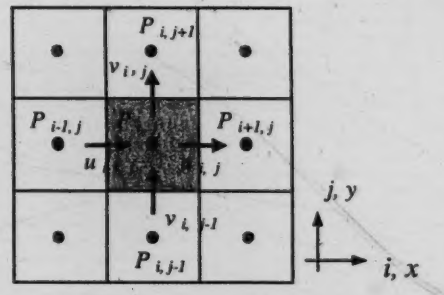

Figure 4.5 Staggered-grid notation (shaded cell represents cell *i, j*)

Figure 4.4 illustrates part of the flow field being discretized into a uniform mesh of finite volumes called *cells*. Figure 4.5 displays the notation used to develop the modeling equations, with positive flows moving to the right and up. The fluid pressure is defined at the center of the cell (black dots in Figure 4.5) and flow velocities are defined at the face (shown by the arrows). Computing every flow velocity and fluid pressure in the mesh yields an approximate solution to the problem.

The continuity equation (equation 4.4) applied to a control volume corresponding to a computational cell in Figure 4.5, can be expressed as

$$\frac{\partial u}{\partial x}+\frac{\partial v}{\partial y}=0$$

or

$$\frac{u_{i,j}-u_{i-1,j}}{\Delta x}+\frac{v_{i,j}-v_{i,j-1}}{\Delta y}=0 \qquad (4.13)$$

Also the momentum principle is applied to a control volume corresponding to a computational cell in Figure 4.5. The equations can be expressed solely in terms of variables evaluated at the location where they are defined in the staggered-grid convention.

From equation (4.12):

$$\rho g_x - \frac{\partial p}{\partial x} + \mu\left(\frac{\partial^2 u}{\partial x^2} + \frac{\partial^2 u}{\partial y^2}\right) = \rho\left(\frac{\partial u}{\partial t} + u\frac{\partial u}{\partial x} + v\frac{\partial u}{\partial y}\right);$$

$$\rho g_y - \frac{\partial p}{\partial y} + \mu\left(\frac{\partial^2 v}{\partial x^2} + \frac{\partial^2 v}{\partial y^2}\right) = \rho\left(\frac{\partial v}{\partial t} + u\frac{\partial v}{\partial x} + v\frac{\partial v}{\partial y}\right).$$

Applying these equations in the finite volume grid and they become:

$$\rho g_x - \frac{p_{i+1,j} - p_{i,j}}{\Delta x} + \mu\left(\frac{u_{i+1,j} - 2u_{i,j} + u_{i-1,j}}{\Delta x^2} + \frac{u_{i,j+1} - 2u_{i,j} - u_{i,j-1}}{\Delta y^2}\right) = \rho\frac{\partial u}{\partial t}$$

$$+\rho\left(\frac{(u_{i,j} + u_{i+1,j})u_{i,j/i+1,j} - (u_{i-1,j} + u_{i,j})u_{i-1,j/i,j}}{2\Delta x} + \frac{(v_{i,j} + v_{i+1,j})u_{i,j/i,j+1} - (v_{i,j-1} + v_{i+1,j-1})u_{i,j-1/i,j}}{2\Delta y}\right);$$

$$\rho g_y - \frac{p_{i,j+1} - p_{i,j}}{\Delta y} + \mu\left(\frac{v_{i+1,j} - 2v_{i,j} + v_{i-1,j}}{\Delta x^2} + \frac{v_{i,j+1} - 2v_{i,j} - v_{i,j-1}}{\Delta y^2}\right) = \rho\frac{\partial v}{\partial t}$$

$$+\rho\left(\frac{(u_{i,j+1} + u_{i,j})v_{i,j/i+1,j} - (u_{i-1,j+1} + u_{i-1,j})v_{i-1,j/i,j}}{2\Delta x} + \frac{(v_{i,j} + v_{i,j+1})v_{i,j/i,j+1} - (v_{i,j-1} + v_{i,j})v_{i,j-1/i,j}}{2\Delta y}\right).$$

It may be observed that some special terms appear in the equation, for instance, $u_{i,j/i+1,j}$ or $u_{i-1,j/i,j}$. These terms are resulted from the technique called *upwind differencing* or *donor-cell differencing*, which is used to provide a simple stable formulation. A double subscripted term means a variable dependent on the flow direction. It is approximated by the nearest value "upwind" from the boundary. For example, $u_{i,j/i+1,j}$ is approximated by $u_{i,j}$ if the flow is in the positive direction but by $u_{i+1,j}$ if the flow is in the negative direction. The upwind formulation has two shortcomings: first it is more complicated to program into the computer and second it may affect the accuracy of the solution by introducing some numerical effects, termed in fluid mechanics "artificial viscosity" or "numerical viscosity".

Now consider the time derivative terms. The time at which the flow rates are evaluated is chosen according to the scheme that is used (explicit or implicit schemes). A superscript, $(\ )^n$, is used to identify time. If the flow rates are evaluated at an earlier time (time n), the only unknown is the new time flow rate in the cell and the equations are solved explicitly. Hence this is called the *explicit scheme*. On the other hand, if the flow rates are evaluated at the new time (time $n+1$), the equation will contain several unknowns. This is known as the *implicit scheme*. Both schemes have their advantages and disadvantages. The explicit scheme is simpler in concept, formulation and calculation, since each individual equation can be solved directly for new time unknowns, but without introducing instability it is limited by the size of the time step. The implicit scheme can have a larger time step but requires more computations per step meaning lots of overhead is needed. In this research, the explicit scheme was chosen.

Thus, the terms of time derivative are expanded and equation (4.12) becomes

$$\frac{(u_{i,j})^{n+1}-(u_{i,j})^n}{\Delta t}=-\frac{1}{\rho}\frac{p_{i+1,j}-p_{i,j}}{\Delta x}+\frac{\mu}{\rho}\left(\frac{u_{i+1,j}-2u_{i,j}+u_{i-1,j}}{\Delta x^2}+\frac{u_{i,j+1}-2u_{i,j}-u_{i,j-1}}{\Delta y^2}\right)+g_x$$

$$-\left[\frac{(u_{i,j}+u_{i+1,j})u_{i,j/i+1,j}-(u_{i-1,j}+u_{i,j})u_{i-1,j/i,j}}{2\Delta x}\right]$$

$$-\left[\frac{(v_{i,j}+v_{i+1,j})u_{i,j/i,j+1}-(v_{i,j-1}+v_{i+1,j-1})u_{i,j-1/i,j}}{2\Delta y}\right];$$

$$\frac{(v_{i,j})^{n+1}-(v_{i,j})^n}{\Delta t}=-\frac{1}{\rho}\frac{p_{i,j+1}-p_{i,j}}{\Delta y}+\frac{\mu}{\rho}\left(\frac{v_{i+1,j}-2v_{i,j}+v_{i-1,j}}{\Delta x^2}+\frac{v_{i,j+1}-2v_{i,j}-v_{i,j-1}}{\Delta y^2}\right)+g_y$$

$$-\left[\frac{(u_{i,j+1}+u_{i,j})v_{i,j/i+1,j}-(u_{i-1,j+1}+u_{i-1,j})v_{i-1,j/i,j}}{2\Delta x}\right]$$

$$-\left[\frac{(v_{i,j}+v_{i,j+1})v_{i,j}/i,j+1-(v_{i,j-1}+v_{i,j})v_{i,j-1}/i,j}{2\Delta y}\right]. \qquad (4.14)$$

Applying this equation and equation (4.13) to every cell in the whole mesh and combining the equations for cells at the flow boundaries, they form a set of algebraic equations relating the flow velocity and the fluid pressure for the entire domain.

4.2.3 Boundary Conditions

At the beginning of every computational step the flow variables at the boundary of the meshes are set to some specified values so that when all variables are solved for the interior cells the correct boundary conditions can be imposed at the flow boundary. There are two types of boundary conditions: the flow boundary condition and the pressure boundary condition.

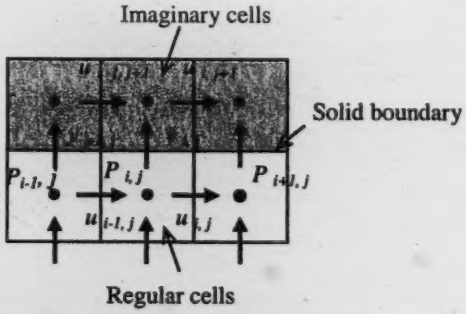

Figure 4.6 Cell configurations for implementing boundary conditions.

Consider Figure 4.6. The boundary between the gray cells and the white cells is a no flow boundary condition representing a solid boundary. The vertical velocities along the solid boundary are simply set equal to zero: $v_{i-1,\,j} = v_{i,\,j} = 0$. Also the no-slip boundary condition is required at the solid boundary due to the effect of fluid viscosity.

The pressure boundary condition is needed at the entrance or exit of a flow field. Referring to Figure 4.6, if cell (i, j) is assumed to be the entrance cell, the value of $P_{i,j}$ is set equal to the fluid pressure at the entrance.

4.2.4 Solution Algorithm

Consider equations (4.13) and (4.14). The problem of modeling incompressible, constant property fluid flow through the discretized flow field has now been reduced to the solution of simultaneous algebraic equations for the primary variables u, v, and p. However, the problem is still complicated by the fact that the fluid pressure, p, does not appear as a variable in the continuity equation. The approach that is adopted here is called a *pressure correction algorithm*.

The solution procedure starts by specializing the basic governing differential equations for two-dimensional, unsteady, incompressible flow:

$$\frac{\partial u}{\partial x}+\frac{\partial v}{\partial y}=0;$$

$$\rho g_x-\frac{\partial p}{\partial x}+\mu\left(\frac{\partial^2 u}{\partial x^2}+\frac{\partial^2 u}{\partial y^2}\right)=\rho\left(\frac{\partial u}{\partial t}+u\frac{\partial u}{\partial x}+v\frac{\partial u}{\partial y}\right);$$

$$\rho g_y-\frac{\partial p}{\partial y}+\mu\left(\frac{\partial^2 v}{\partial x^2}+\frac{\partial^2 v}{\partial y^2}\right)=\rho\left(\frac{\partial v}{\partial t}+u\frac{\partial v}{\partial x}+v\frac{\partial v}{\partial y}\right).$$

Expanding the time derivative in difference form, the momentum equations become:

$$u^{n+1}=u^n-\frac{\Delta t}{\rho}\frac{\partial p}{\partial x}+\Delta t\left[\frac{\mu}{\rho}\left(\frac{\partial^2 u}{\partial x^2}+\frac{\partial^2 u}{\partial y^2}\right)+g_x-\left(u\frac{\partial u}{\partial x}+v\frac{\partial u}{\partial y}\right)\right];$$

$$v^{n+1}=v^n-\frac{\Delta t}{\rho}\frac{\partial p}{\partial y}+\Delta t\left[\frac{\mu}{\rho}\left(\frac{\partial^2 v}{\partial x^2}+\frac{\partial^2 v}{\partial y^2}\right)+g_y-\left(u\frac{\partial v}{\partial x}+v\frac{\partial v}{\partial y}\right)\right]. \qquad (4.15)$$

The explicit numerical scheme is applied in this work. Therefore, most of the right-hand-side terms in the equation (4.15) are evaluated at time n. Now, there are three unknowns (u, v, and p) and only two equations. A third equation can be found by considering continuity of flow. Continuity must be enforced at the new time to ensure that the velocity field calculated at each time satisfies continuity. That is

$$\left(\frac{\partial u}{\partial x}\right)^{n+1} + \left(\frac{\partial v}{\partial y}\right)^{n+1} = 0 \tag{4.16}$$

The calculation difficulties mentioned earlier can be seen here. The fluid pressure does not appear in the continuity equation, so the pressure, p^n, of an earlier time n could not be used to calculate the new time pressure, p^{n+1}, precisely. Since the solution procedure is based on a pressure correction algorithm, the continuity equation must be rewritten so that the fluid pressure appears as a variable in the third equation and the new time pressure can be calculated.

If the momentum equations (4.15) are solved by employing a fully explicit formulation, the new time velocities (u^{n+1}, v^{n+1}) do not necessarily satisfy continuity. This is due to using the previous time pressure in the approximation of velocities at the new time n+1. In order for the velocities estimated by the momentum equations to satisfy continuity at the new time, the pressure field is updated from the old time values to new time values using the continuity equation. The momentum equations are revised using an implicit evaluation of the pressure gradient terms as:

$$u^{n+1} = u^n - \frac{\Delta t}{\rho}\left(\frac{\partial p}{\partial x}\right)^{n+1} + \Delta t\left[\frac{\mu}{\rho}\left(\frac{\partial^2 u}{\partial x^2} + \frac{\partial^2 u}{\partial y^2}\right) + g_x - \left(u\frac{\partial u}{\partial x} + v\frac{\partial u}{\partial y}\right)\right]^n;$$

$$v^{n+1} = v^n - \frac{\Delta t}{\rho}\left(\frac{\partial p}{\partial y}\right)^{n+1} + \Delta t\left[\frac{\mu}{\rho}\left(\frac{\partial^2 v}{\partial x^2} + \frac{\partial^2 v}{\partial y^2}\right) + g_y - \left(u\frac{\partial v}{\partial x} + v\frac{\partial v}{\partial y}\right)\right]^n. \tag{4.17}$$

The pressure gradient terms can be split into:

$$\left(\frac{\partial p}{\partial x}\right)^{n+1} = \left(\frac{\partial \Delta p}{\partial x}\right) + \left(\frac{\partial p}{\partial x}\right)^{n}$$

and

$$\left(\frac{\partial p}{\partial y}\right)^{n+1} = \left(\frac{\partial \Delta p}{\partial y}\right) + \left(\frac{\partial p}{\partial y}\right)^{n}.$$

where $\Delta p \equiv p^{n+1} - p^{n}$.

Using this formulation for the pressure gradient, equation (4.17) can be expanded as:

$$u^{n+1} = u^{n} - \frac{\Delta t}{\rho}\frac{\partial \Delta p}{\partial x} + \frac{\Delta t}{\rho}\left[-\frac{\partial p}{\partial x} + \mu\left(\frac{\partial^2 u}{\partial x^2} + \frac{\partial^2 u}{\partial y^2}\right) + \rho g_x - \rho\left(u\frac{\partial u}{\partial x} + v\frac{\partial u}{\partial y}\right)\right]^{n};$$

$$v^{n+1} = v^{n} - \frac{\Delta t}{\rho}\frac{\partial \Delta p}{\partial y} + \frac{\Delta t}{\rho}\left[-\frac{\partial p}{\partial y} + \mu\left(\frac{\partial^2 v}{\partial x^2} + \frac{\partial^2 v}{\partial y^2}\right) + \rho g_y - \rho\left(u\frac{\partial v}{\partial x} + v\frac{\partial v}{\partial y}\right)\right]^{n}.$$

or

$$u^{n+1} = u^{n} - \frac{\Delta t}{\rho}\frac{\partial \Delta p}{\partial x} + Q_x^{n};$$

$$v^{n+1} = v^{n} - \frac{\Delta t}{\rho}\frac{\partial \Delta p}{\partial y} + Q_y^{n}. \qquad (4.18)$$

where $Q_x^{n} = \frac{\Delta t}{\rho}\left[-\frac{\partial p}{\partial x} + \mu\left(\frac{\partial^2 u}{\partial x^2} + \frac{\partial^2 u}{\partial y^2}\right) + \rho g_x - \rho\left(u\frac{\partial u}{\partial x} + v\frac{\partial u}{\partial y}\right)\right]^{n}$ and

$$Q_y^{n} = \frac{\Delta t}{\rho}\left[-\frac{\partial p}{\partial y} + \mu\left(\frac{\partial^2 v}{\partial x^2} + \frac{\partial^2 v}{\partial y^2}\right) + \rho g_y - \rho\left(u\frac{\partial v}{\partial x} + v\frac{\partial v}{\partial y}\right)\right]^{n}.$$

These expressions for the new time velocities are substituted into the continuity equation or equation (4.16), and it becomes:

$$\left(\frac{\partial u}{\partial x}+\frac{\partial v}{\partial y}\right)^{n}-\frac{\Delta t}{\rho}\left(\frac{\partial^2 \Delta p}{\partial x^2}+\frac{\partial^2 \Delta p}{\partial y^2}\right)+\left(\frac{\partial Q_x}{\partial x}+\frac{\partial Q_y}{\partial y}\right)^{n}=0 \qquad (4.19)$$

The first term on the left-hand side of equation (4.19) is simply the continuity expressed at time n and is therefore equal to zero. Since the Q terms are evaluated at time n, their values are known. The continuity equation applied at time n+1 can now be written as:

$$\left(\frac{\partial^2 \Delta p}{\partial x^2}+\frac{\partial^2 \Delta p}{\partial y^2}\right)=\nabla^2(\Delta p)=\frac{\rho}{\Delta t}\left(\frac{\partial Q_x}{\partial x}+\frac{\partial Q_y}{\partial y}\right)^{n}. \qquad (4.20)$$

The continuity equation is now expressed in terms of pressure, which can be used to make a "correction" to the pressure. Solving this equation and substituting a solution for Δp into the momentum equations will update the velocity field to the new time n+1.

An iterative procedure is used to solve equation (4.20). The procedure begins by computing the first approximation of the new time velocities. A numerical superscript, X^{1st}, X^{2nd}, denotes an iterative level. The first estimation is computed from a fully explicit formulation of the momentum equations, where $\Delta p^{1st}=0$, so:

$$u^{1st}=u^{n}+Q_x^{n};$$

$$v^{1st}=v^{n}+Q_y^{n}.$$

Now the explicit part of the momentum equation is embedded into the first estimated velocity field:

$$u^{2nd}=u^{n}-\frac{\Delta t}{\rho}\left(\frac{\partial \Delta p}{\partial x}\right)^{2nd}+Q_x^{n}=u^{1st}-\frac{\Delta t}{\rho}\left(\frac{\partial \Delta p}{\partial x}\right)^{2nd};$$

$$v^{2nd}=v^{n}-\frac{\Delta t}{\rho}\left(\frac{\partial \Delta p}{\partial y}\right)^{2nd}+Q_y^{n}=v^{1st}-\frac{\Delta t}{\rho}\left(\frac{\partial \Delta p}{\partial y}\right)^{2nd}.$$

To obtain an improved estimation of the velocities, a pressure correction must be computed according to the continuity equation:

$$\frac{\partial u^{2nd}}{\partial x}+\frac{\partial v^{2nd}}{\partial y}=\frac{\partial u^{1st}}{\partial x}-\frac{\Delta t}{\rho}\left(\frac{\partial^2 \Delta p}{\partial x^2}\right)^{2nd}+\frac{\partial v^{1st}}{\partial y}-\frac{\Delta t}{\rho}\left(\frac{\partial^2 \Delta p}{\partial y}\right)^{2nd}=0. \qquad (4.21)$$

Equation (4.21) becomes

$$D^{1st}-\frac{\Delta t}{\rho}\left[\left(\frac{\partial^2 \Delta p}{\partial x^2}\right)^{2nd}+\left(\frac{\partial^2 \Delta p}{\partial y}\right)^{2nd}\right]=0$$

or

$$\nabla^2\left(\Delta p^{2nd}\right)=\frac{\rho}{\Delta t}D^{1st}. \qquad (4.22)$$

where $D^{1st}=\frac{\partial u^{1st}}{\partial x}+\frac{\partial v^{1st}}{\partial y}$.

The equation (4.22) is resolved as

$$\Delta p_{i,j}^{2nd}\approx\frac{\rho}{\Delta t}\frac{-D^{1st}}{2\left[1/(\Delta x)^2+1/(\Delta y)^2\right]}. \qquad (4.23)$$

So the second iterative approximations give the new pressure and velocity fields:

$$p^{2nd}=p^{1st}+\Delta p^{2nd}; \qquad (4.24)$$

$$u^{2nd}=u^{1st}-\frac{\Delta t}{\rho}\left(\frac{\partial \Delta p}{\partial x}\right)^{2nd}; \qquad (4.25)$$

$$v^{2nd}=v^{1st}-\frac{\Delta t}{\rho}\left(\frac{\partial \Delta p}{\partial y}\right)^{2nd}. \qquad (4.26)$$

These second iterative velocities may not satisfy continuity exactly, but the deviation from continuity will be decreased compared to the first approximation. The

iteration pattern is quite clear now. With each iteration, the deviation in the field will be decreased and so will the subsequent pressure correction. Typically the iteration procedure is repeated until the maximum deviation in the cell has decreased to less than a user-specified tolerance:

$$\left|D^{nth}\right| < tolerance\,. \tag{4.27}$$

4.2.5 Critical Time-Step Determination in Fluid Flow Simulation

The size of the time-step may affect the accuracy of the solution and may also significantly affect the calculation stability, particularly when the explicit scheme is used. If the selected time interval is outside the acceptable range of values, the numerical method will become unstable and fail to provide meaningful results.

The first stability criterion is related to how fast mass is convected through a computational cell. To obtain a stable solution, the time-step size must be smaller than the following limit:

$$\Delta t \le \frac{1}{\left|\Delta x/u\right| + \left|\Delta y/v\right|} \tag{4.28}$$

This criterion is often referred to as the Courant-Friedrichs-Lewy (CFL) condition and may be inferred as a condition limiting the distance that a fluid particle travels in a single time step to no further than the size of the cell. If the selected time-step exceeds this condition, information can be transmitted at such a great distance in a single time step that it may completely skip over a cell, thus never affecting the variables associated with that cell. The velocity of information travel depends on the speed of the wave in the

material. Due to the assumption of fluid incompressibility, the wave speed will become infinite. Thus the critical time-step in this criterion will be very small or an instantaneous time-step. However, the small tolerance occurring in the calculation of the continuity equation allows the information to travel at a finite speed. This should be taken into account for the critical time-step determination.

The second stability criterion is related to momentum transfer by viscosity. The condition is:

$$\Delta t \leq \frac{\rho}{2\mu}\left|\frac{\Delta x^2 \Delta y^2}{\Delta x^2 + \Delta y^2}\right| \tag{4.29}$$

This criterion may be interpreted as a condition limiting the transport of momentum by the action of viscosity to no more than a single cell in a single time step. The smaller of these two limiting time steps determined by the equations (4.28) and (4.29) must be enforced as an upper limit of Δt to ensure stability.

4.3 *EXPLANATION OF COMPUTER CODES*

The computer code for modeling fluid flow has been grouped into three main functions (in computer language C or C++, functions are subprograms which perform specified calculations). The first function performs the discretization process: to discretize the flow field into subregions and to assign the coordinate and fluid property in each subregion. The other two main functions are related to the calculation process. The first one approximates the primary variables from the Navier-Stokes equation and the second one makes corrections of the fluid pressure and thereby adjusts the flow velocity

to satisfy the continuity equation. After that, the flow velocities are displayed into graphical form using graphical modules. The entire process is depicted in Figure 4.7

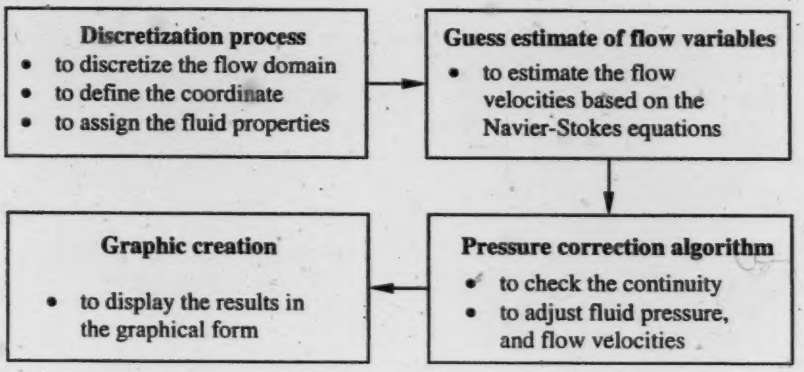
Discretization process
• to discretize the flow domain
• to define the coordinate
• to assign the fluid properties
Guess estimate of flow variables
• to estimate the flow velocities based on the Navier-Stokes equations
Pressure correction algorithm
• to check the continuity
• to adjust fluid pressure, and flow velocities
Graphic creation
• to display the results in the graphical form

Figure 4.7 Entire process of fluid flow simulation

4.3.1 Discretization Process

The main purpose of this function is to discretize the specified flow field and assign the global coordinate to the positions of all variables. First the flow space is defined: the maximum and minimum x and y coordinates are specified. In order to know the mesh size, the number of cells in the flow domain plus two imaginary cells for the boundaries must be given. Due to the fact that the flow variables are not defined at the same location, fluid pressures are defined at the center and velocities on the boundary of the cells (see in Figure 4.8). The positions of each variable are, thus, specified separately. Note that the horizontal and vertical velocities of the same cell are defined at different locations. When assigning coordinates, the fluid viscosity is also assigned for the entire flow field.

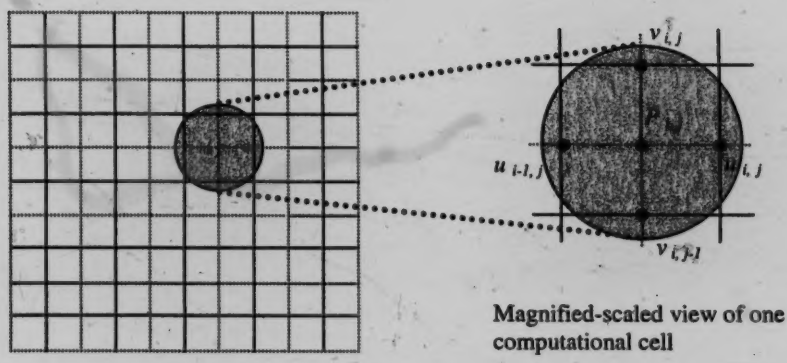

Discretized flow field

Magnified-scaled view of one computational cell

Figure 4.8 Discretization

4.3.2 First Approximation of Flow Variables

The first approximation function will provide an estimate of the velocity field based on the current pressure gradients. It is the first step in the iterative procedure as discussed in Section 4.2.4 "*Solution Algorithm*". The pressure gradients are computed at time *n*. Thus, the new velocities (u^{n+1}, v^{n+1}) obtained in this step do not necessarily satisfy continuity.

Due to the very small grid-size, the abrupt change in pressure between neighboring nodes can cause numerical instability. To prevent this problem in specifying the fluid pressures, the pressures are incremented in small amounts at each time-step until it reaches the intended value. Therefore the fluid pressure will not change drastically between neighboring nodes.

To approximate flow velocities for interior cells, the quantities at the boundary nodes are specified first. The conditions of no-flow across and no slip boundary are included in the simulation. As a result of using the upwind differencing technique, the

program must select the nearest "upwind" node from the boundary in the approximation of the flow velocities from the Navier-Stokes equation.

4.3.3 Pressure Correction Algorithm

After the first approximation of the fluid flow velocities calculated based on the pressure gradient at time n, the next step is to calculate the fluid pressures for the new time, n+1, and simultaneously make corrections of the velocity field to satisfy continuity. This is accomplished using an iterative procedure. First, the approximated velocity values are substituted into the continuity equation. The substituted equation may not exactly equal zero. The numerical result that differs from zero is called the "deviation" of the velocity field. Based on this value of the deviation, changes in fluid pressures are computed. The adjustment of the fluid pressures causes changes in the velocity field. The new velocity field should satisfy continuity better than the previous step, or the value of the deviation should become smaller. An iterative procedure is used until the deviation of the velocity field is smaller than a specified tolerance or it means that the continuity equation has been satisfied at a certain level. At the end of the scheme, the program will update the information of the primary variables. A new time step will be imposed and the procedure will march in time. Figure 4.9 illustrates the flow chart for this iterative procedure.

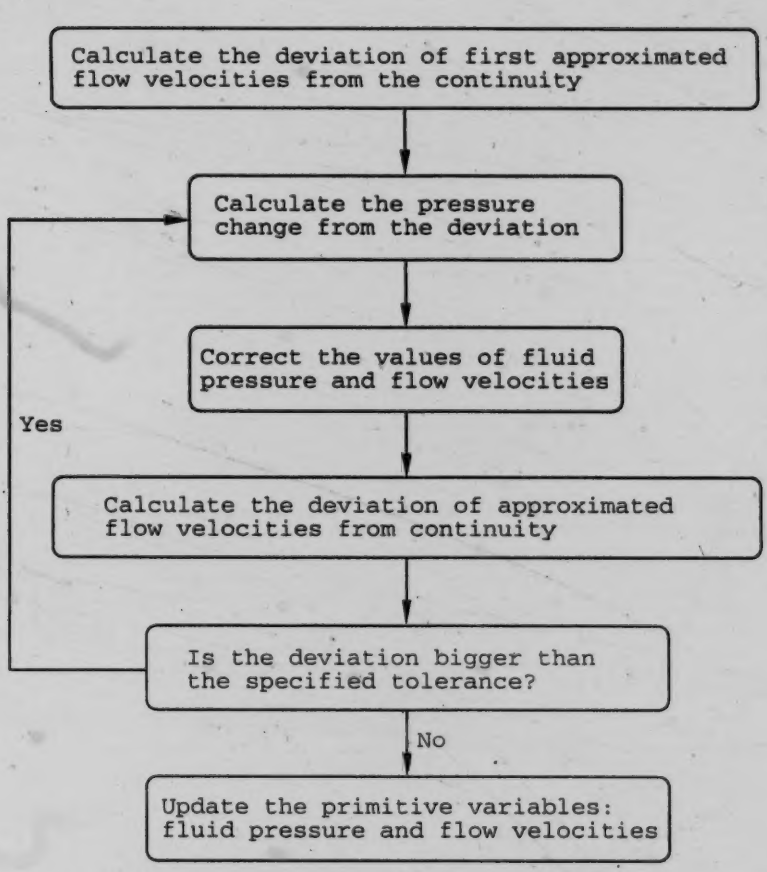
Calculate the deviation of first approximated flow velocities from the continuity
Calculate the pressure change from the deviation
Correct the values of fluid pressure and flow velocities
Yes
Calculate the deviation of approximated flow velocities from continuity
Is the deviation bigger than the specified tolerance?
No
Update the primitive variables: fluid pressure and flow velocities

Figure 4.9 Flow chart of pressure correction algorithm

4.3.4 Creation of Graphical Result

At the end of each time step, the program will give solutions of the primary variables, such as flow velocities and fluid pressure. To visually interpret the solutions, numerical results are converted to graphical format. Because flow velocities are defined at the cell boundaries, there are 4 flow velocities in each cell: two horizontal and two vertical velocities. However, it is desired to represent a cell with one velocity vector, therefore an averaging technique is used. The velocity vector is drawn as a line starting at

the center of the cell or the location of fluid pressure with its length proportional to the average velocities both in the horizontal and vertical directions.

4.4. *LIMITATIONS AND SHORTCOMINGS OF FLUID FLOW SIMULATION*

4.4.1 Computer Time Consumption

The demand for computer time comes from several sources. It is related to the computer scheme, programming technique, fluid property, mesh-size, etc. The explicit scheme has its drawbacks. Obviously, the explicit scheme has limitations on the size of the time-step compared to the implicit scheme. The size of the critical time-step is related to the mesh-size, fluid velocity and fluid property according to the equations (4.28) and (4.29) in this simulation. Based on experience, the actual time-step can be as small as 1/1000 of the theoretical maximum time step to obtain numerical stability.

Another computer intensive task is the treatment of boundary conditions. For instance, to specify pressure at the pressure boundary, if the mesh-size is small, the fluid pressure cannot be set equal to the intended value in one step. Imposing a large jump in pressure at the boundary can introduce a shock wave to the system causing instability. To avoid this problem it is necessary to increase the pressure in small increments. Therefore a larger number of time steps is required to obtain a solution.

4.4.2 Range of Solvable Problems

The present work is limited by the assumptions made in the formulation, such as incompressible flow, constant viscosity and the Navier-Stokes equations. The scheme is assumed to limit for laminar flow of low Reynolds numbers. To model turbulent flow, it is required to reformulate the problem and include other flow phenomena in the formulation.

4.4.3 Shortcomings of Upwind Differencing Technique

The upwind differencing technique provides numerical stability, but it has two shortcomings. First it increases the complexity of computer coding to include the logic of selecting the upwind values. Second, it introduces "artificial viscosity", which may reduce the accuracy of the solution at some locations. The scheme has been checked and the results are presented in the next section.

4.5 *VERIFICATION PROBLEM*

4.5.1 Problem Statement

To verify the formulation, methodology and computer coding, a flow problem was solved. The problem involved fluid flow between two parallel and fixed plates. The computed velocities and fluid pressures were compared with the results calculated from closed form solution.

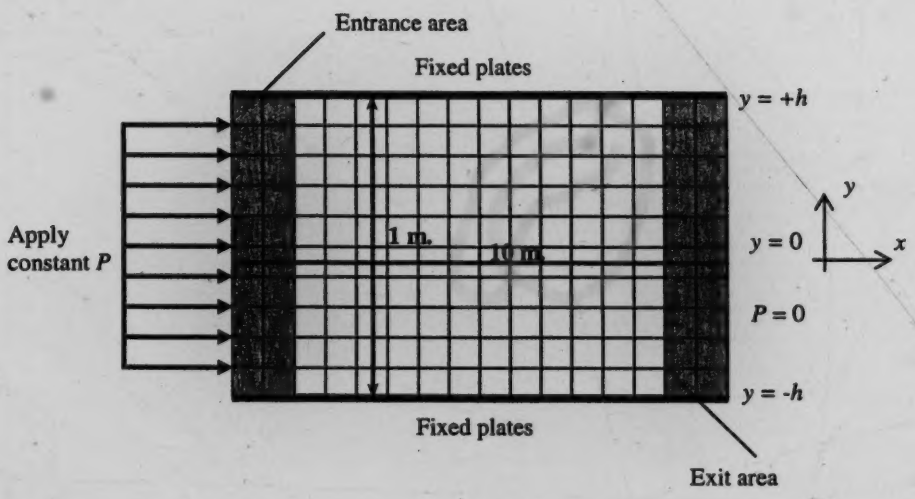

Figure 4.10 Physical model

Figure 4.10 shows the problem to analyze. The problem was a two-dimensional, ($\partial/\partial z = 0$), incompressible viscous flow between two parallel plates of $2h$ apart with no gravity effects. Both plates had a length of 10.0 meters and were located 1.0 meter apart. The fluid was assumed to have constant viscosity and density. An initial condition of a zero pressure field was specified with a no-slip boundary imposed at each plate because of viscous effects. To generate fluid flow, the pressure was raised at the left boundary.

4.5.2 Closed-Form Solution

A closed form solution for flow between very wide and very long plates was obtained. Applying a pressure gradient in the flow space generated flow. Positive pressures were specified at the left boundary and simultaneously the fluid pressure at the exit, right side, was set equal to zero. That caused a pressure variation and fluid flow in one direction, from left to right (refer to Figure 4.10).

Under the specified pressure gradient, the variations of velocities and pressure are given by (White, 1999):

$$\partial p/\partial x = \text{const},$$

$$u = -\frac{dp}{dx}\frac{h^2}{2\mu}\left(1-\frac{y^2}{h^2}\right),$$

$$v = 0.$$

where $y = 0$ refers to the mid point of the flow space where the flow velocity was at its maximum value.

4.5.3 Numerical Model

The two-dimensional incompressible fluid flow was modeled using the pressure correction algorithm in the finite volume scheme. As mentioned before, the flow field was divided into a finite number of subregions. The continuity and Navier-Stokes equations were both applied to those small areas. The initial and boundary conditions were also imposed. Finally, marching the scheme forward through time obtained a solution for the unsteady fluid flow problem. A steady state solution was achieved by observing the development of flow until all the primary variables did not change with time.

Typical values of fluid properties, viscosity and density, were used in the simulation, shown in Table 4.1. Gravity was neglected in this example.

Table 4.1 Fluid Properties in Numerical Simulation

Properties	Values
Density of fluid (kg/m^3)	998
Fluid Viscosity ($N\text{-}s/m^2$)	0.001
Time-step (s)	0.001

4.5.4 Results

The variations of flow velocities and fluid pressure arising from the application of fluid pressure gradient were compared with the ones calculated from the closed-form solution. Table 4.2 represents the comparison of flow velocities resulted from the numerical simulation with the ones from the analytical formulation.

Fluid properties that were used in the simulation are described as follows: fluid density ρ equal to 998 kg/m^3 and viscosity μ equal to 0.001 $N\text{-}s/m^2$. Fluid flow was generated by defining a pressure gradient (0.01 Pa over the horizontal distance of 10.0 meters) across the flow field. Table 4.2 compares the analytical results with the numerical results at various locations in the flow regime. It can be seen in Table 4.2 that the calculated velocities agree well with the closed-form solution. The numerical results also show that the changes in fluid pressure are constant with respect to the horizontal distance, shown in Figure 4.11, similarly to the closed-form solution ($\partial p/\partial x$ = constant).

Table 4.2 The comparison of flow velocities

Location in the flow space	*Numerical*	*Analytical*
At the middle point of flow space	0.1250	0.1250
0.05 far from the middle point	0.12375	0.12375
0.15 far from the middle point	0.11375	0.11375
0.25 far from the middle point	0.09375	0.09375
0.35 far from the middle point	0.06375	0.06375
0.45 far from the middle point	0.02375	0.02375

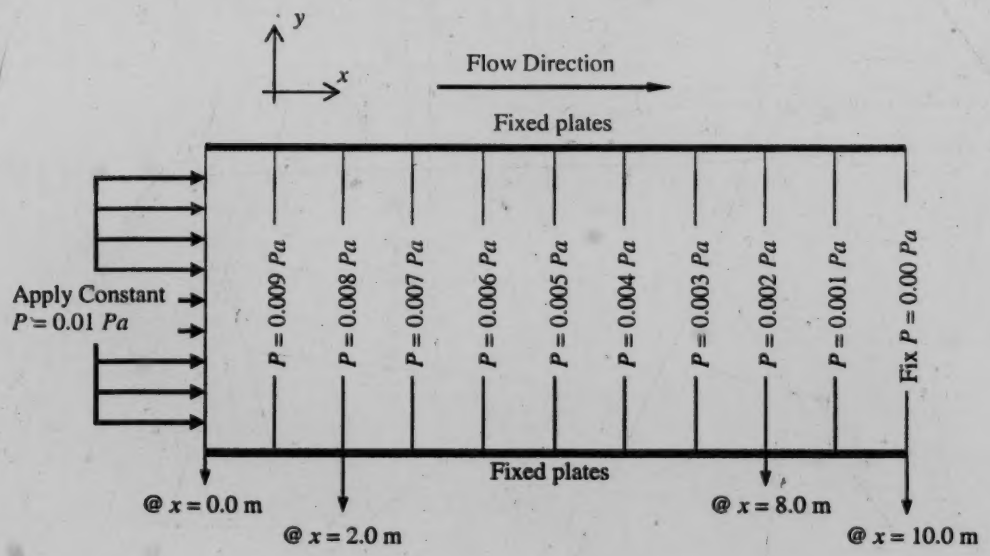

Figure 4.11 Simulated variations of fluid pressure

CHAPTER 5 FLUID-SOLID COUPLING

In Chapter 3 and 4, the details of the discontinuum approach to model granular material movement and the continuum approach to model fluid flow have been presented. The coupling of those two approaches is developed here to simulate wet granular flow. The term "wet" refers to the flow of granular material in water or other type of fluid. The coupling mechanisms are explained in terms of fluid/particle interactions, which can be separated into the effect of fluid on the granular particle and the effect of the particle on the flowing fluid. An explanation of computer codes in the coupling part is presented. Finally, limitations in the coupling scheme will be discussed.

5.1 *MODELING SOLID-FLUID COUPLING*

In DEM modeling, discussed in Chapter 3, contact between particles results in contact force. To determine the motion of the particles, the resultant of all forces is computed and Newton's Law of Motion is applied. While a particle is submerged in a flowing fluid, drag, lift and buoyant forces are the basic effects that a fluid has on the granular particles. In this work, drag and buoyant forces are included in the force resultant when calculating the movement of the particle. At the same time, the presence of the particles will affect the fluid flow. The particle reduces the flow domain and imposes impedance to the flowing fluid. Therefore it is necessary to change the flow velocity accounting for this effect.

5.1.1 Effects of Fluid on the Granular Particles

5.1.1.1 Drag Force

A moving object immersed in a stagnant fluid, a motionless object immersed in a flowing fluid, or a moving object immersed in a fluid flowing at a different velocity all experience forces caused by relative movements between the fluid and the object. Drag is, therefore, a force caused by the fluid on an immersed object along the line of the relative movement between the object and the fluid. The total drag acting on an object is comprised of two components: the *skin-friction drag* and *pressure drag*. The skin friction drag results from shearing stresses in the fluid layer adjacent to the object's surface (the boundary layer). Pressure drag results from disturbances of the flow stream as it passes around the object and produces pressure differential between lowered pressure at the rear of the object in the turbulent wake and higher pressure at the front of the object. Either skin-friction drag or pressure drag may predominate depending upon the situation. The basic principles of drag force can be found in the general text of fluid mechanics. The author refers to two textbooks: Fundamentals of Fluid Mechanics by Evett and Liu (1987) and Viscous Fluid Flow by White (1974).

Drag force for the granular particle can be evaluated using the following equation (Evett and Liu, 1987):

$$D_j = C_D \rho \frac{v_j^2}{2} A \qquad (5.1)$$

where D_j is the drag force of the granular particle j; C_D is the drag coefficient; ρ is the fluid density; v_j is the relative velocity of the fluid with respect to the granular particle j;

and A is the projected area of the granular particle on a plane perpendicular to the direction of flow.

The drag coefficient, C_D, is a dimensionless parameter that is generally dependent on the particle's shape and the Reynolds number. Different shapes have different empirical relationships for determining the drag coefficient.

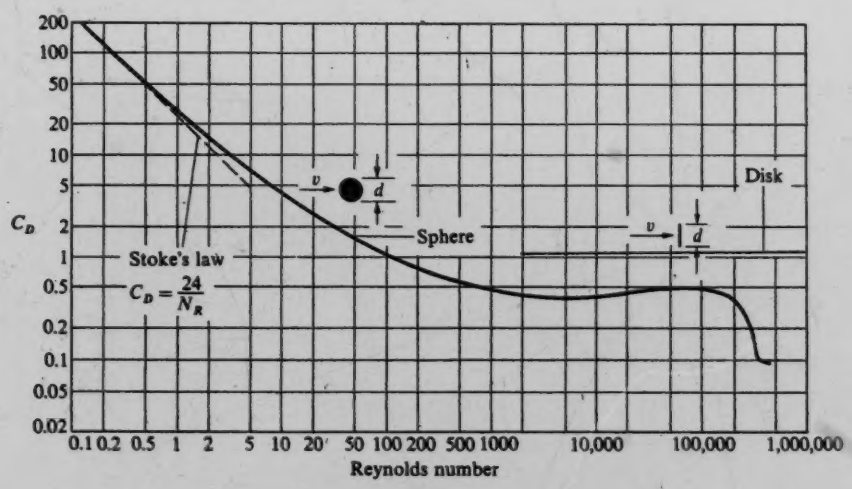

Figure 5.1 Drag coefficients for sphere and circular shaped objects: Evett and Liu (1987).

The focus of this work is sphere-shaped particles and therefore it is of interest to determine the drag coefficient for spherical particles. Figure 5.1 can be used to determine the drag coefficient for spheres as a function of the Reynolds number, and for circular disks with axes perpendicular to the direction of flow. The distance d indicated on the figure is used to compute the Reynolds number. This figure is based almost entirely on experimental data. For convenient use in numerical work, White (1974) suggested the following expression based on curve fitting:

$$C_{D,sphere} \approx \frac{24}{\mathrm{Re}} + \frac{6}{1+\sqrt{\mathrm{Re}}} + 0.4 \quad , \mathrm{Re} < 2\times10^5 \tag{5.2}$$

where Re is the Reynolds number. This expression cannot be used for Reynolds number exceeding 2×10^5.

5.1.1.2 Buoyancy

An object submerged in a fluid is subjected to a fluid pressure. The horizontal components of the fluid pressure cancel each other for both sides. There are two vertical components of the fluid pressure acting on a submerged object. One is the downward component of the total pressure exerted on the upper surface of the object, and the other is the upward component exerted on the lower surface of the object. Because fluid pressure increases with depth, the upward component at the bottom of the object is greater than the downward one at the top, thus resulting in a net upward force acting on the object. The net upward force on a submerged object is, therefore, equal to the weight of the fluid displaced by the submerged object and is independent of the depth of submergence, provided the object is totally submerged.

The buoyant forces on a submerged particle j can be computed from

$$B_j = (\rho - \rho_j) g V_j \tag{5.3}$$

where B_j is the vertical buoyant force of particle j, ρ_j is the density of particle j, ρ is the unit weight of the fluid and V_j is the displaced volume and g is the gravitational constant.

5.1.1.3 Lift

Lift is a force caused by fluid acting on an immersed body in the direction perpendicular to the line of movement of the body or fluid. The lift force can be evaluated using the following expression.

$$L = C_L \rho \frac{v^2}{2} A \tag{5.4}$$

where L is the lift force on the body; C_L is the lift coefficient; ρ is the fluid density; v is the relative velocity of the fluid with respect to the body; and A is the projected chord area.

As explained by Gerhart et al. (1992), 'the fluid passing over the "top" of the airfoil must travel faster than the fluid passing over the "bottom". In a steady flow, this condition means that the "topside" fluid must have, on average, a higher velocity than the "bottomside" fluid. Bernoulli's equation implies that the "topside" pressure is lower than the "bottomside" pressure, generating a net upward (lift) force.' Bernoulli's equation can be expressed as following:

$$\frac{p}{\rho} + \frac{v^2}{2} + gz = Const. \tag{5.5}$$

where p is the fluid pressure at any point, ρ is the fluid density, v is the fluid velocity at any point, z is the elevation of the fluid, and g is the gravity.

In this work, the velocity and pressure differences between "topside" and "bottomside" of the particle are assumed to be negligible due to the small size of the particles. Therefore, the lift force is neglected in this simulation.

5.1.2 Effect of Granular Particle on the Fluid

From the discrete element method, the locations of the granular particles are known at every time-step. The presences of the granular particles in the flow region can be imagined as occupying the flow space that would have been otherwise available for fluid flow. The reduction in the flow channel leads to changes in flow velocity and fluid pressure. Basically, at the location of the granular particles, the fluid flow velocity will be less than that for free flow. To model the effect of the particle against fluid flow, a reduction factor is applied directly on the calculation of Navier-Stokes equation. It is assumed that the particle will cause a decrease in the fluid velocity in the direction perpendicular to the flow. Subsequently in the continuum fluid computation the primary variables will be recalculated and adjusted automatically heading towards a new equilibrium condition. The final result is seen as a change in the flow pattern; fluid avoids flowing in the direction of higher resistance. The reduction factor is determined by trial and error. This factor is related to the simulation conditions; i.e., the value of pressure gradient and mesh size. Inappropriate reduction factor can induce more drastic changes in fluid pressure, which may cause calculation instability. The computation of fluid flow velocity for the next time-step, where the granular particles appear, is shown in the following equation; the velocity on the left-handed side of the equation is estimated for the next time-step, while the ones appearing on the right-hand side are the values at the current time-step:

$$\vec{V}_{N+1} = \alpha\vec{V}_N - \frac{\Delta t}{\rho}\vec{\nabla}p + \Delta t\left[\frac{\mu}{\rho}\nabla^2\vec{V} + \vec{g} - \left(\vec{V}\cdot\vec{\nabla}\right)\vec{V}\right] \tag{5.6}$$

where α is the reduction factor.

5.1.3 Calculation Cycle

Both the DEM and fluid flow computations are performed using the explicit scheme; thereby the calculation cycle for the coupled granular-fluid flow involves a time-stepping algorithm. The chosen time-step must be compatible for both systems, otherwise instability in one system can result in the collapse of the coupled systems.

Figure 5.2 depicts the calculation cycle of the fully coupled process. The DEM calculates and gives the positions of all granular particles. From the positions of granular particles, the continuum fluid computation can determine the cells where the granular particles appear as it needs to modify the fluid flow velocities. Fluid flow calculation solves for all primary variables, including fluid pressure and flow velocities, at the end of every time-step. The relative velocities between the fluid and granular particles induce drag forces, which affect particle movement. Buoyant forces occur and resist the downward movement of the granular particles. The calculation cycle continues until the solution is converged.

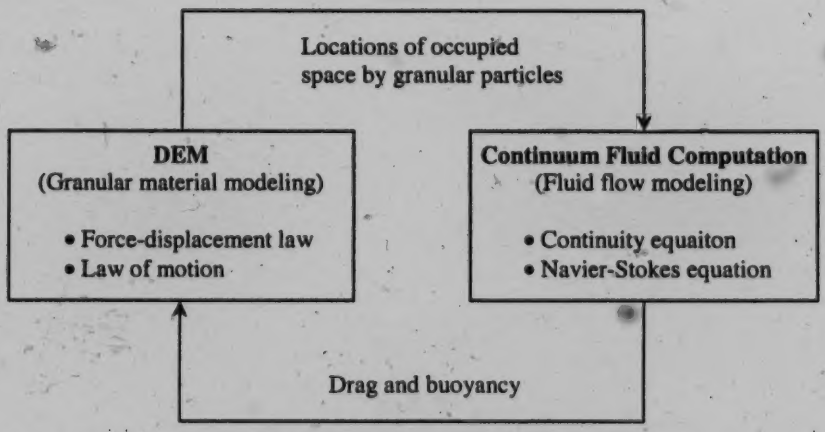

Figure 5.2 Calculation cycle of the whole simulation

5.2 EXPLANATION OF COMPUTER CODES

In this section, a description of computer codes for fluid-solid coupling is given. Fluid-solid interactions are divided into two effects: the effect of fluid on the movement of the particles and the effect of particles on the flowing of the fluid. Drag and buoyancy are considered as the effects of fluid on the granular particles. For each particle, drag and buoyant forces can be computed. Then these forces are added to the resultant of the forces which are come from contact interaction in the DEM calculation. Finally the movement of granular particles can be calculated by applying Newton's Law of Motion. To consider the effect of the particles on the fluid, a reduction factor is used to reduce the fluid flow locally. In order to apply the particle effect on the fluid flow simulation, it is necessary to determine the position of the particle in the finite volume grid. Once the grid point has been determined, the reduction factor is applied at the affected grid points. Note that the local impedance is applied only to the calculation of fluid flow velocity, not for the calculation of fluid pressure. The value of fluid pressure will be automatically adjusted.

5.2.1 Detection of Fluid-Particle Contact

The main purpose of this function is to discover where the granular particle appears in the flow space. It is explained in an earlier section of fluid flow modeling that the specified flow field is divided into a finite number of subregions. The primary variables of fluid flow modeling in one cell are defined at different locations. Even though the horizontal and vertical components of the fluid flow velocity are in the same

cell, they are defined at different positions. However since the locations of the primary variables in fluid flow modeling and granular particles are referred to the same coordinate, the program is thereby capable of making the comparison between the coordinates of the granular particles and the flow velocities making it possible to detect which nodes in the flow space are occupied by a granular particle. This information is recorded by the program and will be used later.

To map all granular particles into the flow space, the program needs to know the coordinates of both granular particles and flow space. The program starts by restoring the maximum and minimum x- and y-coordinates of the flow field. It then calculates the mesh size based on the total number of nodes defined by the user. The information of the granular particles, including x- and y-coordinates of the particle mass center as well as the radius of particles, is recalled. Based on this information, the program can finally map all granular particles one by one into the flow space. Since the horizontal components of the fluid velocities are defined at different locations than the vertical components of the fluid velocities, the mappings of the granular particle into the flow space are made twice.

5.2.2 Simulation of Particle Interaction

After the program determines which nodes in the flow space are occupied by the granular particles, the program now can apply the reduction factor to the calculation of fluid flow velocities. That induces changes in the flow pattern at the next time-step. The fluid pressure will automatically be adapted in the calculation correspondingly to the first approximated value of the fluid flow velocities. The reduction factor is defined as the adjusted fluid flow velocity over the unadjusted velocities expressed as percentage. The

percentage should not be too low, otherwise it will cause an abrupt change in the calculation of fluid flow velocity and can cause numerical instability.

5.2.3 Calculation of Drag and Buoyant Forces

This part of the program, as shown in Figure 5.3, works on the computation part of fluid-granular interactions. It computes the drag and buoyant forces. Drag force is computed based on the relative velocities between the fluid and the granular particle. Buoyant force on a granular particle is equal to the weight of the fluid displaced by that particle. After calculating these forces, the program calculates the resultant of all forces acting on the granular particle, including gravitational force. The resultant force will be used later to calculate the movement of the granular particles in the next time-step.

The calculation process begins with the forces acting on each granular particle due to gravity. It is then followed by the computation of the horizontal and vertical drag forces and buoyant force in the vertical direction. After the program completes all the computations, the computed values of the forces are added immediately to update the record of total forces, which will be used to calculate the movement of the granular particle.

In the case of particles dropping into the flowing fluid, the submerged volume is changing with time. This has an effect on the drag and buoyant forces. Figure 5.4 shows all possible cases of a partially submerged particle.

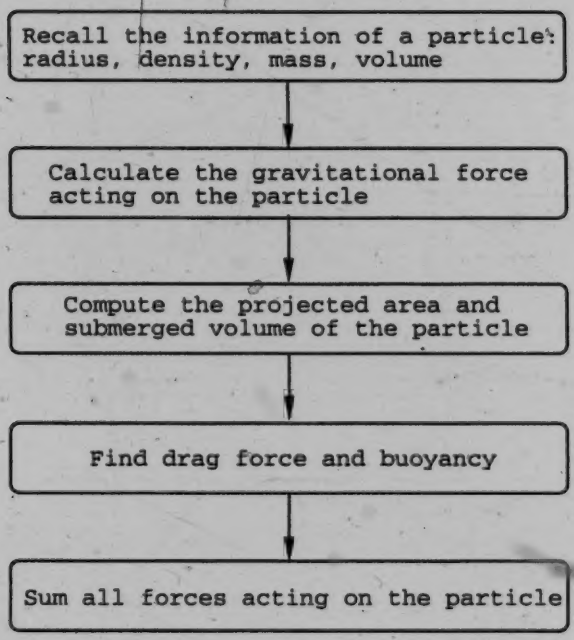
Recall the information of a particle: radius, density, mass, volume
Calculate the gravitational force acting on the particle
Compute the projected area and submerged volume of the particle
Find drag force and buoyancy
Sum all forces acting on the particle

Figure 5.3 Simulation of fluid interaction

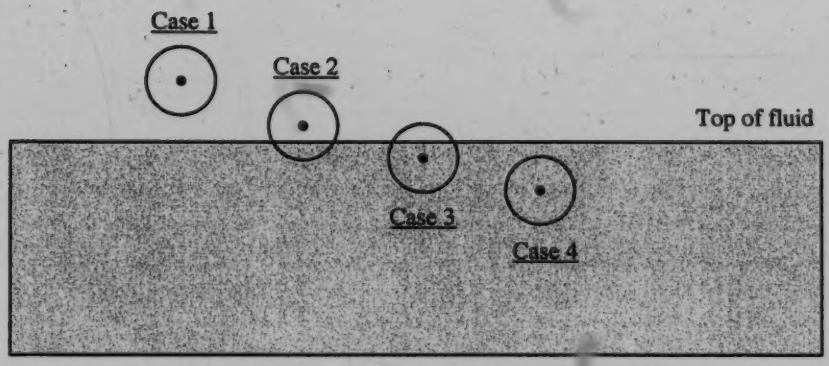

Figure 5.4 All possible cases of particle dropping into fluid

Case 1: a granular particle is above the fluid surface: no drag and no buoyancy are applied.

Case 2: a small part of granular particle submerges into the fluid; the particle center is still above the fluid; drag and buoyant forces partly act on the granular particle.

Case 3: over than half of a granular particle immerses into the fluid, the particle center is below the surface of the fluid; drag and buoyant forces partly act on the granular particle.

Case 4: the whole particle submerges into the fluid; full drag and buoyant forces are applied.

5.3 *LIMITATIONS AND DRAWBACKS*

5.3.1 Range of Solvable Problems

The formula to calculate the drag coefficient is based on an empirical formula that is valid for Reynolds number less than 200,000. If the calculated Reynolds number is higher than 200,000, this formula will not be applicable.

5.3.2 Resolution of the Flow Field

In order for the program to identify a granular particle moving in the flow field, the size of the smallest granular particle should be larger than the biggest mesh size. If the particle is smaller than the mesh size, it is possible for the particle to go through the fluid in between the grids without being detected. Also if the particle occupies several grid points, it provides better interaction with the fluid calculation. The large difference between the particle and the mesh size gives a better appearance of the particle effect. For example in Figure 5.5, two different mesh sizes are shown. Even though the particles in both cases have the same size, mesh size in Case A is twice as large as mesh size in Case B. The number of nodes that are occupied by the particle in Case A is less than the

number of occupied nodes in Case B. This will affect the manifestation of particle effect in Case B and also in Case A. The finer mesh in Case B is likely to give more detail of particle effect than the coarser mesh in Case A does.

Another point that can be noticed in Figure 5.5 is the appearance of the particle. In Case A with the coarse mesh-size, the particle is thought as a circle in the cross section, but it appears in the flow field as a rectangle. Even though with finer mesh in Case B, the particle appearance is not perceived as absolutely circular.

The decrease in the mesh size means an increase in computational time. Therefore, in Case B it will take more time to compute the solution of one loop calculation than in Case A.

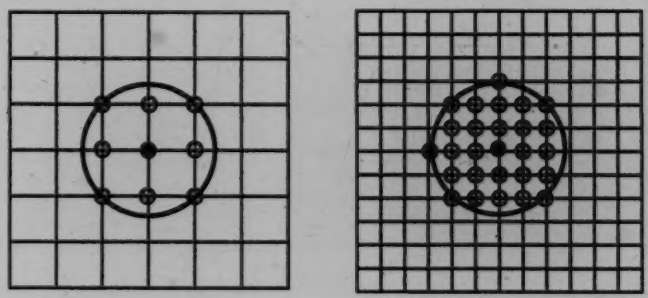

Case A. Case B.

Figure 5.5 Two different mesh sizes

5.3.3 Limitation of the Two-Dimensional Model

When the program detects the nodes in the flow field that are occupied by the granular particles, the same reduction factor is applied to every part of the particle in the two-dimensional model. However, in reality it is noted that different parts of a granular particle have different effects on fluid flow. For example, fluid can flow through the outside area of the granular particle, around the particle periphery, in higher amounts than

that through the inside area, particularly at the central zone of the granular particle. This can be stated as the limitation of a two-dimensional model compared with a three-dimensional model.

5.3.4 Fluid/Particle Interaction

According to the classification of fluid/particle interactions by Cundall (1999), there are five or six major types of fluid/particle interactions. Detailed modeling of the fluid flow using a discontinuum approach by considering small water particles, including all effects of local three-dimensional pore geometry, gives realistic solid-fluid coupling but may require unaffordable computational resources. This work tries to capture two simple situations: hydrostatic pressure and medium concentration of particles in a fluid. It neglects other effects, such as the possible surface tension in the inter-particles pore or the possible pressure gradient in the void between granular particles.

5.3.5 Calibration Process

The model parameters are determined using a calibration process. For example, the reduction factor and the particle stiffness would be adjusted to find possible ranges of values. However, the calibration process for some parameters is very difficult, requiring further laboratory testing. For instance, it is stated in many fluid mechanics texts that drag coefficients are derived from experimental data. However the formula may have neglected other possible effects, i.e., the different surface roughness of the granular particle, three-dimensional and two-dimensional effects, etc.

CHAPTER 6 EXAMPLES OF COUPLED GRANULAR AND FLUID FLOW MODELING

Illustrative examples are presented in this chapter to demonstrate the effectiveness of the coupling method. There are two types of simulations according to the fluid boundary conditions; the first example is to simulate the granular-fluid flow between two parallel plates and the second example is to simulate dropping of granular particles into a flowing fluid of finite depth. The discussion of the illustrative examples is given at the end of the chapter.

6.1 Flow of Fluid and Granular Particles between Two Fixed Parallel Plates

The flow field of 10 units wide by 1 unit high was modeled by a finite volume domain (see in Figure 6.1). Both top and bottom sides of the flow field were fixed and presented as two parallel planes. A constant pressure boundary was applied at the left boundary while at the right boundary a zero pressure boundary was maintained. The pressure gradient between the boundaries caused the fluid to flow from left to right. Flow velocities were highest in the middle region of the flow domain and became zero at the fixed plates due to viscous effects. Granular particles were introduced into the flow space after the flowing fluid was generated and the flow has stabilized. Three different cases (Ex 6.1.1, 6.1.2 and 6.1.3) with different numbers of particles (1, 6 and 45, respectively) were considered to show the effect of particle density on the simulation. The flow domain consisted of 100×10 nodes in Ex 6.1.1 as well as in Ex 6.1.2, but 200×20 nodes in Ex 6.1.3. Grid size of the flow domain was defined correspondingly to the smallest particle size. The model parameters used in each example are shown in Table 6.1. The values

were selected to demonstrate the simulation within a reasonable computational time, not necessarily to represent any real specific material. Drag coefficients were computed based on a Reynolds number following equation (5.2). Figures 6.2, 6.3 and 6.4 show the sequences of simulation of granular particle moving in fluid.

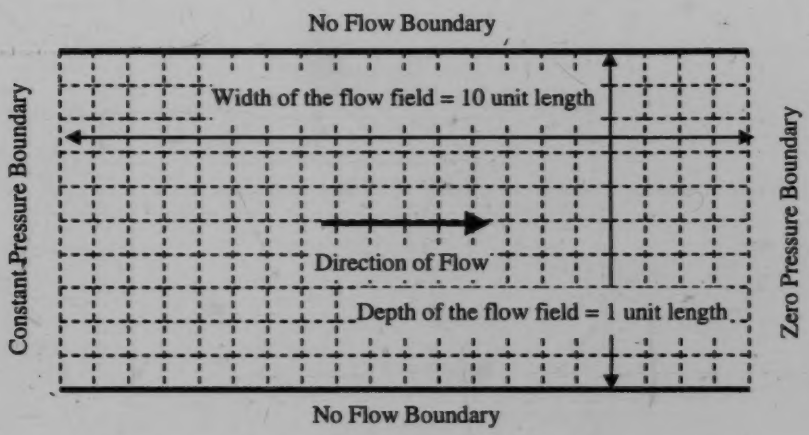
No Flow Boundary
Width of the flow field = 10 unit length
Constant Pressure Boundary
Zero Pressure Boundary
Direction of Flow
Depth of the flow field = 1 unit length
No Flow Boundary

Figure 6.1 Schematic of flow between two fixed plates

Table 6.1 Summary of Model Parameters in the Examples 6.1.1, 6.1.2, and 6.1.3

Properties	Ex 6.1.1	Ex 6.1.2	Ex 6.1.3
Number of particle(s)	1	6	45
Density of granule(g/cm^3)	2.65	2.65	2.65
Density of fluid(g/cm^3)	1.00	1.00	1.00
Coefficient of friction (°)	5	5	5
Cohesion(kPa)	0	0	0
Reduction factor	0.985	0.985	0.995

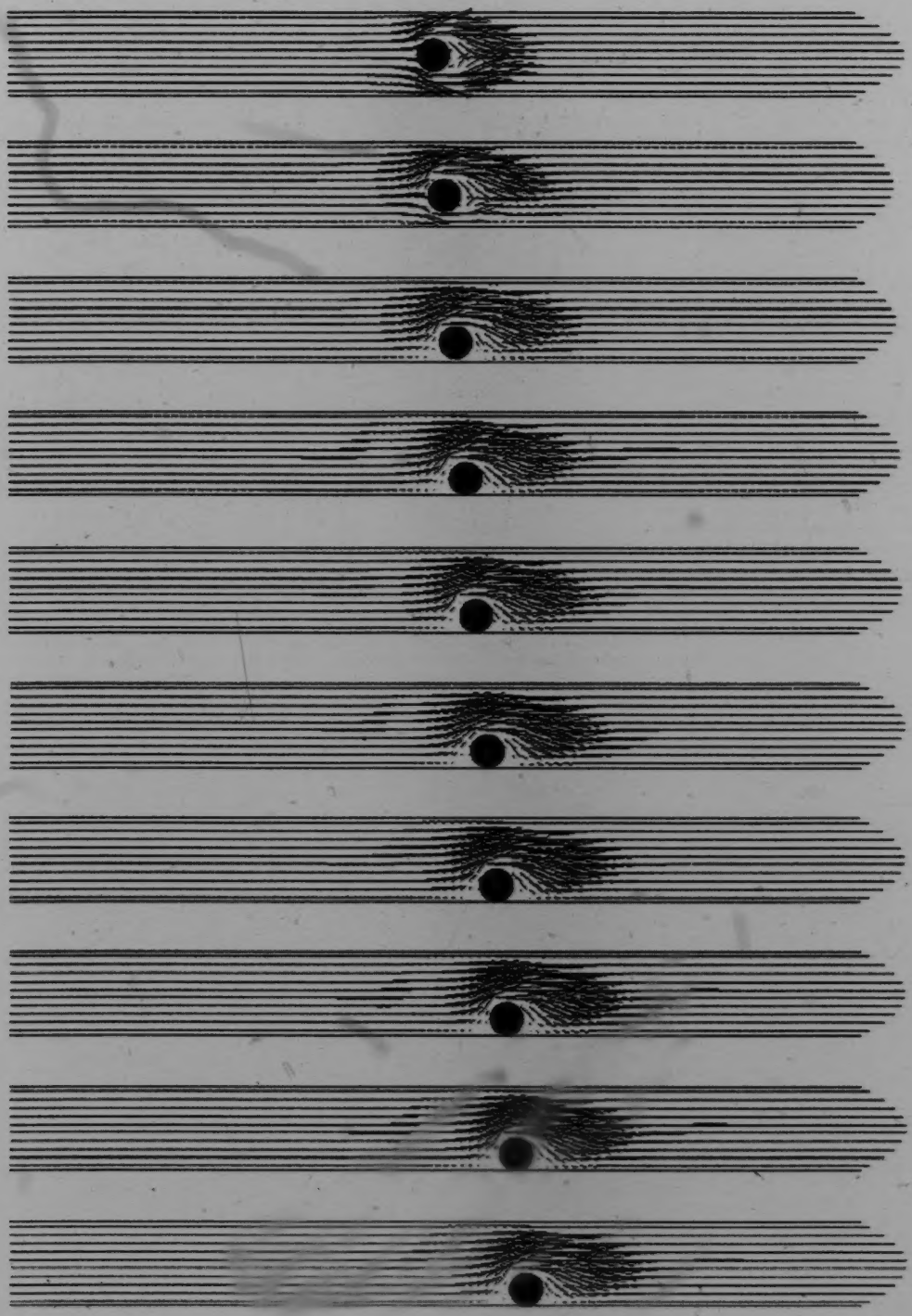

Figure 6.2 The simulation of granular and fluid flow between two fixed plates

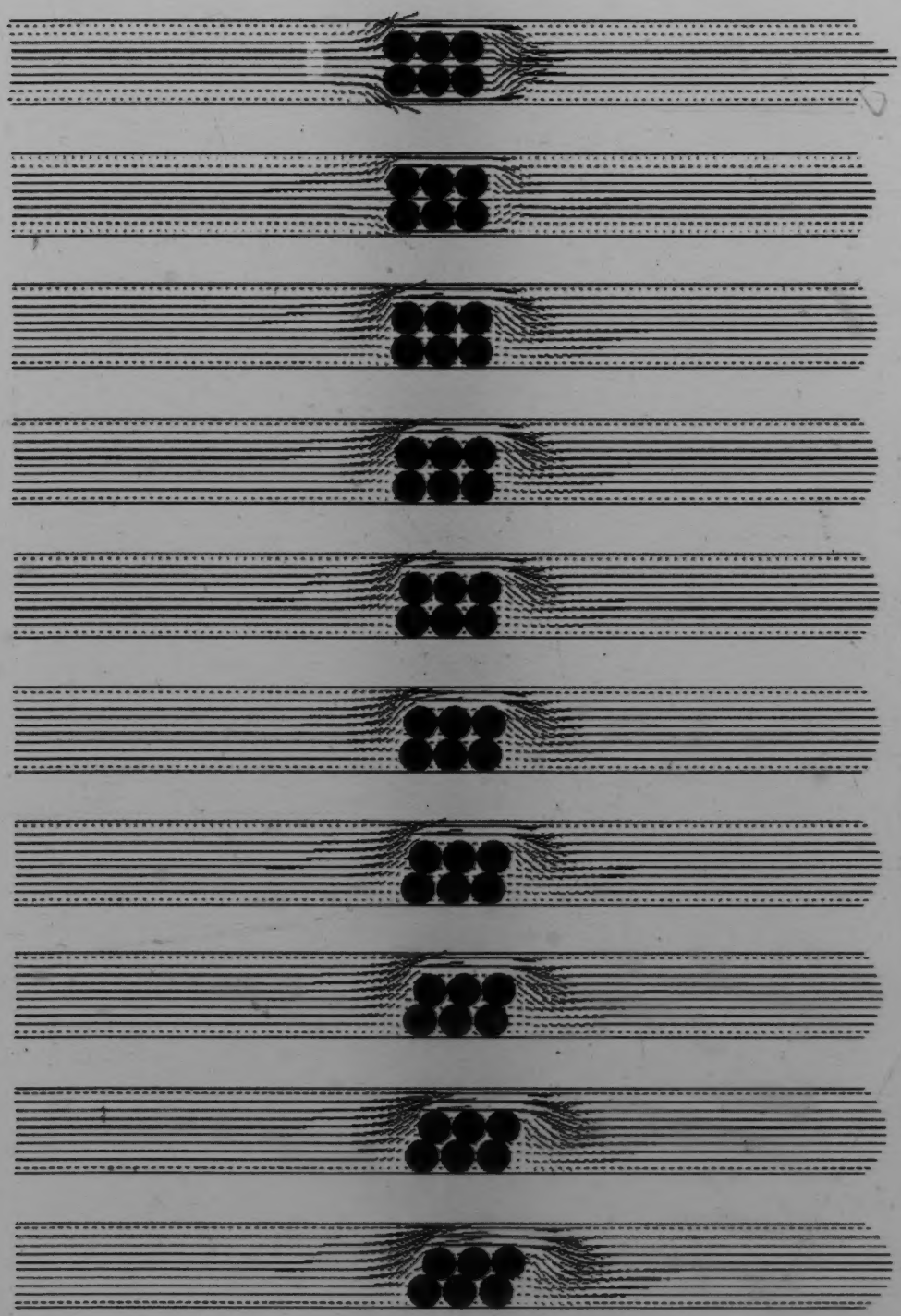

Figure 6.3 The simulation of 6 granular particles and fluid flow between two fixed plates

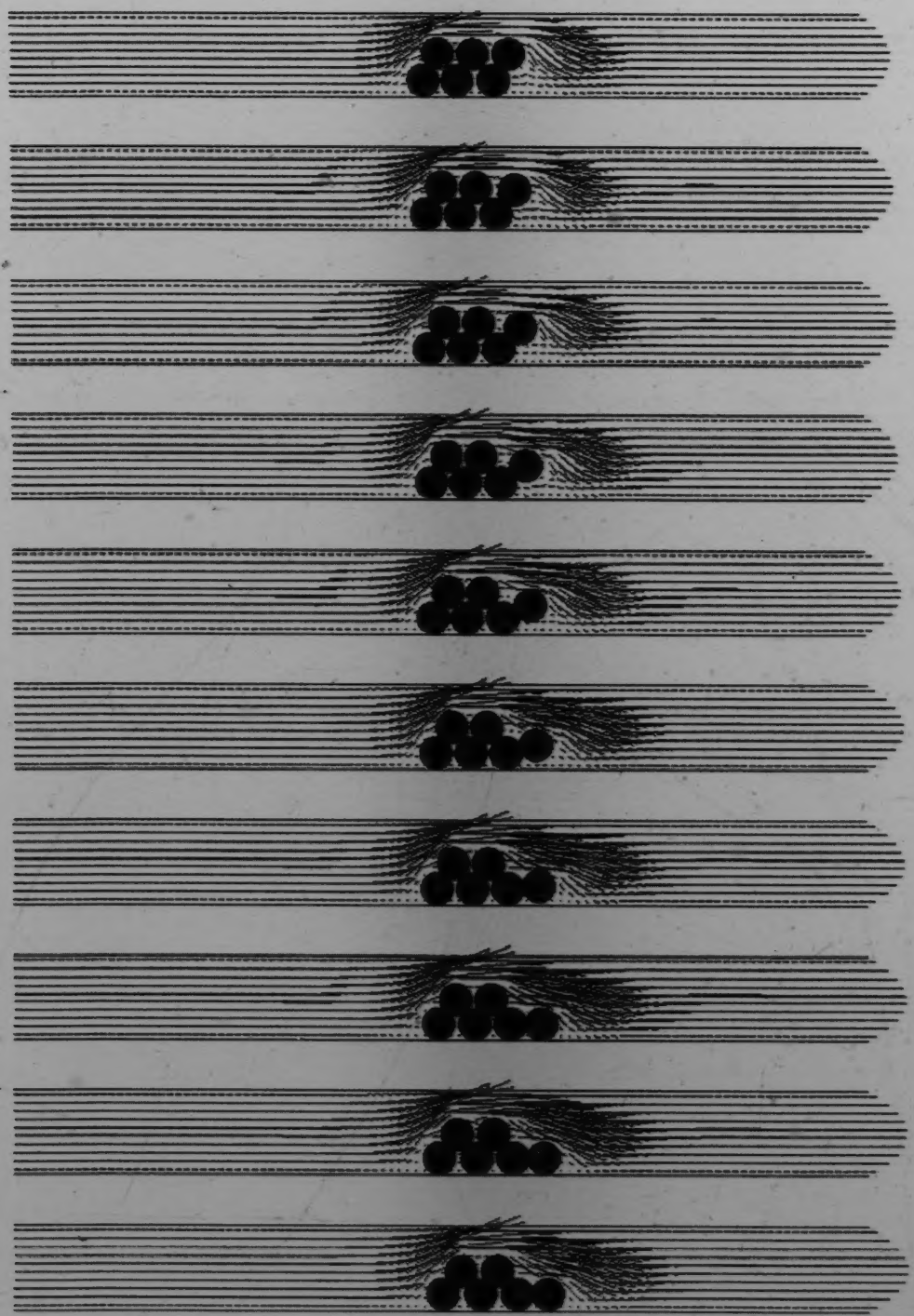

Figure 6.3 The simulation of 6 granular particles and fluid flow between two fixed plates (cont)

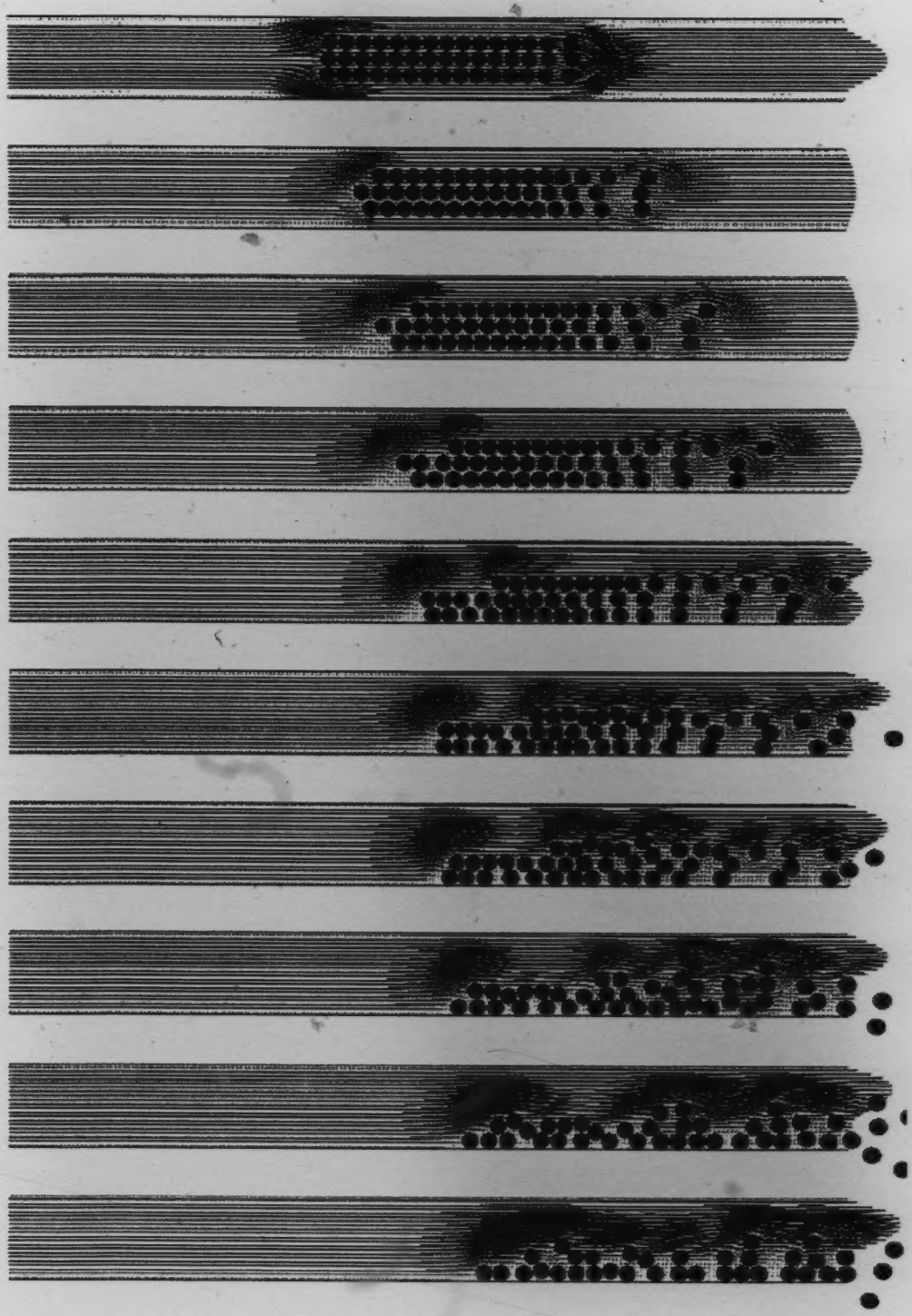

Figure 6.4 The simulation of 45 granular particles and fluid flow between two fixed plates

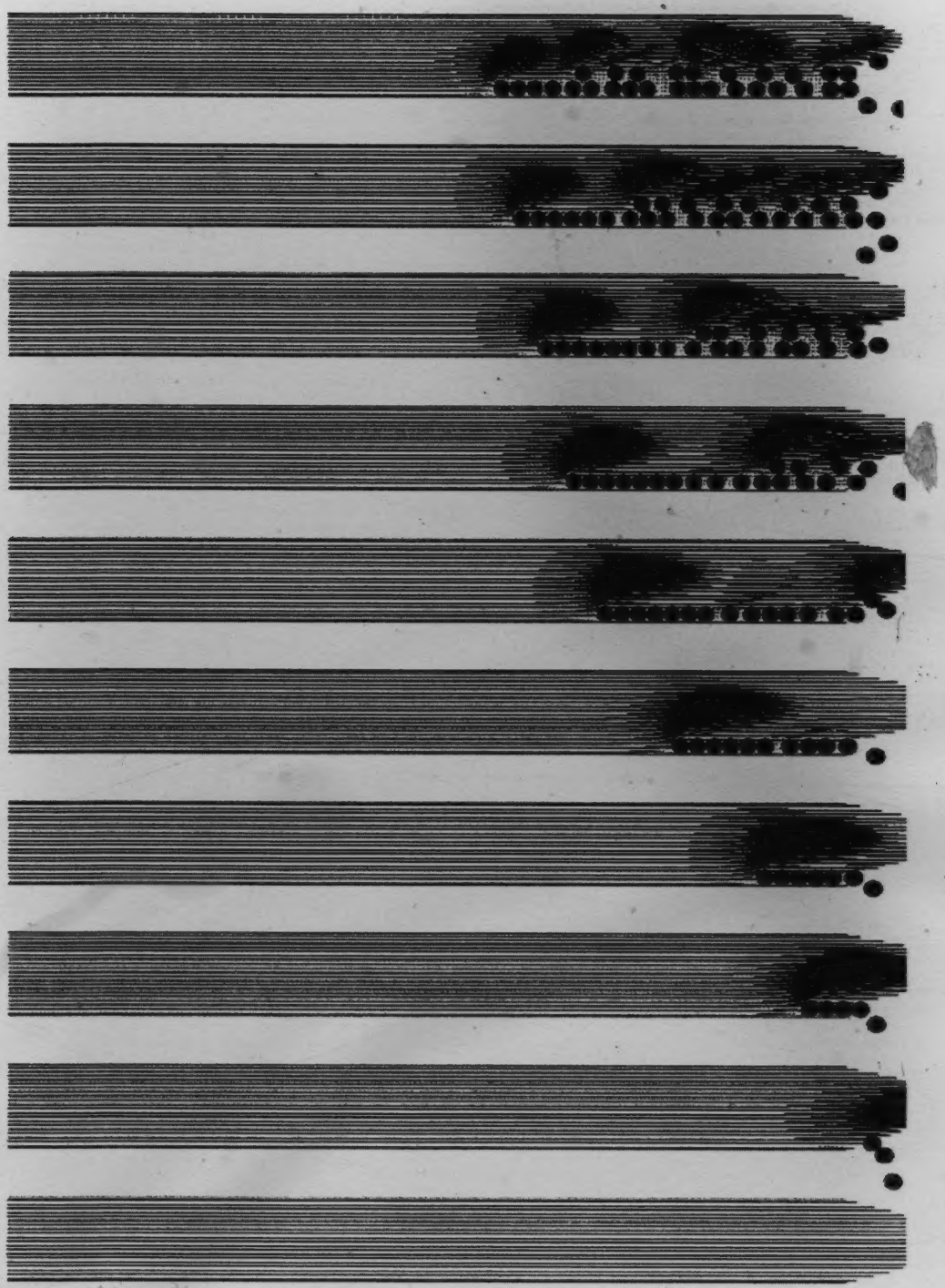

Figure 6.4 The simulation of 45 granular particles and fluid flow between two fixed plates (cont)

6.2 Granular Particles Dropped into Flowing Fluid

The flow field consisted of 10 units wide by 1unit high was modeled by a finite volume domain (see in Figure 6.5). The bottom of the flow field was a fixed plane, whereas the top part was a free surface. A constant pressure boundary was applied at the left boundary, while at the right boundary a zero pressure boundary was maintained. The pressure gradient between the boundaries caused the fluid to flow from left to right. The fluid velocities were the highest at the top surface and became zero at the bottom boundary. Granular particles were dropped into the fluid after the flow of fluid was generated and the flow stabilized. Three different cases (Ex 6.2.1, 6.2.2 and 6.2.3) with different numbers of granular particles (1, 6 and 45, respectively) were considered to show the effect of particle density on the simulation. Similar to Section 6.1, the flow domain consisted of 100×10 nodes in Ex 6.2.1 as well as in Ex 6.2.2, but 200×20 nodes in Ex 6.2.3. The grid size of the flow domain was defined correspondingly to the smallest particle size. The model parameters used in each example are shown in Table 6.2. The values were selected to demonstrate the simulation within a reasonable computational time, not necessarily to represent any real specific material. Drag coefficients were computed based on a Reynolds number following equation (5.2). Figures 6.5, 6.6 and 6.7 show the sequences of simulation of granular particle dropped in fluid.

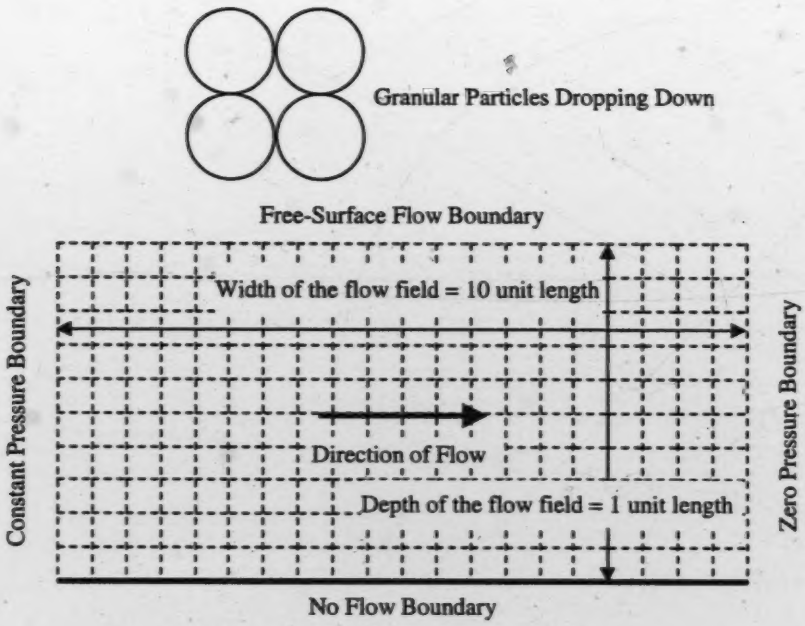
Granular Particles Dropping Down
Free-Surface Flow Boundary
Width of the flow field = 10 unit length
Constant Pressure Boundary
Zero Pressure Boundary
Direction of Flow
Depth of the flow field = 1 unit length
No Flow Boundary

Figure 6.5 Schematic of flow in the flow field with free surface on top

Table 6.2 Summary of Model Parameters in the Examples 6.2.1, 6.2.2, and 6.2.3

Properties	Ex 6.2.1	Ex 6.2.2	Ex 6.2.3
Number of particle(*s*)	1	6	45
Density of granule(g/cm^3)	2.65	2.65	2.65
Density of fluid(g/cm^3)	1.00	1.00	1.00
Coefficient of friction (°)	5	5	5
Cohesion(*kPa*)	0	0	0
Reduction factor	0.995	0.995	0.9995

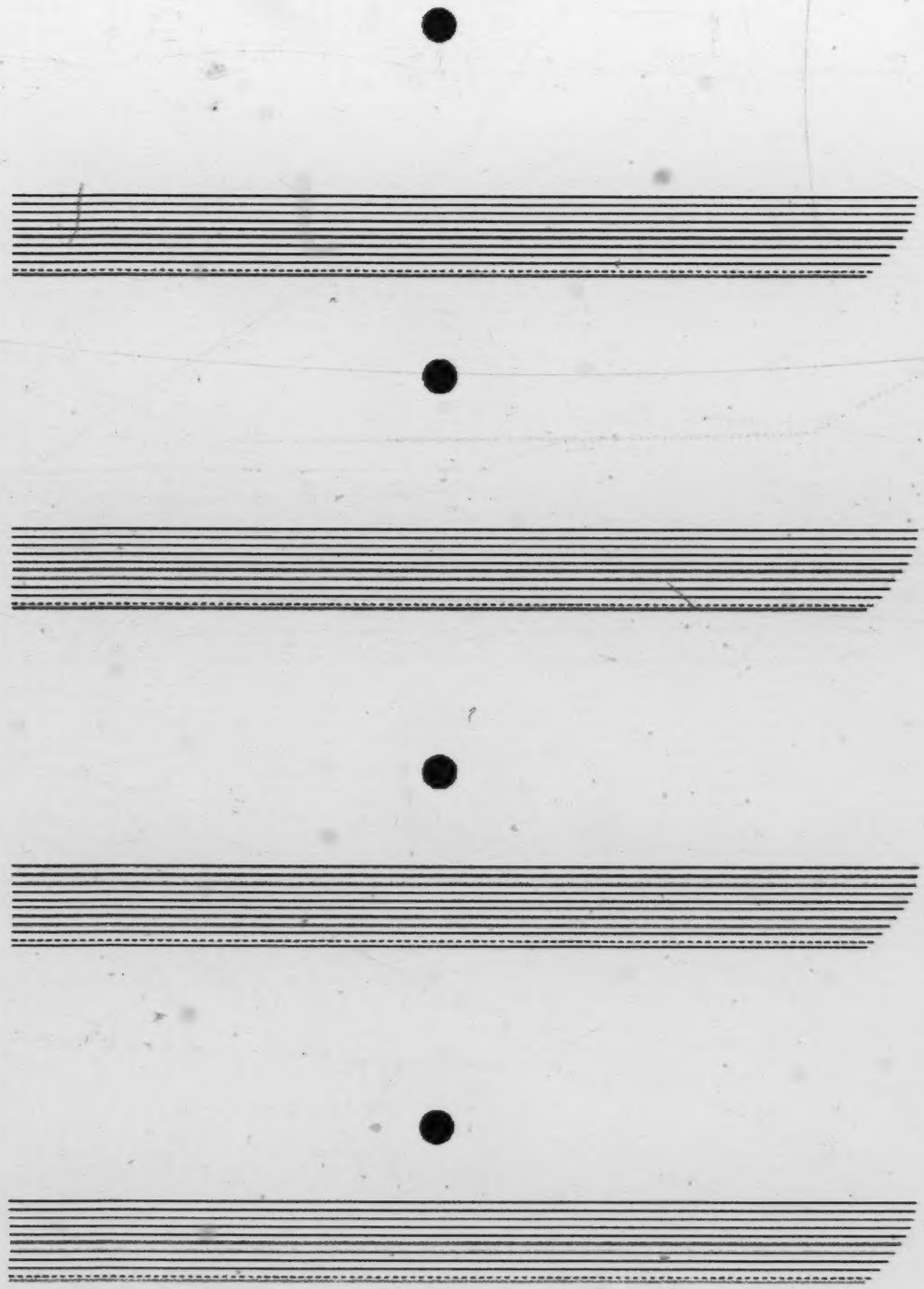

Figure 6.6 The simulation of granular and fluid flow in the free-surface flow space

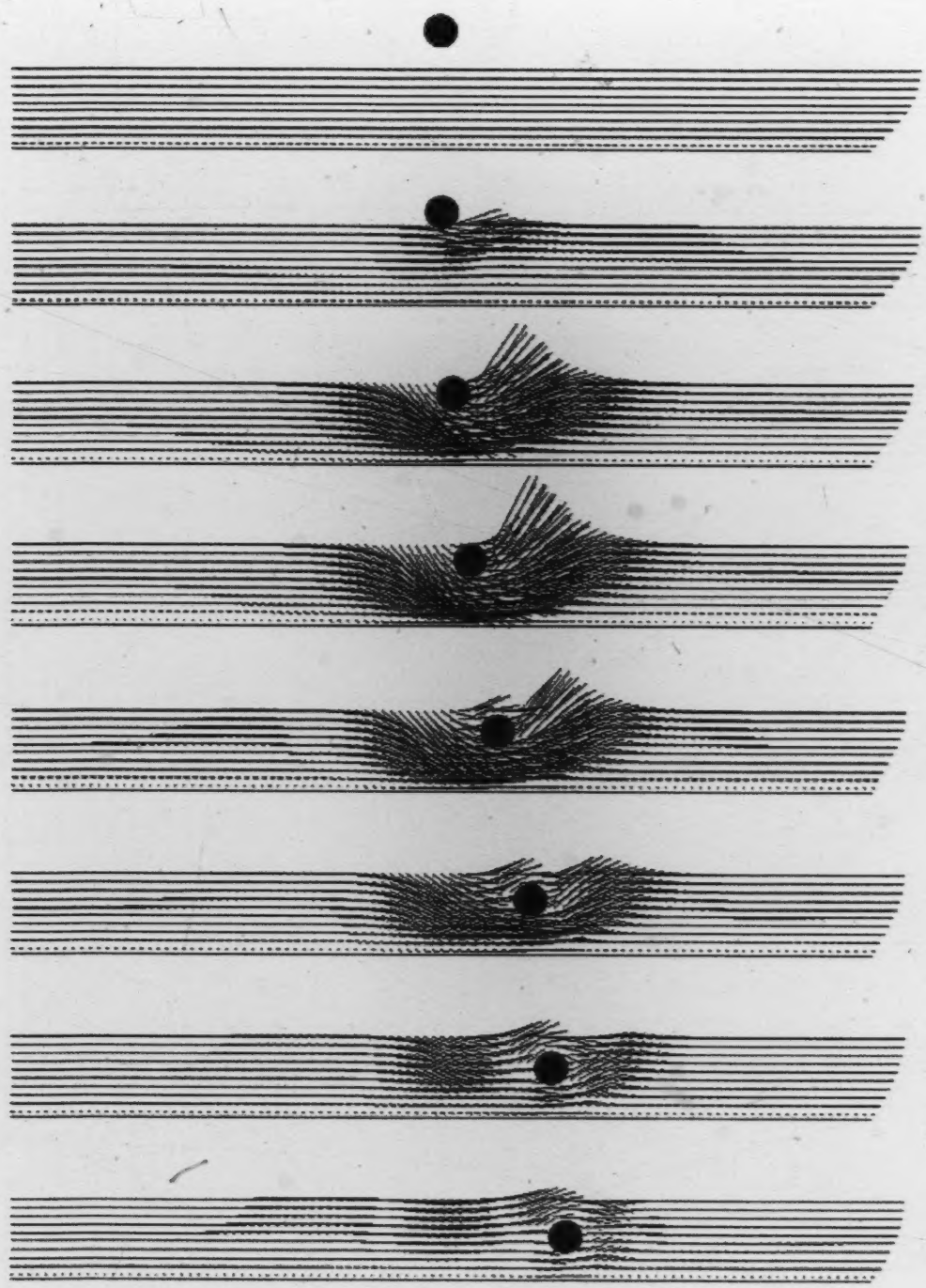

Figure 6.6 The simulation of granular and fluid flow in the free-surface flow space (cont)

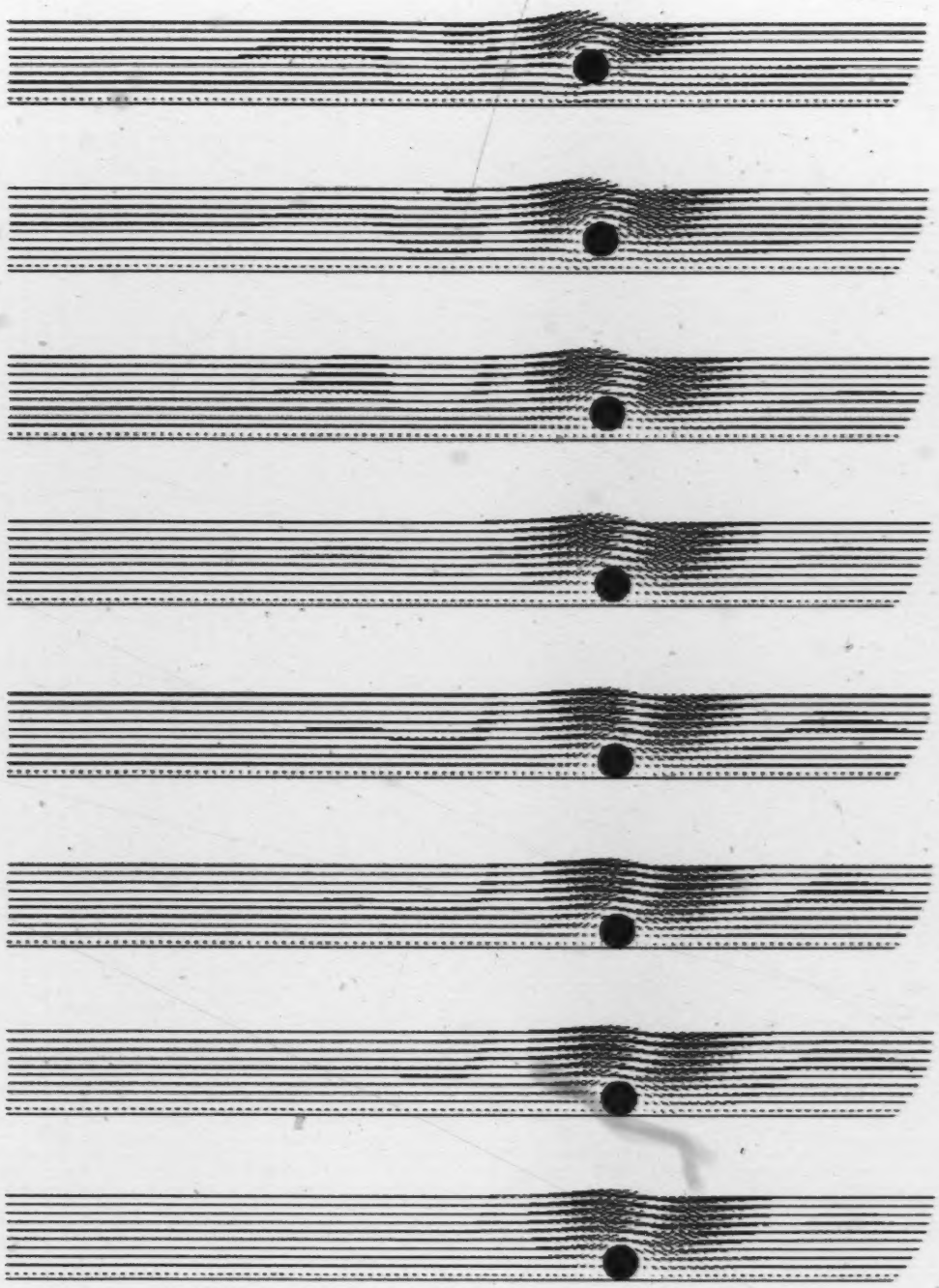

Figure 6.6 The simulation of granular and fluid flow in the free-surface flow space (cont)

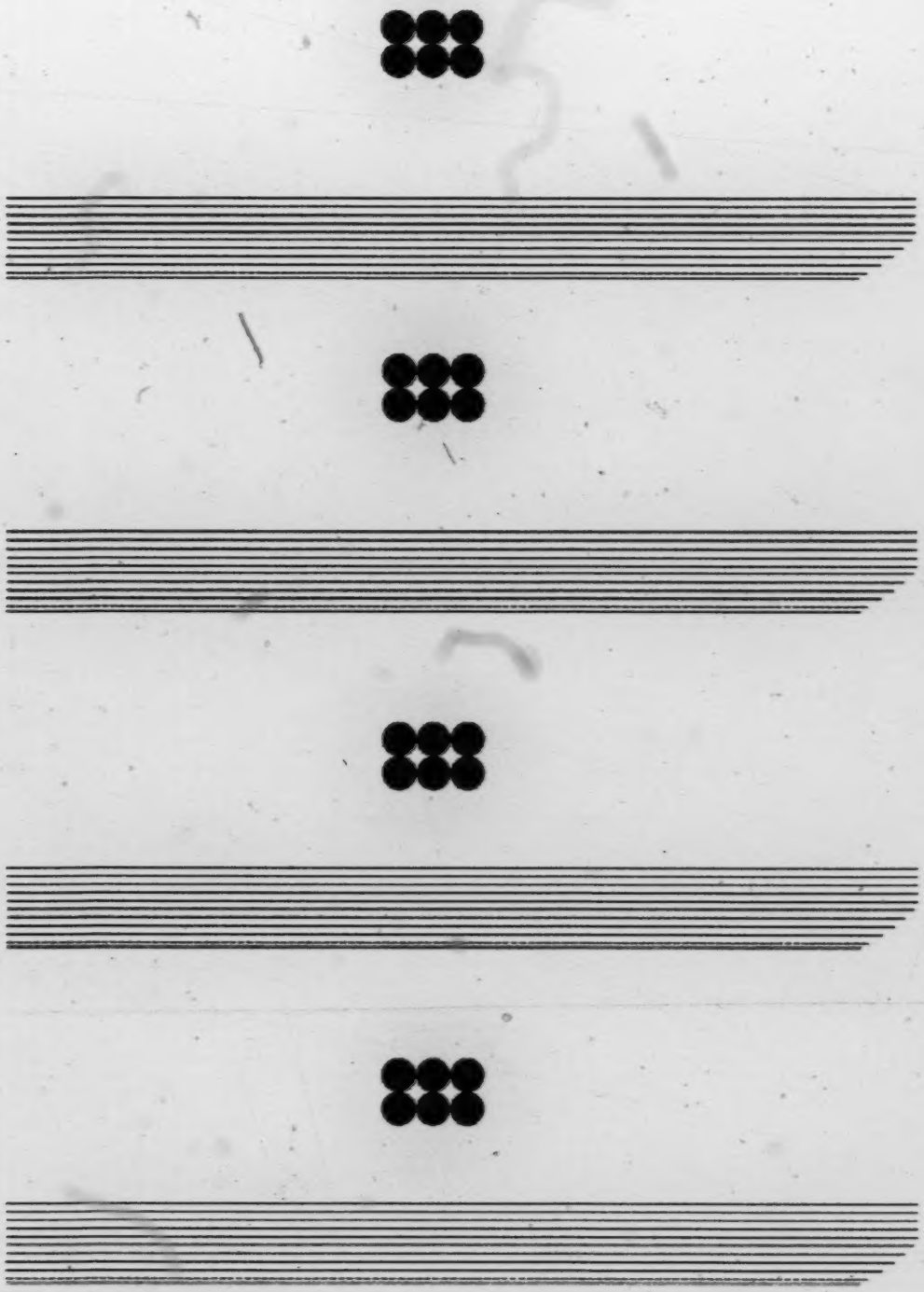

Figure 6.7 The simulation of 6 granular particles and fluid flow in the free-surface flow space

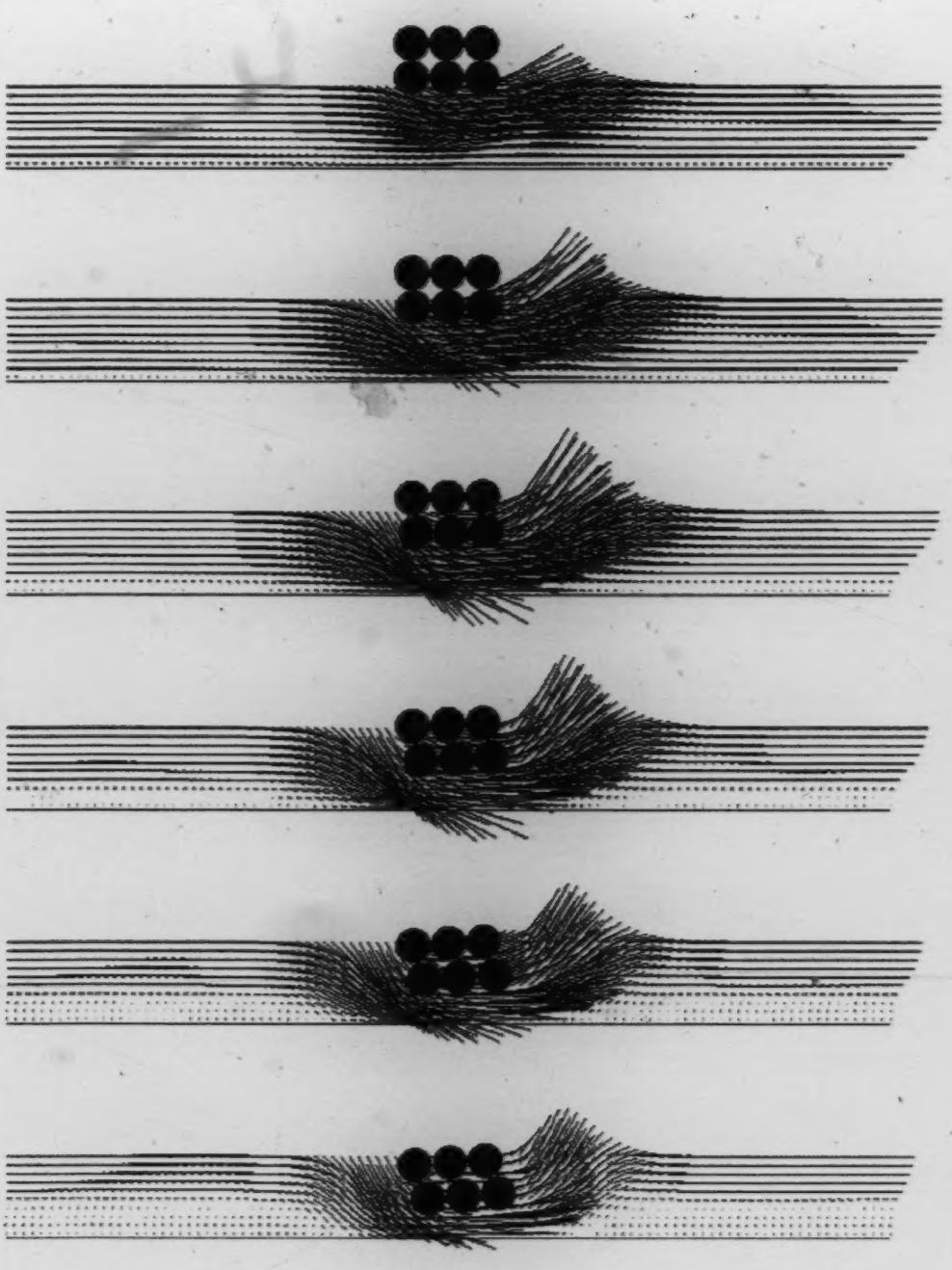

Figure 6.7 The simulation of 6 granular particles and fluid flow in the free-surface flow space (cont)

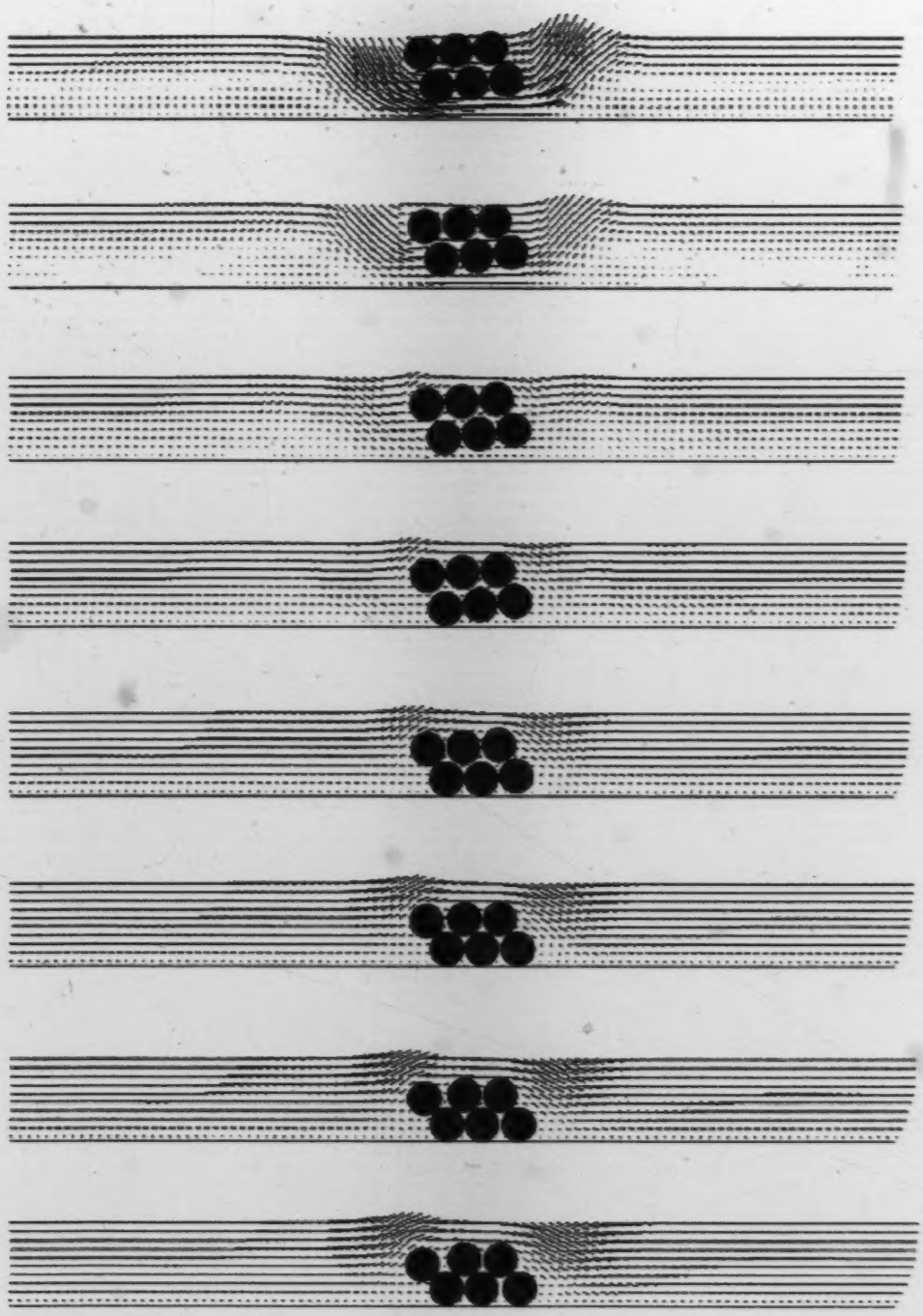

Figure 6.7 The simulation of 6 granular particles and fluid flow in the free-surface flow space (cont)

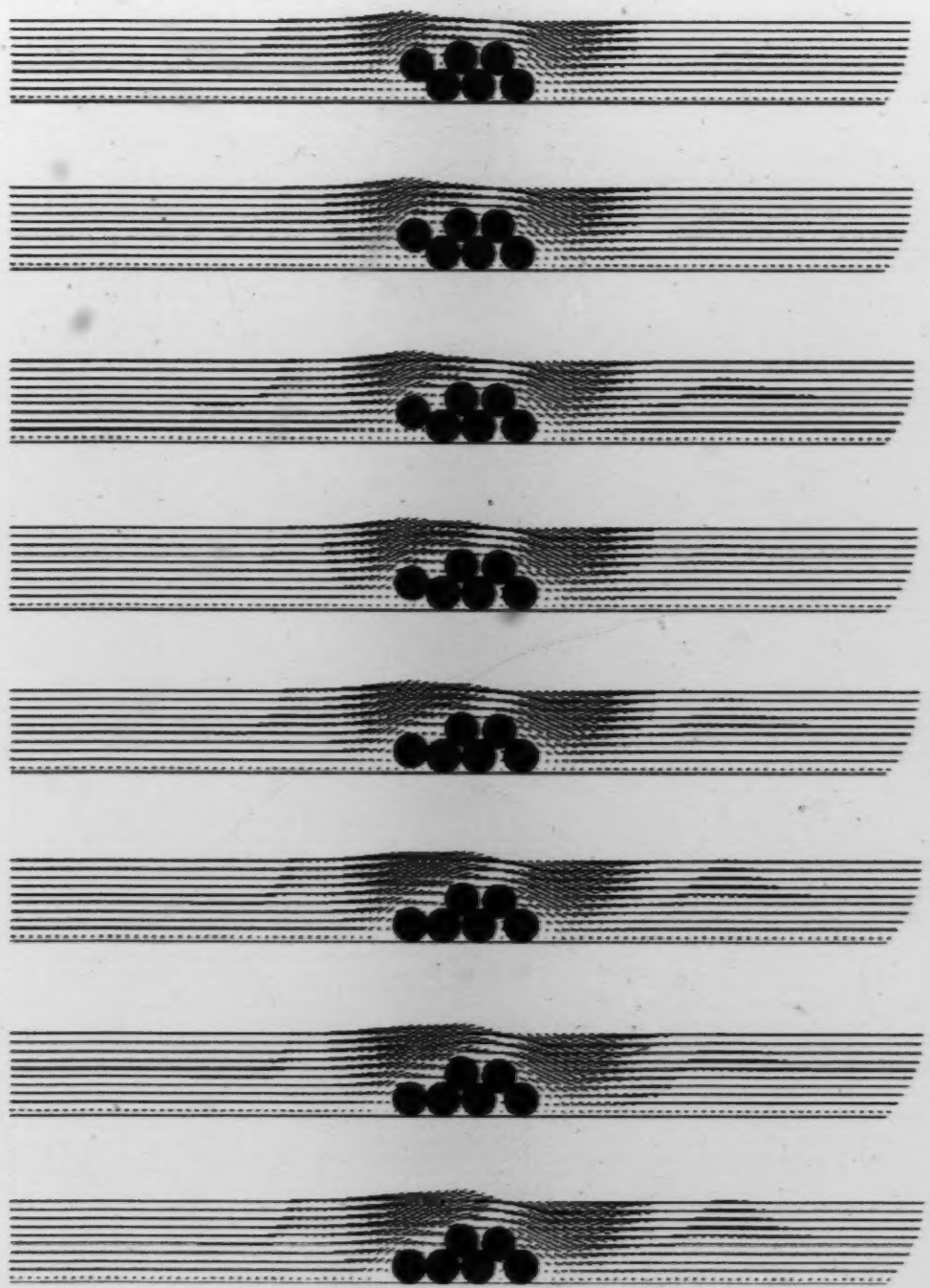

Figure 6.7 The simulation of 6 granular particles and fluid flow in the free-surface flow space (cont)

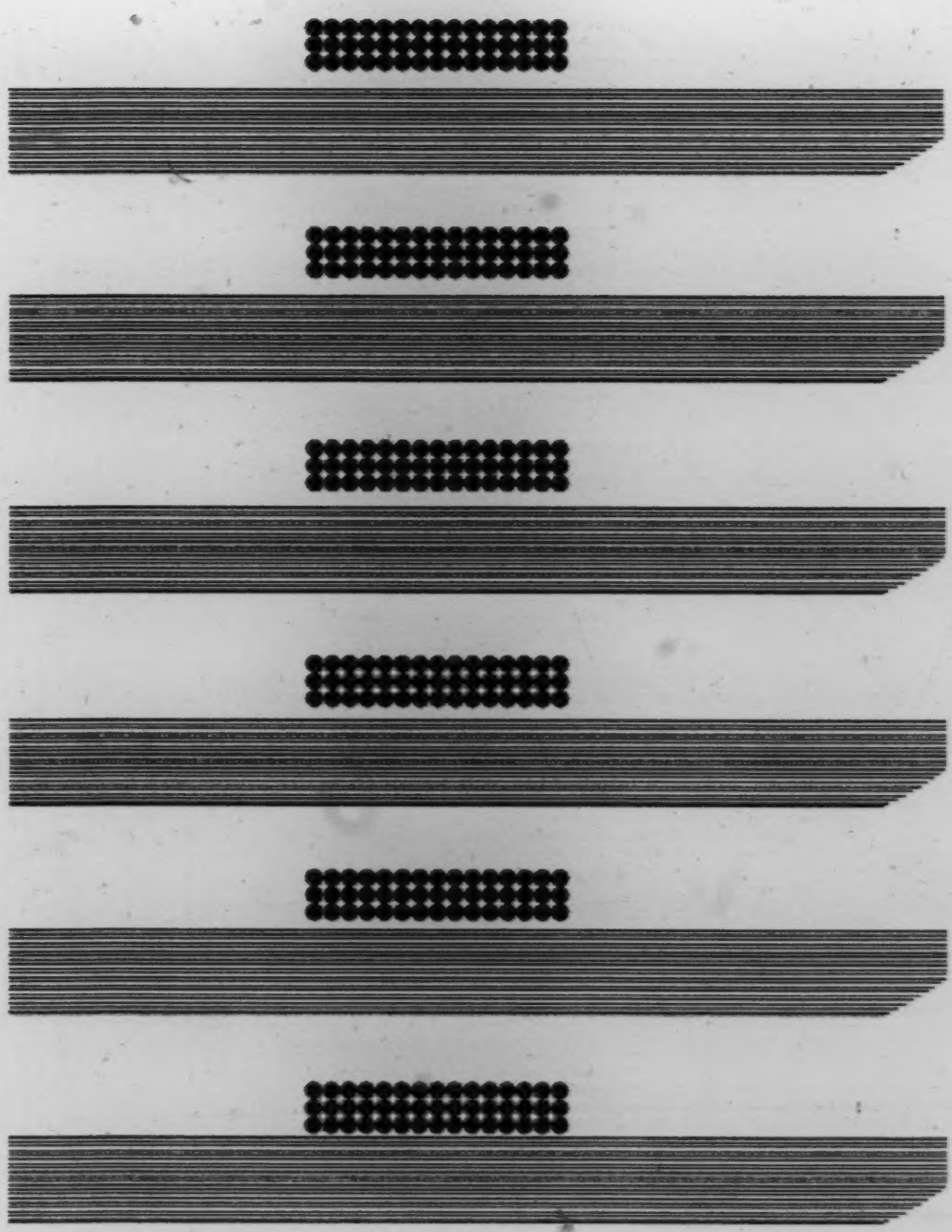

Figure 6.8 The simulation of 45 granular particles and fluid flow in the free-surface flow space

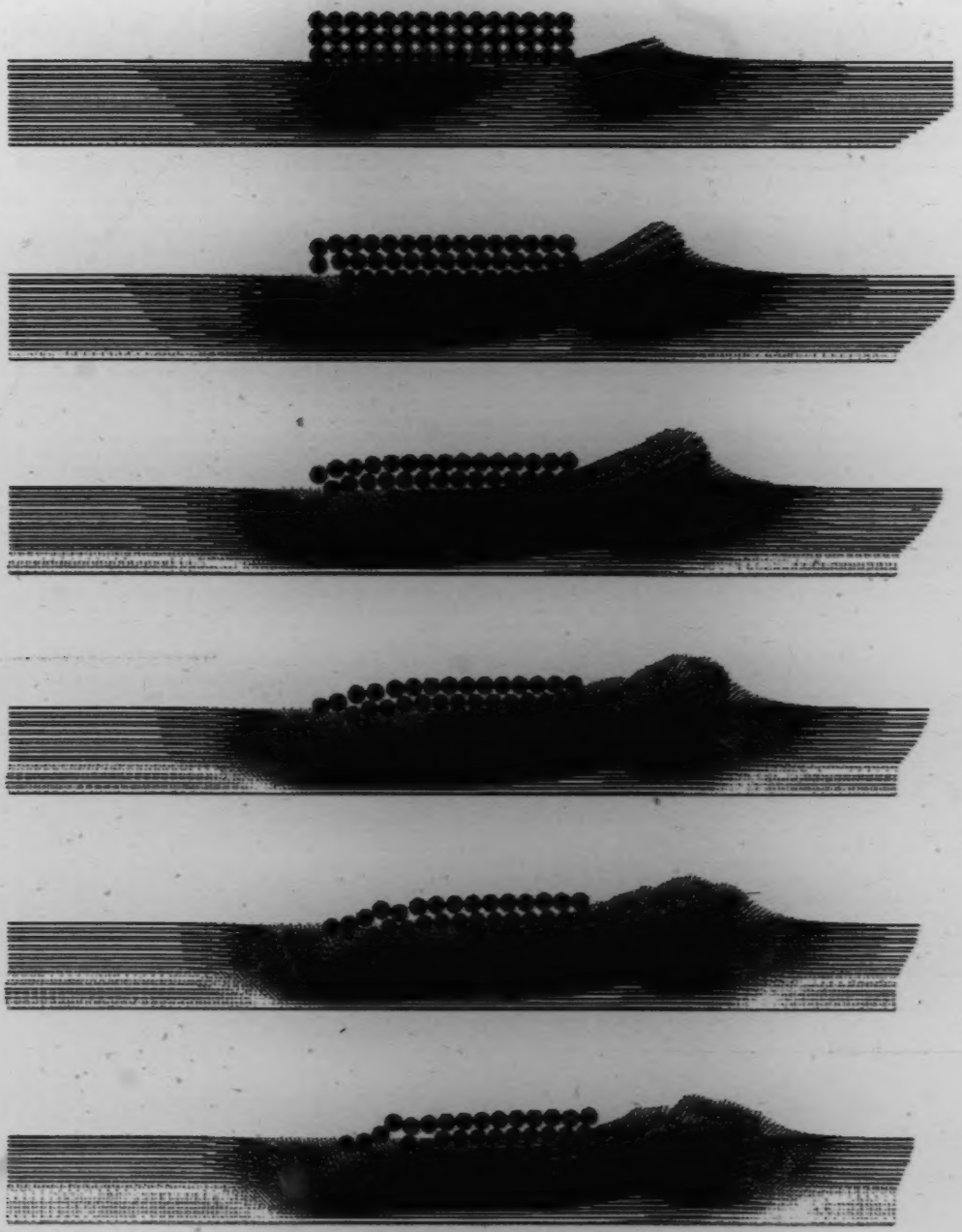

Figure 6.8 The simulation of 45 granular particles and fluid flow in the free-surface flow space (cont)

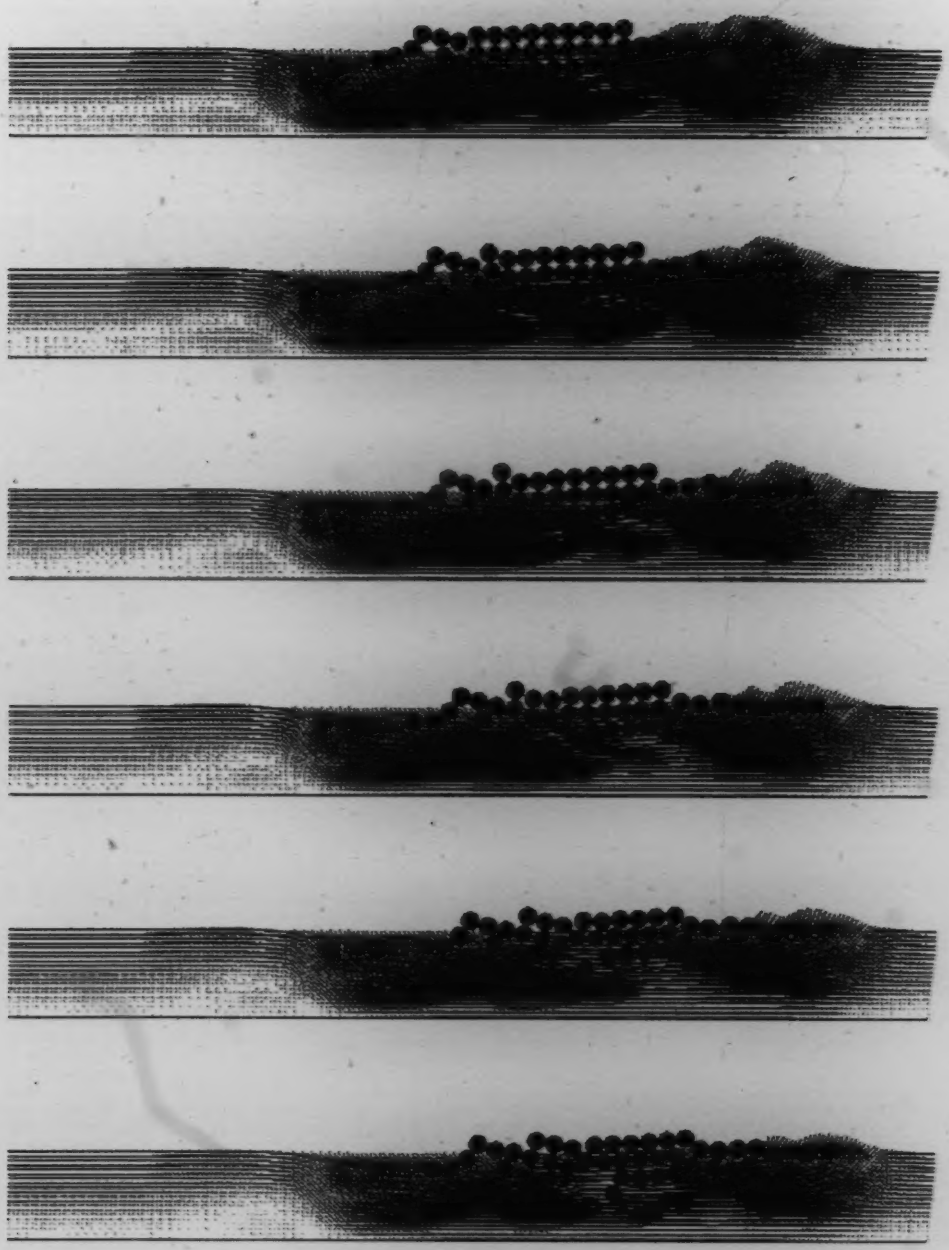

Figure 6.8 The simulation of 45 granular particles and fluid flow in the free-surface flow space (cont)

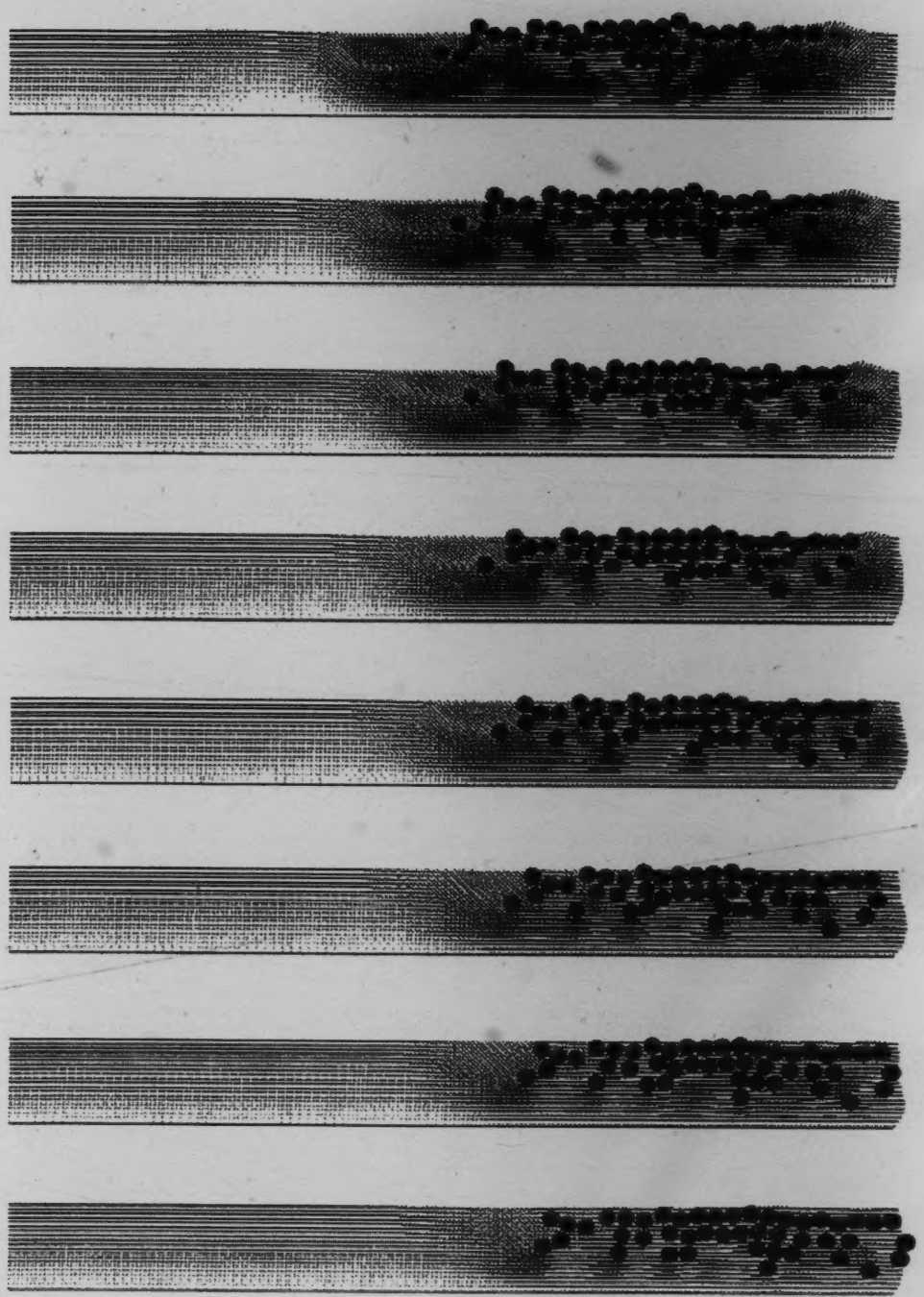

Figure 6.8 The simulation of 45 granular particles and fluid flow in the free-surface flow space (cont)

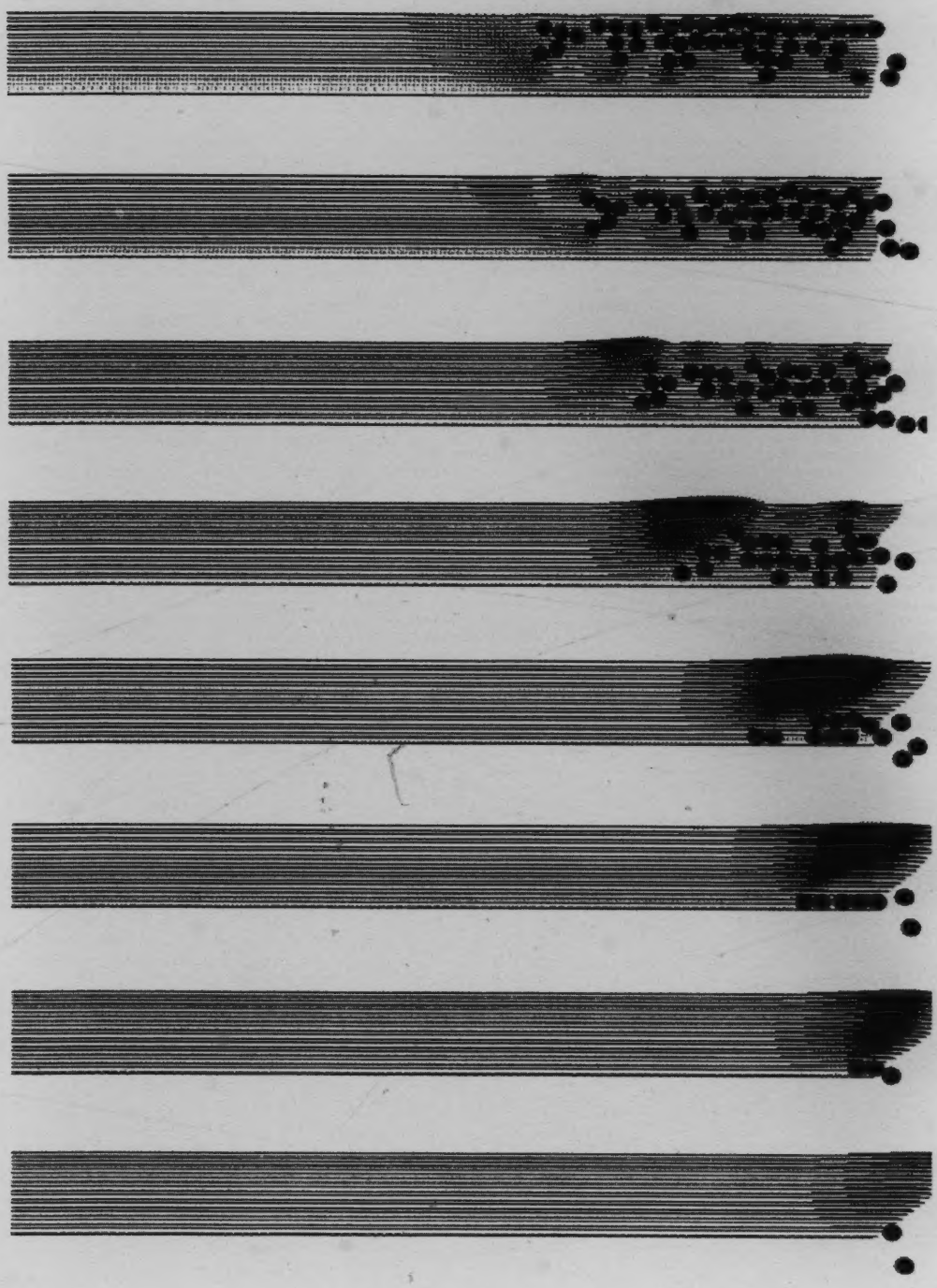

Figure 6.8 The simulation of 45 granular particles and fluid flow in the free-surface flow space (cont)

6.3 Discussions

In the first example, flow between two parallel plates was considered. To display the graphical results, granular particles were represented by red circles and the fluid velocity vectors were shown by the straight lines with their length proportional to their velocities. As expected, the fluid velocities were the highest in the middle region between two fixed plates, and became zero value near the plates. It is seen that the presence of the granular particle caused the fluid to flow around the particle at the same time allowing some fluid (less than usual) to flow "through" the granular particle. Since the granular particles were much heavier than the fluid in all cases, they quickly settled to the bottom. The fluid induced drag forces that moved the granular particles from left to right. Finally, the granular particles passed the edge of the plate and dropped into space under the action of gravity. Considering the impact of particle density on the simulation, three different numbers of granular particles were used. In each case, the results are roughly described as follows. In Ex 6.1.1, a granular particle was dragged along the flowing fluid. When the particle reached the flow boundary, its movement was deterred by friction. The event of a fluid flowing around the particle was displayed most apparently in this situation. In Ex 6.1.2, the pack of 6 granular particles sank down to the bottom of the flow field. The contact force between particles caused one particle to move around the others. In Ex 6.1.3, the collection of 45 granular particles was dragged along the flowing fluid. The particle movements were also deterred when they were in contact with the flow boundary. When particles were moving out of the flow space, they dropped down due to the gravitational forces.

The second illustrative examples modeled the granular particle being dropped into the flowing fluid. The fluid velocities were the highest value at the top free surface and became zero value at the bottom fixed plate. Initially, granular particles were dropped into the fluid. They fell vertically in space under gravity. After they came into contact with the fluid, drag and buoyancy were introduced. Simultaneously the top surface of the fluid was moving up and down due to the particle impact. Drag forces induced by the fluid flow caused the granular particles to move from the left to right side following the direction of fluid flow. Buoyant force was acting up against gravity and retarded the movement of the granular particle in the vertical direction. Again, since granular particles were much heavier than the fluid, they quickly settled at the bottom. Eventually, the granular particles passed the edge of the plate and dropped into space under gravity. Three different situations with different numbers of granular particles were simulated as well. The results resembled the ones in the first illustrative example. In Ex 6.2.1, after a granular particle dropped and came into contact with the fluid, it was being dragged along the flowing fluid. Its movement was deterred by friction forces, when the particle was in touch with the flow boundary. In Ex 6.2.2, the pack of 6 granular particles dropped and sank down to the bottom of the flow field. The contact force between the particles caused one particle to move around the others. In Ex 6.2.3, the collection of 45 granular particles was dropped into the flow domain. They were dragged along the flowing fluid from left to right. The particle movement was also deterred when the particle was in touch with the flow boundary.

As a consequence of the explicit numerical scheme employed in both DEM and fluid flow calculations; the time-step selected must be smaller than the critical time-step.

An inappropriate choice of time-step can cause numerical problems and unexpected results. The effects of inappropriate time-step size are summarized here.

a) Effect on the continuum fluid computation

- *Inaccurate result*: The values of fluid flow velocity are not exactly the same as the one computed from the closed form solution.
- *Instability calculation*: The time-step size is much larger than the critical time-step which causes numerical instability.

b) Effect on the DEM calculation

- *Inappropriate contact force*: The causes of this unwanted result may come from both the inappropriate time-step size and improper specification of the contact stiffnesses. Figure 6.9 and Figure 6.10 show examples of inappropriate contact force. Figure 6.9 shows the case where the contact force was not developed causing too much overlap between particles. When the contact forces were too large, as in Figure 6.10, the particles were bouncing excessively, causing divergence. Particles can eventually move past the flow boundary without being detected.

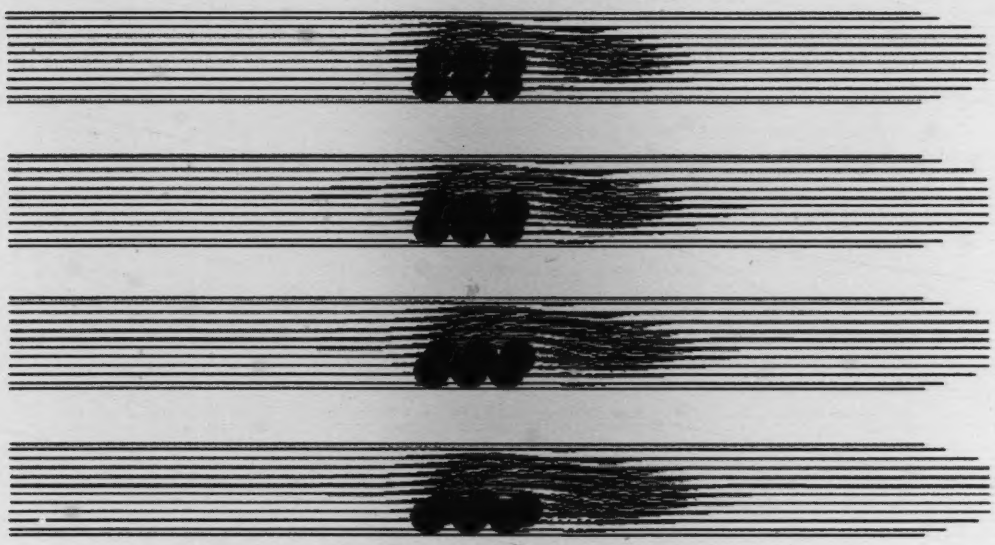

Figure 6.9 Huge amount of overlap between particles

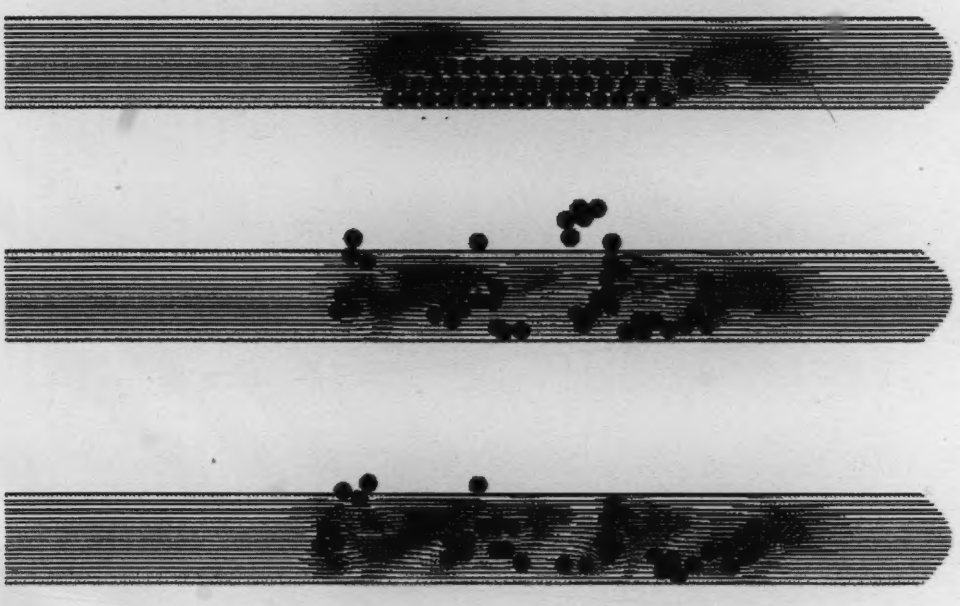

Figure 6.10 Too large contact forces

- *Unsuitable particle movement*: Granular particle can move too fast and not smoothly. This can cause inaccurate calculation or even numerical instability.

c) Effect to the fluid/particle interaction

- *Instability calculation*: This resulted from the time-step being larger than the critical time-step either in one or both of the simulations. It can cause the incorrect solution or even numerical instability of the whole system. Figure 6.11 shows the case of particles dropping too fast causing numerical instability. (This may also be the result of unsuitable velocity reduction factor.)

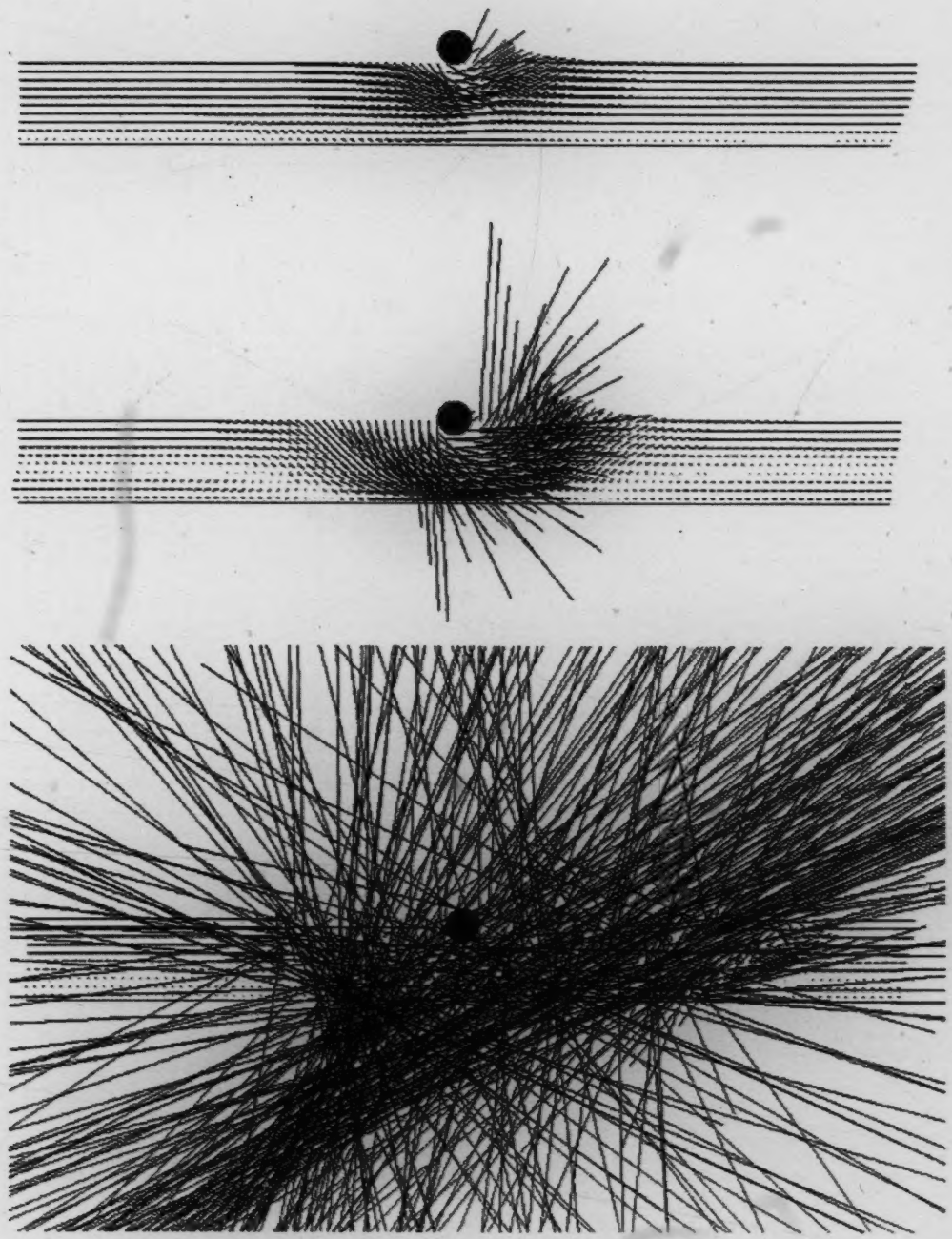

Figure 6.11 Instability calculation

CHAPTER 7 CONCLUSION

A method of coupling the discontinuum approach to model the movement of granular material and the continuum approach to simulate the fluid flow is proposed. A program is implemented in Microsoft Visual C++ version 6.00 based on these approaches with the coupling mechanisms. The transient fluid flow is modeled using the finite volume scheme, whereas the movement of granular material is simulated by the discrete element method. The solution of fluid flow simulation is obtained by solving the 2-D Navier-Stokes equations with the continuity equation. To couple these two different physical systems, the interactions between fluid and granular particle are incorporated into the simulation: drag, buoyancy and the velocity reduction factor. Since the explicit numerical scheme is used to obtain a solution both in DEM and fluid flow simulation, the size of the time-step must be selected carefully. Two types of illustrative examples were presented graphically to demonstrate the effectiveness of the proposed technique.

It can be observed that the drag coefficients and velocity reduction factors play an important role in the simulation of wet granular flow. The concept of the drag coefficients relies heavily on experimental data that is broadly developed in fluid mechanics. While the notion of velocity reduction factor is an ideal numerical method to represent the particle effect, it still requires improvement to increase robustness. The idea of velocity reduction factor can be developed further relating to the concept of permeability. In the case of low or medium concentrations of granular particles in a fluid, this combination of fluid-particle interactions seems to be appropriate. However, if the simulation conditions are changed (i.e., particles are closely spaced and surface tension or pressure is generated

in the void between particles due to the trapped fluid), it will be necessary to include other kinds of fluid-particle interaction into the coupling method.

Finally, recommendations for further research are given. The proposed method here is still in its development stage. In order to compare the simulation results with real behavior of wet granular flow quantitatively, many issues need to be addressed, such as:

- The development of a 3D simulation method;
- Coupling other kinds of fluid-solid interactions;
- The improvement of the concept of velocity reduction factor both numerically and theoretically;
- The development of a fluid flow simulation method from the finite volume method to the finite element method;
- The requirements of experimental tests under some specific conditions.

Furthermore, there are other useful topics such as the effect of flow turbulence, particle fabric, particle arrangement, particle rotation, etc. that should be studied additionally. These related topics would expand the scope of the problems more extensively and more practically. Nevertheless, the proposed method provides a sensible framework to model solid-fluid interaction.

REFERENCES

Antony, S. J. (2000). "Evolution of force distribution in three-dimensional granular media." Physical Review E, vol.63, 011302.

Babic', M., and Shen, H. H. (1990). "Simulations of gravity-driven channel flows of disks floating on the flowing viscous fluid." Mechanics Computing in 1990's and Beyond, vol.2 Structural and Material Mechanics, May 20-22, 1991. 1259-1263.

Chan, D. H. (1993). "Numerical simulation of wet granular flow." The International Conference on Soft Soil Engineering, November 8-11, 1993. 68-73.

Chang, C. S., and Misra, A. (1989). "Computer simulation and modeling of mechanical properties of particulates." Computers and Geotechnics, vol.7, 269-287.

Cleary, P. W., Metcalfe, G., and Liffman, K. (1998). "How well do discrete element granular flow models capture the essentials of mixing processes?" Applied Mathematical Modelling, vol.22, 995-1008.

Cundall, P. A. (1971). "A computer model for simulating progressive large scale movements in blocky rock systems." Proceedings of the Symposium of the International Society of Rock Mechanics, Nancy, Vol. 1, paper no.II-8.

Cundall, P. A. (1988). "Formulation of a three-dimensional distinct element model—part I. A scheme to detect and represent contacts in a system composed of many polyhedral blocks." International Journal of Rock Mechanics, Mining Sciences and Geomechanics, vol.25, no.3, 107-116.

Cundall, P. A. (1999). "Technical Note: The incorporation of fluid coupling into PFC."

Cundall, P. A., and Hart, R. D. (1992). "Numerical modeling of discontinua." Engineering Computations, vol.9, 101-113.

Cundall, P. A., and Strack, O. D. L. (1979). "A discrete numerical model for granular assemblies." Geotechnique, vol.29, No. 1, 47-65.

Detournay, C., and Cundall, P. A. (1999). "Numerical modeling of free surface flow in porous media using *FLAC3D*." FLAC and Numerical Modeling in Geomechanics, Detournay & Hart (eds), Balkema, Rotterdam, 155-161.

Evett, J. B. and Liu, C. (1987). Fundamentals of Fluid Mechanics, McGraw-Hill, Inc. New York. 1987.

Gavrilov, D., and Vinogradov, O. (1997). "Recursive inverse matrix algorithm in granular mechanics applications." Computational Mechanics, vol.20, 407-411.

Gerhart, P. M., Gross, R. J., and Hochstein, J. I. (1992). Fundamentals of Fluid Mechanics 2nd edition, Addison-Wesley Publishing Company. Reading, Mass., 1992.

Hart, R., Cundall, P. A., and Lemos, J. (1988). "Formulation of a three-dimensional distinct element model—part II. Mechanical calculations for motion and interaction of a system composed of many polyhedral blocks." International Journal of Rock Mechanics, Mining Sciences and Geomechanics, vol.25, no.3, 117-125.

Hopkins, M. A. (1992). "Numerical simulation of systems of multitudinous polygonal blocks." CRREL REPORT 92-22.

Itasca Consulting Group, Inc. (1999). PFC2D (Particle Flow Code in 2 Dimensions) Manual, Version 2.0, ICG, Minneapolis, Minnesota.

Jensen, R. P., Bosscher, P. J., Plesha, M. E., and Edil, T. B. (1999). "DEM simulation of granular media—structure interface: effects of surface roughness and particle shape." International Journal for Numerical and Analytical Methods in Geomechanics, vol.23, 532-547.

Minchinton, A., and Lynch, P. M. (1996). "Fragmentation and heave modeling using a coupled discrete element gas flow code." Rock Fragmentation by Blasting, Mohanty Ed., 71-80.

Munjiza, A. and Andrews, K. R. F. (1998), "NBS contact detection algorithm for bodies of similar size", International Journal for Numerical Methods in Engineering 43, 1998. 131-149.

Ng, T. T. (1999). "Fabric study of granular materials after compaction." Journal of Engineering Mechanics, vol.125, no.12, 1390-1394.

Perkins, E. and Williams, J. R. (2001), "A fast contact detection algorithm insensitive to object sizes", Engineering Computations, Vol. 18, No. 1/2, 48-61.

Potyondy, D. O., and Cundall, P. A. (1998). "Modeling notch-formation mechanisms in the URL mine-by test tunnel using bonded assemblies of circular particles." International Journal of Rock Mechanics and Mining Sciences, vol.35: 4-5, paper no. 67.

Potyondy, D. O., Cundall, P. A., and Lee, C. A. (1996). "Modeling rock using bonded assemblies of circular particles." Rock Mechanics, Aubertin, Hassani & Mitri (eds.), Balkema, Rotterdam, 1937-1944.

Potyondy, D. O., Cundall, P. A., and Sarracino, R. S. (1996). "Modeling of shock- and gas-driven fractures induced by a blast using bonded assemblies of spherical particles." Rock Fragmentation by Blasting, Mohanty Ed., 55-62.

Rothenburg, L., and Bathurst, R. J. (1991). "Numerical simulation of idealized granular assemblies with plane elliptical particles." Computers and Geotechnics, vol.11, 315-329.

Sun, Y. and Vinogradov, O. (1998). "Numerical simulation of jamming of solid particles transported by fluid in planar channels." Computer Modeling & Simulation in Engineering, February98, Vol. 3. 27-32.

Taylor, L. M., and Preece, D. S. (1992). "Simulation of blasting induced rock motion using spherical element models." Engineering Computations, vol.9, 243-252.

Thallak, S., L. Rothenburg and Dusseault, M. (1990). "Hydraulic fracture (parting) simulation in granular assemblies using the discrete element method." AOSTRA Journal of Research, Vol. 6, 141-153.

Ting, J. M. (1992) "A robust algorithm for ellipse-based discrete element modeling of granular materials." Computers and Geotechnics, vol.13, 175-186.

Ting, J. M., Meachum, L. R., and J.D. Rowell, J. D. (1995). "Effect of particle shape on the strength and deformation mechanisms of ellipse-shaped granular assemblages." Engineering Computation, vol.12, 99-108.

Trent, B. C., and Margolin, L. G. (1994). "Modeling fracture in cemented granular materials." ASCE, Fracture mechanics applied to geotechnical engineering, 54-69.

Vinogradov, O. (1992). "Explicit equations of motion of discrete system of disks in two dimensions." Journal of Engineering Mechanics, vol.118, no.9, 1850-1858.

Vinogradov, O. (1993). "Dynamic equations for system of irregularly shaped plane bodies." Journal of Engineering Mechanics, vol.119, no.11, 2226-2237.

Vinogradov, O. (1997). "Scalar form of dynamic equations for a cluster of bodies." Structural Engineering and Mechanics, vol.5, no.2, 209-220.

Vinogradov, O., and Sun, Y. (1997). "Multibody approach in granular dynamics simulations." Computational Mechanics, vol.19, 287-296.

White, F. M. (1974). Viscous Fluid Flow, McGraw-Hill, Inc. New York. 1974.

White, F. M. (1999). Fluid Mechanics 4th edition, WCB-McGraw-Hill. Boston, Mass., 1999.